JCU ePrints

This file is part of the following reference:

Keall, Rebecca M. (2005) ***Molecular and genetic analysis of Drosophila Rad21: a gene and protein involved in sister chromatid cohesion.***
PhD thesis, James Cook University.

Access to this file is available from:

http://eprints.jcu.edu.au/2088

JCU
JAMES COOK UNIVERSITY

CHAPTER 1: INTRODUCTION

1.1 THE CELL DIVISION CYCLE AND CHROMOSOME SEGREGATION

1.1.1 IDENTIFICATION OF CHROMOSOMES AS BEARERS OF HEREDITARY INFORMATION

The problem of how a cell divides is a fundamental issue in biology. Not only is correct cell division essential for an organisms growth and survival, but correct dissemination of the genetic material is critical for the continuation of life.

Cell division has fascinated biologists for centuries, but it wasn't until the description of chromatin, by Walther Flemming, that our modern understanding of the molecular basis of inheritance began to emerge. In 1882 Flemming described a cellular substance which he called chromatin. He noted that during cell division this chromatin transformed into threadlike strings, and in doing so provided the first description of chromosome condensation (Paweletz, 2001).

In the period from 1887-1890, Theodor Boveri published a number of papers that significantly contributed to our current understanding of chromosomes as the bearers of hereditary information. Studying embryos of the nematode worm *Ascaris megalocephala* Boveri observed that chromosomes exist as consistently organised and individual structures throughout cell division. Based on these observations, Boveri theorised that as the properties of chromosomes met the key requirement of hereditary material (to be constant and unchanging), chromosomes may be the bearer of hereditary material (Baltzer, 1967).

In 1900, following the re-discovery of Mendel's 1866 paper outlining the basic laws of inheritance, both Boveri and Sutton individually proposed that the chromosomes could bear the material of heredity. Through his studies of sea urchin eggs Boveri had recognised that each chromosome contains unique factors that are required for development, providing empirical proof of the theory first put forward by Wilhelm Roux in 1883 that the total hereditary substance required for development is spread across the chromosomes. From the same set of experiments Boveri hypothesised that the chromosomes must also be bipolar.

At around the same time, Sutton was working with grasshopper chromosomes to prove Mendel's laws of inheritance. In 1902 Sutton proposed that "the association of paternal and maternal chromosomes in pairs and their subsequent separation during the reduction division …may constitute that basis of the Mendelian law of hereditary" (Crow and Crow, 2002).

The Sutton-Boveri chromosome hypothesis remained controversial until 1915 when Morgan's work on the white eyed *Drosophila melanogaster* mutant was able to confirm not only Mendel's laws of inheritance, but also that genes are located on chromosomes (Moore, 1972). This pioneering work laid the foundation for what we now refer to as classical genetics and the emergence of one of the great genetic models: *Drosophila melanogaster.*

1.1.2 CELL DIVISION

1.1.2.1 Overview

It is essential that the genome be disseminated into daughter cells accurately and with high fidelity. As early as 1902, based on his studies on sea urchin eggs, Boveri recognised that perturbations of cell division could result in cell death, and indeed the death of an entire organism.

The canonical eukaryotic cell cycle consists of two main phases: M-phase, whereby nuclear (mitosis) and cytoplasmic (cytokinesis) division occurs, and interphase during which cells grow and replicate their DNA (Figure 1.1). Interphase can be divided into G1 phase (the gap between mitotic exit and DNA synthesis); S-phase (when DNA synthesis occurs) and G2 phase (the gap between S-phase and the subsequent M-phase). From the time that the chromosomes are segregated in anaphase until the following S-phase diploid cells have a DNA content of 2N. Following DNA-replication the DNA content is doubled to 4N. In order to ensure the even distribution of chromosomes to daughter cells highly ordered and controlled mechanisms have evolved to regulate the two main types of nuclear division in eukaryotes. In somatic cells these process culminate in **mitosis** and in germ cells in **meiosis**.

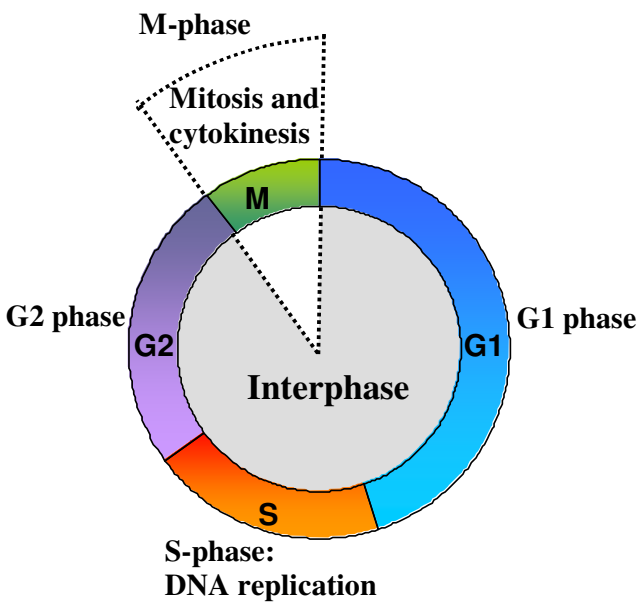

Figure 1. 1: *The typical eukaryotic cell cycle*

The cell cycle consists of four phases. The nuclear and cytoplasmic divisions, mitosis and cytokinesis respectively, occurring during M-phase. DNA replication takes place in S-phase, and the newly replicated chromosomes are called sister chromatids. Adapted from Griffiths et al (2000).

1.1.2.2 The basic mechanisms of mitosis

Mitosis is the process by which all somatic cells divide (Figure 1.2). It is therefore central to biological phenomena such as the size and regeneration of tissues. The first step in mitosis is the formation of a mitotic spindle. The mitotic spindle is a large microtubular structure that commences formation during prophase. As the chromosomes condense, microtubules begin to grow from the microtubule organising centre (or centrosome as it is known in animals). During pro-metaphase the nuclear envelope breaks down and the kinetochores of the attached sister chromatids commence capturing spindle microtubules and congressing, or aligning, at the centre of the spindle. Metaphase is achieved when all chromosomes have achieved bipolar spindle attachment and congressed to the metaphase plate. The spindle checkpoint functions to ensure that there is tension across all kinetochores and that all chromosomes have congressed before anaphase is initiated. During anaphase the replicated chromosomes (sister chromatids) synchronously separate and

move to opposite poles of the spindle, partly aided by the shortening of the kinetochore microtubules and the elongation of the spindle. Telophase is marked by the chromosomes arriving at the spindle poles and beginning to decondense. At the end of telophase, following nuclear envelope reassembly, cells contains two identical daughter nuclei with the cytoplasm commencing division via the formation of actin/myosin contractile ring. In cytokinesis the contractile ring forms a cleavage furrow which pinches the cells into two, to completing cytokinesis and forming two daughter cells.

1.1.2.3 The basic mechanism of meiosis

The primary objective of mitosis is to produce two daughter cells that are genetically identical to the original (mother) cell. Meiosis, on the other hand, is a specialised form of cell division that not only differs from mitosis in that the end products are haploid (1N) gametes, but also in the fact that one of the main objectives of meiosis is to generate genetic diversity (Figure 1.3). Meiosis is characterised by one round of DNA replication followed by two rounds of nuclear division. Table 1.1 summarises the key features of mitosis and meiosis (adapted from Strachan and Read, 1999).

Table 1. 1: Comparison of the main features of mitosis and meiosis

Feature	Mitosis	Meiosis
Location	All tissues	Germline tissues only
Products	Diploid somatic cell	Haploid germ cell
DNA replication	One round of replication	One round of replication
Cell division	One round of division	Two rounds of division
Length of prophase	Short (approximately 30 minutes in human cells)	Long and complex, can take years to complete
Homologous chromosome pairing	None	Homologues pair in Meiosis I
Recombination	None (very rarely occurs and is abnormal)	During meiosis I
Genotype of products	Identical diploid cells	Genetically diverse haploid gametes

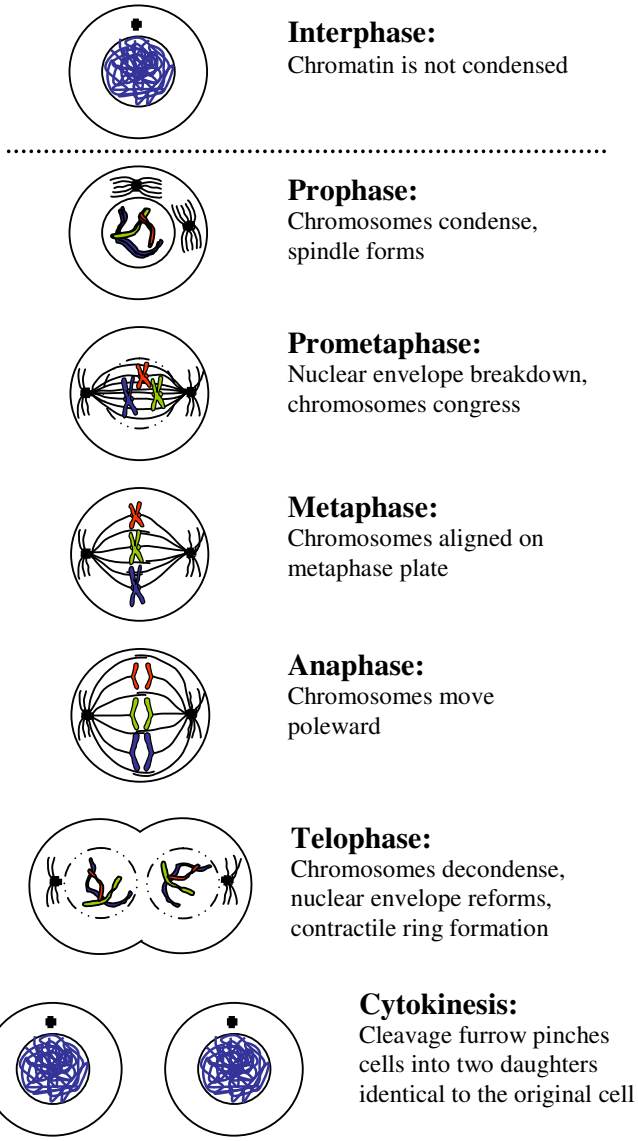

Figure 1. 2: *The cytological features of mitosis*

The main cytological features of mitosis are represented diagrammatically under the dotted line. Brief descriptions of each stage are situated next to the appropriate diagram. Adapted from Griffiths et al (2000).

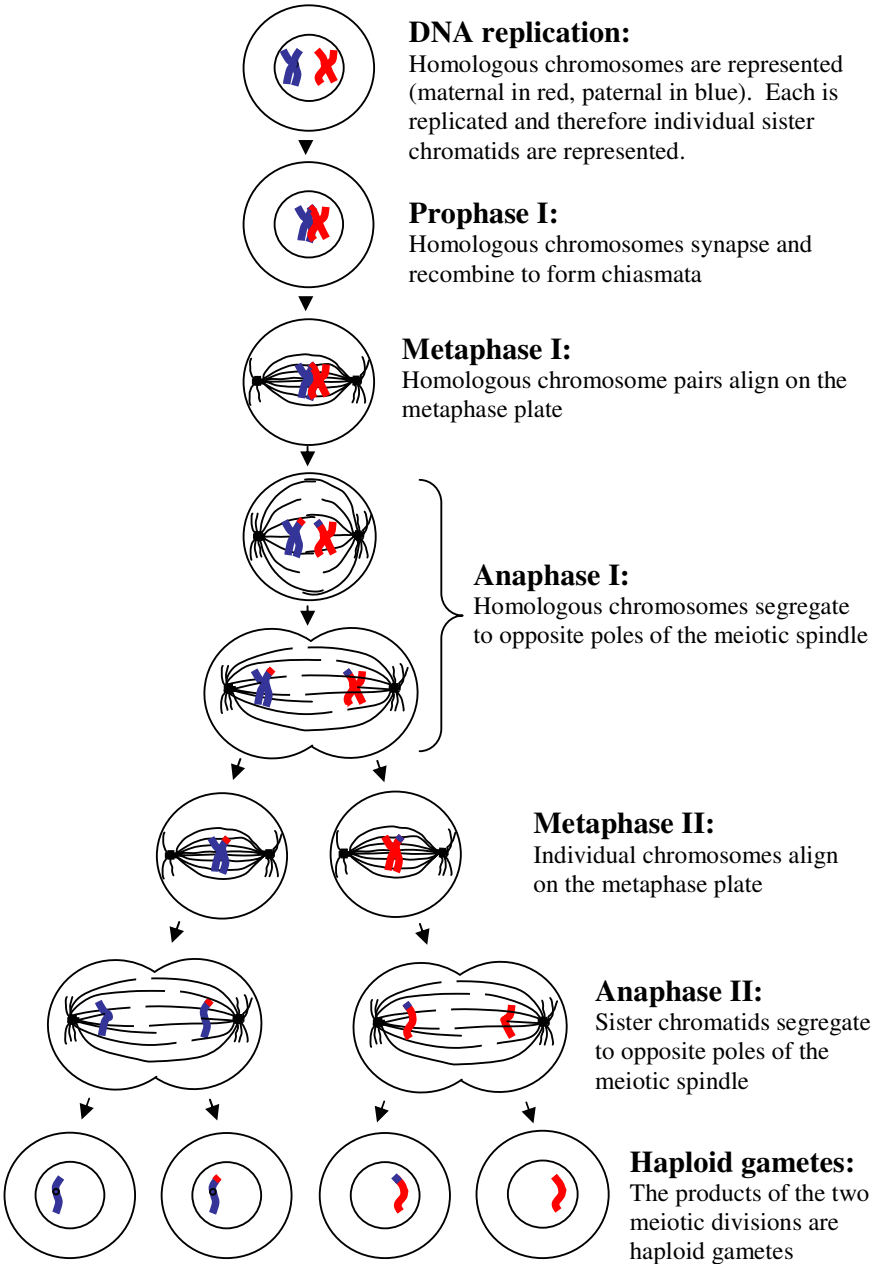

Figure 1. 3: *The cytological features of meiosis*

In meiosis there are two distinct rounds of division, one reductional, the other equational. Homologous chromosomes pair and undergo recombination during prophase I. Meiosis I involves reductional division and the resolution of chiasmata. During meiosis I centromeres of sister chromatids remain attached allowing only for the segregation of homologues. In the equational division of meiosis II sister chromatids segregate to opposite spindle poles allowing for the formation of haploid gametes. Adapted from Griffiths et al (2000).

Each diploid cell consists of two copies of each chromosome, one derived from the maternal parent and the other derived from the paternal parent. Following DNA replication in pre-meiotic S phase these chromosomes, in the form of sister chromatids, are held together and in meiotic prophase I the pairs of homologous chromosomes associate, or synapse. The process by which homologous maternal and paternal chromosomes are able to identify each other is not clear but is known to involve the recombination machinery (for recent review see Shinohara and Shinohara, 2004). During meiosis I, homologous chromosomes segregate to opposite poles of the spindle in what is also known as the reductional division.

The second meiotic division resembles mitosis in that the sister chromatids segregate to opposite spindle poles following the dissolution of sister chromatid cohesion. The key difference, however, is that the meiotic products contain half the number chromosomes compared to the products of mitosis.

During meiosis diverse gametes are generated by the random segregation of maternal and paternal chromosomes in metaphase I. An additional level of genetic diversity is also generated by recombination of the synapsed homologous chromosomes. This recombination is a critical feature of meiosis I and homologue separation in anaphase I requires the resolution of such cross overs, or chiasmata.

1.1.2.4 Sister Chromatid Cohesion

DNA replication results in the duplication of chromosomes, which are termed sister chromatids. It is important that the cell has a means to distinguish sister chromatids from one another so that each daughter cell inherits one and only one copy of each chromosome. To achieve this, sister chromatids are held together along their length from the time of their formation in S-phase, when DNA replication occurs, until they are separated at anaphase. This association is called sister chromatid cohesion and allows the sister chromatids to align at the metaphase plate and is necessary for the bipolar attachment of the sister kinetochores to microtubules emanating from the spindle poles (Biggins and Murray, 1999, Cohen-Fix, 2001, Tanaka et al., 2001). The pulling forces of the spindle microtubules are counteracted by the cohesive force of sister chromatid cohesion, and its subsequent dissolution allows the sister chromatids to migrate to opposite spindle poles during anaphase (Tanaka et al., 2000,

Vagnarelli et al., 2004). Sister chromatid cohesion is therefore one of the mechanisms involved in the maintenance of genomic integrity. Through ensuring that sister chromatids do not segregate randomly, cohesion plays a crucial role in the prevention of chromosome missegregation and aneuploidy in both mitotic and meiotic cells.

Correct chromosome segregation in both mitosis and meiosis requires sister chromatid cohesion (Figure 1.4). During mitosis equational division requires the simultaneous loss of arm and centromeric cohesion for the segregation of sister chromatids at anaphase. Following DNA replication meiotic cells undergo two different forms of nuclear division, the first of which is reductional and the second equational. This results in the generation of four haploid cells. Sister chromatid cohesion is important during both meiotic nuclear divisions; however, its regulation is different to accommodate the different types of division that occur. Tension across the metaphase I spindle is produced by sister-chromatid cohesion distal to the chiasmata which resists the pulling forces of the meiotic spindle. During the reductional divisions of meiosis I, cohesion is lost from chromosome arms but maintained at the centromere (Losada et al., 1998). This allows for the resolution of chiasmata and disjunction of homologous chromosomes. During meiosis II centromeric cohesion is lost to allow for the segregation of sister chromatids during the equational division that occurs. Interestingly, most incidences of aneuploidy that lead to birth defects can be traced to chromosome segregation errors of maternal origin (>80%), with the majority of these (>60%) occurring during meiosis I (Hassold and Hunt, 2001).

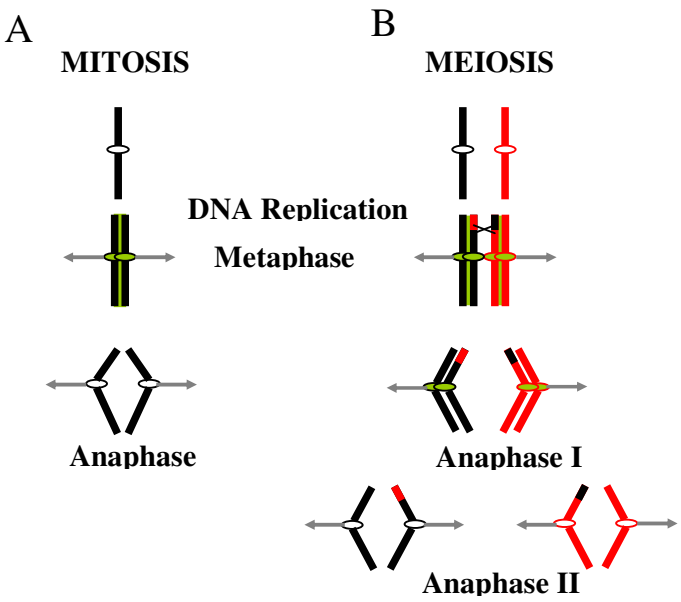

Figure 1. 4: *Correct chromosome segregation in mitosis and meiosis required sister chromatid cohesion*

A: During mitosis sister chromatids are separated by a single equational division. Following DNA replication sisters are held together along the arms and at the centromere by sister chromatid cohesin (green). At the metaphase to anaphase transition cohesion is lost simultaneously along the arms and centromeres. Dissolution of cohesion allows the sisters to move away from one another and segregate to opposite poles of the mitotic spindle (grey arrows represent spindle microtubules, with the arrowhead indicating the direction of the spindle pole).
B: In meiosis there are two distinct rounds of division, one reductional, the other equational. Homologous chromosomes pair and undergo recombination during prophase I. Meiosis I involves reductional division and cohesion is lost along the arms, allowing for the resolution of chiasmata, whereas centromeric cohesion is maintained allowing only for the segregation of homologues. In meiosis II, the loss of centromeric cohesion at the onset of anaphase II allows sister chromatids to segregate during equational division, providing for the formation of haploid gametes.

1.1.3 ERRORS IN CHROMOSOME SEGREGATION

Loss of integrity of cell division during mitosis or meiosis can lead to the unequal distribution of genetic material, which in turn can result in a range of detrimental consequences such as aneuploidy and cell death.

Aneuploidy is defined as the presence of an abnormal amount of DNA in the cell. This deviation from the normal diploid chromosome compliment can be the result of either gains or losses of entire chromosomes or parts thereof. In addition, aneuploidy is often associated with structural changes in chromosomes such as translocations, duplications and deletions (Rajagopalan and Lengauer, 2004).

Aneuploidy is an almost ubiquitous feature of spontaneous and experimentally induced tumours. As early as 1914, Boveri noticed a correlation between aneuploidy and cancer and proposed the "aneuploidy theory of cancer" based on these observations and the fact that aneuploid sea urchin eggs fail to develop properly. Whilst the contribution of aneuploidy to the development of cancer remains controversial, there is a growing body of evidence that supports a role for aneuploidy as a discrete event contributing to malignancy (Sen, 2000) rather than a consequence. Specific aneuploid karyotypes correlating with distinct tumour phenotypes have been observed in several primary tumours. In addition, aneuploid tumour cell lines and experimentally transformed rodent cells have increased chromosomal instability, further implicating aneuploidy as a distinct chromosomal event that is associated with transformation. Recently, further support for this proposition has come from the discovery of mutations of mitotic genes, such as the *hBub1* spindle checkpoint gene, in human cancers (Hanks et al., 2004, Cahill et al., 1998). The debate as to whether aneuploidy is a cause or consequence of cancer will no doubt continue, however, the body of evidence indicating that aneuploidy specifically and frequently correlates with certain phenotypes, stages and prognoses of cancer continues to grow.

Chromosomal missegregation during meiosis is a major cause of miscarriage in humans (for recent reviews see Rubio et al., 2005, Page and Hawley, 2003). The majority of human aneuploidy has no obvious cause, with the only established risk factor being maternal age. Aneuploid pregnancies that go to term lead to birth defects. The specific defect depends upon the aneuploid chromosome configuration

with, for example, trisomy 21 causing Downs Syndrome, and monosomy X causing Turners syndrome. Whilst Turners syndrome only affects approximately 1 in 2500 live births, it is estimated that 10% of spontaneous abortions can be attributed to this aberrant chromosomal configuration (Robinow et al., 1980). It is likely that errors in meiotic chromosome segregation also significantly contribute to human infertility (Cohen, 2002).

1.2 UNDERSTANDING THE CELL CYCLE: GENETIC APPROACHES

1.2.1 KEY CELL CYCLE REGULATORS REVEALED BY GENETIC SCREENS IN YEAST

Our current understanding of cell cycle has largely come from experimental studies performed in yeast. Whilst the temporal events of cell division had been well characterised in the early 20th century, it was not until the late 1960's and early 1970's that an understanding of the molecular events of cell division began to emerge. This understanding came following the pioneering work of Hartwell, who worked with the budding yeast *Saccharomyces cerevisiae*. Hartwell and colleagues used photomicroscopy to screen temperature sensitive mutants of *S. cerevisiae* (Hartwell et al., 1970), leading to the identification of almost 100 cell division cycle (cdc) mutants. Following nitrosoguanidine mutagenesis of haploid cells, temperature sensitive mutants were identified by failure to grow at 36ºC (the restrictive temperature). These temperature sensitive mutants were grown at the permissive temperature (23ºC) and then spotted on agar and maintained at the restrictive temperature. Whilst at the restrictive temperature photographs of the cells were taken and cell cycle defects were identified based on cell morphology. This screen relied upon the fact that the size of the developing bud is indicative of the cell cycle stage. Therefore, by comparing the size of the bud with that of the parent cell, the point of the cell cycle at which arrest occurred could be identified. Using these criteria, Hartwell and colleagues were able to identify temperature sensitive mutants in which the entire cell population of the colony behaved in a uniform pattern consistent with a cell cycle defect, and thus identify genes that when mutated impaired cell cycle progression. Key to this work was the identification of *CDC28* which is required for the initiation of DNA synthesis and regulates the "start" point of the *S. cerevisiae* cell cycle (Hagan and Nurse, 2005).

Following essentially the same approach as that used in *S. cerevisiae,* Nurse began identifying cdc mutants in the fission yeast *Schizosaccharomyces pombe* (Nurse et al., 1976). The phenotypes of the cdc mutants of both budding and fission yeast, revealed that later cell cycle events relied on the execution of earlier events and highlighted the interdependence of the cell cycle. The identification of *cdc2,* the *S. pombe* homologue of *CDC28,* was a breakthrough in cell cycle research, and highlighted the conservation of the cell cycle machinery. Given that *S. cerevisiae* and *S. pombe* are as distantly related to each other as either is to animals (Sipiczki, 2000), this conservation indicated that the regulation of cell cycle progression may be conserved across all eukaryotes. This supposition was confirmed through the isolation of the human homologue of *cdc2* based on its ability to complement a temperature sensitive *cdc2* allele of *S. pombe* (Lee and Nurse, 1987).

Other genetic approaches used in yeast to understand important cell cycle events have involved the analysis of mutants that are sensitive to DNA damaging agents such as ionising radiation or chemical mutagens. The repair of DNA during the cell cycle is an important means by which cells maintain their genetic integrity, by preventing the propagation of deleterious mutations in future generations. Our understanding of the molecular mechanisms of eukaryotic DNA repair pathways has been greatly influenced by genetic studies in yeast. The identification and characterisation of radiation sensitive (rad) mutants of *S. pombe* has greatly aided our understanding of cell cycle regulation and cell responses to DNA damage (Jimenez et al., 1992). This is exemplified by the checkpoint pathways which operate during three main cell cycle transitions, G1/S, intra-S and G2/M, that act to prevent the cell entering the next phase of the cell cycle until the previous phase has been completed correctly. Central to all three checkpoint response pathways is the Rad3-like ATR and its related protein ATM. Members of this protein family play a key role in the maintenance of genomic integrity through the activation of cell cycle checkpoints.

1.2.2 *DROSOPHILA* SCREENS FOR CELL CYCLE MUTANTS

Early genetic research using *Drosophila* such as that conducted by Morgan and colleagues relied on the identification of mutant flies arising out of otherwise wild-type cultures. This process was laborious and involved the screening of thousands, if not millions of flies for the identification of each phenotypic alteration, and hence new mutation. To overcome the problem of the rarity of spontaneously occurring mutations researchers began to attempt to experimentally induce mutations using radiation and chemical means. The introduction of mutations using these methods sped up the rate of genetic research and also resulted in the identification of strains of flies that were hypersensitive to these treatments.

A breakthrough in *Drosophila* cell cycle research occurred when Gatti and Baker realised that many of the genes involved in radiation and mutagen sensitivity and meiotic recombination are also required for DNA repair and genetic stability in mitotic cells (Gatti et al., 1980, Baker et al., 1978). These observations highlight that the processes involving DNA metabolism, for example in the generation and repair of DNA lesions, are utilised throughout the cell cycle to maintain genomic integrity.

Genetic screens in *Drosophila* can take on many different forms, from the traditional analysis of mutant phenotype, to loss-of-function and gain-of-function genetic interaction screens. External organs such as the eye or wing have been used extensively for genetic screens in *Drosophila*. In both cases phenotypic alterations are relatively easy to score and interpretation of the results is aided by the fact that the development of these tissues is very well understood. Genetic screens have been successful in the dissection of a vast array of biological processes (St Johnston, 2002). For example, genetic screens using eye phenotypes resulting from overexpression of cell cycle regulators such as Cyclin E, Rbf or E2F/Dp in the posterior differentiating cells of the eye imaginal disc have been successful in identifying dominant cell cycle regulators (Staehling-Hampton et al., 1999, Boulton et al., 2000, Duman-Scheel et al., 2002, Lane et al., 2000). Before discussing some *Drosophila* genetic screens that have elucidated mechanisms of cell cycle regulation, the development of the *Drosophila* eye and its use in genetic screens will be introduced.

1.2.2.1 The *Drosophila* eye as a model system

During embryogenesis in *Drosophila* sets of cells are set aside to become the adult structures. During the third instar larval stage these cell populations, called imaginal discs, proliferate and commence differentiation to form the adult structures during pupariation. The adult *Drosophila* eye is formed from the cells of the eye imaginal disc, and cells begin to assume their adult fate during the development of the eye imaginal disc of the third instar larva (Figure 1.5). During this larval period a wave of morphogenesis moves across the single layer epithelium of the eye imaginal disc from posterior to anterior (Thomas and Wassarman, 1999). The progression of this wave is marked by the Morphogenetic Furrow (MF), and it is immediately anterior to and within the MF that the cell cycle and differentiation are co-coordinated. Anterior to the MF cells asynchronously progress through the cell cycle. Cells located immediately anterior to the MF arrest in G1 of the cell cycle. Passage of the MF induces a subset of cells to differentiate into photoreceptor pre-clusters whilst the surrounding cells undergo a synchronous round of DNA replication, followed by a synchronous mitosis, called the second mitotic wave. The eye imaginal disc is an ideal system in which to study the cell cycle as the cell cycle patterns are well defined and understood. An additional advantage of using this system is that perturbations to cell division in the developing eye imaginal disc, for example, by inducing ectopic S-phases through the ectopic expression of *cyclin E*, lead to eye developmental defects. These defects disrupt the ordered hexagonal array of ommatidia and can be seen as a disorganised and roughened adult eye (Richardson et al., 1995). This simple assay system, combined with the fact that the eye is a non-essential organ for a laboratory animal, makes the *Drosophila* eye an ideal model system in which to study disruptions to the cell division cycle.

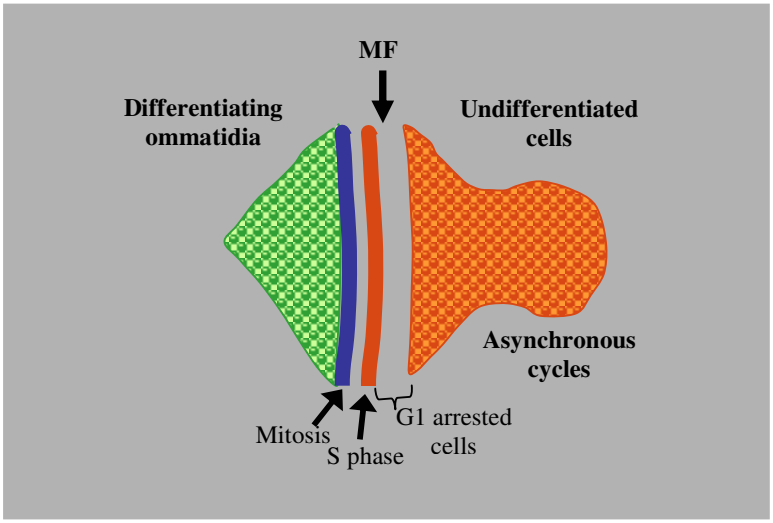

Figure 1. 5: *Schematic of the eye imaginal disc*

Schematic of the progression of the morphogenetic furrow across the eye-antennal imaginal disc. Following asynchronous cell cycles, cells arrest in G1 immediately anterior to the MF. Posterior to the MF a subset of cells differentiate into photoreceptor pre-clusters whilst the surrounding cells undergo a synchronous round of DNA replication, followed by a synchronous mitosis, called the second mitotic wave. Adapted from Richardson et al (1995).

1.2.2.2 Drosophila screens for cell cycle mutants

The power of the *Drosophila* system to identify loci involved in the regulation of the cell cycle can be readily illustrated by a recent study performed by Hariharan and colleagues (Tseng and Hariharan, 2002). This approach used a missexpression screen to identify negative regulators of the cell cycle by virtue of the observation that negative cell cycle regulators, when overexpressed, are likely to restrict growth or cell cycle progression. This overexpression (or gain-of-function) screen was performed using a collection of 2300 *Drosophila* stocks called EP lines (Rorth et al., 1998, Rorth, 1996). This approach takes advantage of the Gal4-UAS system (Figure 1.6), with each EP line having a P-element with Gal4 binding sites and a minimal promoter inserted in the genome. It has been shown that P-elements preferentially insert into the 5' untranslated region (5' UTR) of genes (Zhang and Spradling, 1993), which means that the expression of Gal4 in a specific temporal or spatial pattern should result in the overexpression of genes downstream of the EP insertion. In this study, Hariharan and colleagues used Gal4 expressed from the eyeless promoter (ey-

Gal4) to specifically express 2296 of the individual EP lines in the developing *Drosophila* eye (Tseng and Hariharan, 2002).

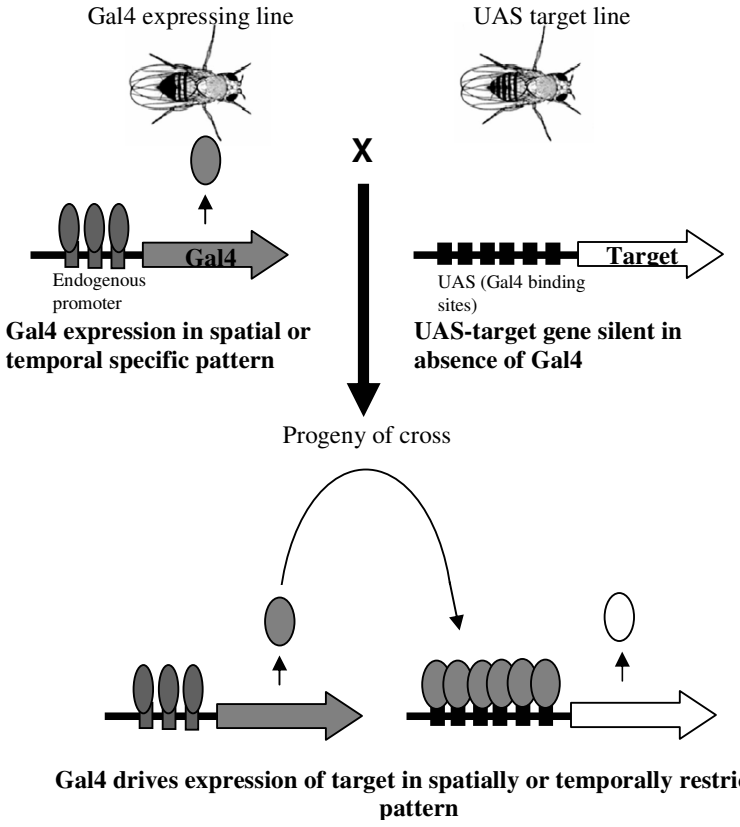

Figure 1. 6: *The Gal4-UAS system*

The Gal4-UAS binary system is used in *Drosophila* to induce gene expression in a tissue and/or developmentally specific pattern. This is achieved by placing Gal4 binding sites (UAS) upstream of the target gene. Expression of the target gene only occurs in the presence of the yeast Gal4 transcription factor, which can be achieved by genetic crossing as depicted. Adapted from Phelps and Brand (1998).

A small eye phenotype was observed upon ey-Gal4 driven expression in 46 individual EP lines, representing 32 loci. EP lines that produced small eye phenotypes were analysed further to eliminate those that were eye specific or were functioning post-mitotically and whether the small eye phenotype could be suppressed by increasing the amount of cell division occurring in the eye imaginal discs (by simultaneous overexpression of the S-phase Cyclin, Cyclin E which induces additional rounds of S-phase and mitosis). Four of the EP lines, representing three loci (*INCENP*, *elB* and *CG11518*) fit all of these criteria and were analysed further. It was shown that their overexpression slows the rate of doubling time as cells from clones expressing the EP element were the same size as their wildtype counterparts but their progress through the cell cycle was delayed. These results illustrate one approach that can be used to identify cell cycle regulators in *Drosophila*.

Another recently reported screen for new DNA repair mutants highlighted the usefulness of *Drosophila* in revealing metazoan specific components of common eukaryotic pathways (Laurencon et al., 2004). In this screen a collection of 6275 *Drosophila* strains homozygous for autosomal mutations (Koundakjian et al., 2004) were analysed for hypersensitivity to the mutagens methyl methane sulfonate (MMS) and nitrogen mustard (NH2). Previous screens for mutagen sensitive in *Drosophila* have identified genes with a mammalian but not a yeast orthologue. For example, mus304, which is a mutation in the *CG7347* locus that encodes the *Drosophila* orthologue of the mammalian ATR interacting protein ATRIP (Cortez et al., 2001) was originally identified in a screen for excision repair mutants (Boyd and Harris, 1981). In the screen for new mutagen sensitive loci in *Drosophila* Burtis and colleagues identified 22 new genes that had not been previously implicated in DNA repair. Given that over 27% of known *Drosophila* mutagen sensitive loci have a mammalian orthologue, but no yeast orthologue, it is likely that this screen has identified several components of the DNA repair machinery that are unique to metazoa.

Other genetic screens in *Drosophila* have identified loci required for the regulation of G1/S progression. Cells that are in the G1 phase of the cell cycle have either just completed mitosis or are about to enter S-phase. Regulation of the progression

through G1 has been characterised most extensively in yeast. Multicellular eukaryotes, however, have distinct cyclin/cdk complexes that regulate the G1 phase of the cell cycle. For example, CyclinE which together with Cdc2 promotes entry into S-phase is not found in single celled eukaryotes. The following examples illustrate the genetic approaches used in *Drosophila* to understand the role of CyclinE in cell cycle progression.

Overexpression of CyclinE in post mitotic cells using the Gal4 UAS system, results in a rough eye phenotype (Richardson et al., 1995). Lehner and colleagues screened a collection of ethyl methane sulfonate (EMS) mutagenised flies for dominant modifiers of this rough eye phenotype (Lane et al., 2000). Identification of loci that both enhanced (worsened) or suppressed (lessened) the rough eye phenotype revealed known CyclinE interactors such as Cdc2 and novel interactors such as *split ends* (*spen*). *spen* encodes an RNP-type RNA-binding protein that is required for wingless signaling in imaginal discs (Lin et al., 2003). Several *spen* alleles have also been shown to suppress the rough eye phenotype of a hypomorphic allele of *cyclinE*, $cyclinE^{JP}$ (Brumby et al., 2004). Suppression of the rough eye phenotype produced upon *CyclinE* overexpression and upon expression of a hypomorphic mutation, by *spen* supports a role for the wingless signaling pathway in the negative regulation of S-phase entry in the eye imaginal disc. Expression of $cyclinE^{JP}$ causes a rough eye phenotype by reducing the number of S-phases in the developing *Drosophila* eye (Secombe et al., 1998). Genetic screens using the $cyclinE^{JP}$ phenotype have identified both known and novel regulators of S-phase entry in *Drosophila* (Brumby et al., 2002, Brumby et al., 2004). Using large deletions (deficiencies), X-ray and EMS mutagenised lines fourteen new loci that had not been previously implicated in the G1/S transition were identified, including proteins with known roles in signaling pathways, chromatin remodeling and cell adhesion (Brumby et al., 2004). Therefore, these two *cyclinE* based genetic screens highlight the fact that the information gained from such experiments depends upon the precise approach taken. Both of the examples discussed have provided insight into the regulation of G1/S progression and by using different approaches have taken advantage of the wealth of tools available to *Drosophila* researchers.

1.3 UNDERSTANDING SISTER CHROMATID COHESION

1.3.1 GENETIC SCREENS IN YEAST REVEAL GENES REQUIRED FOR SISTER-CHROMATID COHESION

Sister chromatid cohesion is required for the correct and timely segregation of sister chromatids during cell division, and to prevent precocious segregation of chromatids. Until recently, however, little was known about the genes that regulate this crucial cellular process. Our understanding of the molecular mechanisms of sister chromatid cohesion has been greatly aided by genetic screens in yeast for chromosome cohesion mutants.

In a screen for chromosome transmission fidelity mutants (ctf), Spencer and colleagues used a visual screen to identify *S. cerevisiae* mutants with increased frequency of chromosome loss (Spencer et al., 1990). Using a non-essential marker chromosome, colonies that exhibited increased chromosomes loss (specifically loss of the marker chromosome) accumulated red pigment which resulted in the formation of red sectors in otherwise white colonies. In this manner, approximately 600 000 EMS mutagenised colonies were screened for the colony sectoring phenotype and therefore decreased fidelity of chromosome transmission. 136 mutant colonies that fall into 11 different ctf complementation groups were identified. The *Ctf7p* gene was first identified at the molecular level in this screen and has since been shown to be essential for the establishment of sister chromatid cohesion (Skibbens et al., 1999).

Colony sectoring phenotypes were also used in a screen for genes required for sister chromatid cohesion in metaphase cells (Michaelis et al., 1997). At the time that this screen was performed it was known that a functional anaphase promoting complex (APC) was required for sister the resolution of sister chromatid cohesion at anaphase as APC mutants failed to segregate sister chromatids (Irniger et al., 1995). Colonies that lost chromosomes at elevated frequencies were first identified based on their colony sectoring phenotype and then subsequently analysed for separation of sister chromatids in the absence of APC function. The rationale for this screen was that products that are essential for sister chromatid cohesion, when mutated, would

decrease the fidelity of cohesion. Therefore, in the absence of APC function, sister chromatids should remain attached unless a mutation in a sister chromatid cohesion gene allowed them to become unattached. With this approach eight independent mutants were isolated (Michaelis et al., 1997). These eight mutants were found to represent four complementation groups. One allele of each of the *SMC1* and *SMC3* genes, which encode structural maintenance of chromosomes proteins, was isolated in the screen. Two alleles of a gene subsequently named sister chromatid cohesion protein 1, *scc1*, were obtained and four alleles of sister chromatid cohesion protein 2, *scc2*, were identified in this screen. Each of *scc1, scc2, SMC1* and *SMC3* play crucial roles in the regulation of sister chromatid cohesion, with SMC1, SMC3 and SCC1 subsequently shown to form a complex which was named cohesin (additional details are presented in Section 1.4.1).

Cohesin proteins have been identified in all eukaryotes examined to date, including *Drosophila* and human. In a separate screen to identify genes required for sister chromatid cohesion in *S. cerevisiae* Guacci et al (1997) identified a gene named *mcd1* for mitotic chromosome determinant 1 which was later shown to be the *scc1* gene identified by Michaelis et al (1997). In addition, the *S. pombe* homologue of *mcd1/scc1* was identified as a radiation sensitive mutant involved in DNA repair and named *rad21* (Birkenbihl and Subramani, 1995). Throughout this thesis RAD21 will be used to refer to MCD1/SCC1/RAD21 proteins irrespective of the species being discussed.

1.3.2 APPROACHES TO SCREEN FOR CHROMOSOME SEGREGATION GENES IN *DROSOPHILA*

Approaches used to analyse chromosome segregation in *Drosophila* have mainly focused on meiotic mechanisms of chromosome missegregation. Such screens ultimately identify genes that are essential for meiosis, and therefore are not specific for identification of genes involved in chromosome segregation.

A more direct approach to identify genes that are required for accurate chromosome transmission was recently conducted by Karpen and colleagues (Dobie et al., 2001) in which the inheritance of minichromosomes that are non-essential for the survival of an organism were used to monitor meiotic chromosome inheritance. This strategy

was used to identify sensitised chromosome inheritance modifiers, or *scim* mutants in *Drosophila* (Dobie et al., 2001). Karpen and colleagues used a modified minichrosomosome called J21A to screen approximately 3000 P-element mutagenised lines. J21A is normally inherited in 27% of progeny, and P-element lines were screened for those that increased or decreased the frequency of J21A transmission. P-element mutagenesis was used in this study to facilitate the subsequent identification of the gene causing the effect. 78 *scim* mutants were isolated in this study. Some of the *scim* mutants were found to be P-element insertions in genes already implicated in chromosome segregation, such as *centrosomin* which is involved in the organisation and function of the mitotic spindle. The majority of *scim* lines, however, corresponded to insertions in previously uncharacterised loci. Interestingly, analysis of mitoses in the larval neuroblasts of homozygous lethal *scim* lines revealed mitotic chromosome defects including the precocious separation of sister chromatids and heterochromatin defects. These results indicate that chromosome segregation in mitosis and meiosis share many important regulatory molecules.

1.4 THE COHESIN COMPLEX

1.4.1 THE YEAST COHESIN COMPLEX

The discovery of the multi-subunit cohesin complex has greatly advanced understanding of the molecular mechanisms involved in sister chromatid cohesion. First identified through genetic screens in *S. cerevisiae* the mitotic cohesin complex is comprised of at least four subunits including two structural maintenance of chromosome proteins, SMC1 and SMC3, and two non-SMC proteins, RAD21 and SCC3 (Figure 1.7). Genome project data from a wide variety of eukaryotic species shows homologous genes present in all genomes examined, suggesting that this complex has been conserved as it performs functions that are essential for cell survival.

SMC proteins have globular N and C termini at the ends of stretches of coiled-coil with a central flexible hinge region. It is this flexible hinge which gives bacterial SMCs their characteristic 'V' conformation (Melby et al., 1988). Bacterial SMC proteins form antiparallel homodimers and the SMCs of higher eukaryotes form

similar antiparallel heterodimers (for review see Losada and Hirano, 2005). The coiled coils of SMC 1 and SMC 3 proteins fold back on themselves to form intramolecular coiled-coils and the proteins form a heterodimer by associating at their hinge regions (Haering et al., 2002).

Sub-unit interaction assays have lead to a model whereby this heterodimer, in combination with the RAD21 cohesin component, form a tripartite ring-like structure (Haering et al., 2002). Indeed, through a series of deletion experiments it was shown that the C-terminus of RAD21 bound the globular domains of SMC1 and not SMC3, and the N-terminus of RAD21 bound the globular domains of SMC 3 and not SMC 1, providing evidence for the proposed model of cohesion function, with RAD21 capable of completing the 'loop' (Figure 1.7). This ring-like structure is consistent with electron micrographs of purified *Xenopus* and human cohesin complexes (Anderson et al., 2002). At present it is thought that this proteinacious ring-like structure facilitates chromosome cohesion by encircling the sister chromatids, although direct evidence supporting this mechanism has yet to come to light.

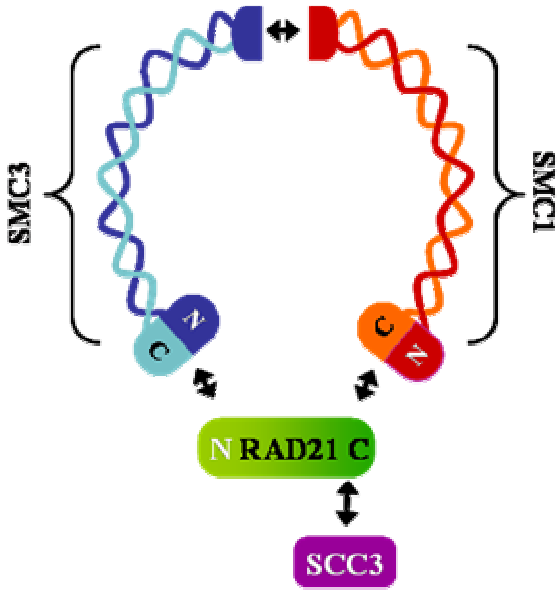

Figure 1. 7: *The cohesin complex*

Arrows indicate known subunit interactions as shown (Haering et al., 2002). Current models of cohesin function suggest that it forms a ring that encircles the sister chromatids.

Although the exact function of the non-SMC cohesin subunits remains to be precisely determined, current models implicate them in regulating the activity of the SMC heterodimers, and in conferring specificity to the SMC containing complex. In *S.pombe* RAD21 localises to the nucleus and its levels are regulated in a cell cycle dependent manner. In early G1, RAD21 is absent from cells and protein expression is observed to peak during S, G2 and metaphase, and subsequently RAD21 levels decline during anaphase (Michaelis et al., 1997, Birkenbihl and Subramani, 1995). *S. pombe* RAD21 is a phosphoprotein and levels of hyperphosphorylated RAD21 are seen to peak in G2. Analysis of the crystal structure of the SMC1 globular ATPase head complexed with RAD21, reveals that the C terminus of RAD21 forms a winged helix (Haering et al., 2004). This motif is found in many DNA-binding proteins; however functional data suggests that RAD21 does not directly bind DNA.

The second non-SMC cohesin component, SCC3 is an integral part of the cohesin complex and is homologous to the stromalin antigen (SA) proteins of higher eukaryotes. SCC3 is a critical regulator of cohesin dissociation in metazoan species, although its precise function in yeast remains to be determined. Depletion of RAD21 in *Drosophila* cultured cells results in the instability of the SCC3 protein (Vass et al., 2003), indicating that the formation of functional cohesin complexes may rely on a feedback loop involving these two proteins.

1.4.1.1 Establishment of cohesion in S-phase

Cohesin binds to chromosomes prior to S-phase and requires the accessory proteins SCC2 and SCC4. In budding yeast *scc2* and *scc4* mutants soluble cohesin complexes form but do not bind to chromatin (Ciosk et al., 2000). Chromatin immunoprecipitation assays in budding yeast were used to identify cohesin attachment sites, and suggested that cohesin was enriched at the centromeres and at some sites along the chromosome arms spanning approximately 1kb and located every 5-10 kb (Blat and Kleckner, 1999, Tanaka et al., 1999b). Further investigation of cohesin attachment sites has recently shown that the chromosomal location of cohesin in much more dynamic that previously thought (Glynn et al., 2004, Lengronne et al., 2004). It is suggested that cohesin is initially loaded onto DNA at the transcriptionally active SCC2/SCC4 binding sites, and once loaded can then slide to a more permanent location on the chromosome. Cohesin localisation appears to

be directed by the active transcription of flanking genes as the complex is found most often at sites of convergent transcription. This suggests that it is actually pushed to these sites by the transcription apparatus (Lengronne et al., 2004) (Figure 1.8). In addition, SCC2/SCC4 complexes may be required to promote the hydrolysis of ATP by the SMC heads, a process that has recently been shown to be required for the stable association of cohesin with chromosomes (Arumugam et al., 2003).

In yeast, cohesion between sister chromatids is established with the aid of another protein, ECO1/CTF7. ECO1 is an essential protein required for establishing cohesion between sisters during S phase but not for the maintenance of cohesion during G2 or M phases of the cell cycle (Skibbens et al., 1999). ECO1 is able to acetylate itself and a number of cohesion related proteins including SMC3 and SCC1 *in vitro* but not *in vivo.* The physiological significance of this activity, therefore, remains to be demonstrated (Ivanov et al., 2002). Indeed, budding yeast expressing acetyltransferase-defective ECO1 as the sole source of ECO1 grow robustly with high fidelity chromosome transmission (Brands and Skibbens, 2005). *eco1* mutants are able to form cohesin complexes which bind chromatin but cohesion between sisters is not established (Toth et al., 1999). Therefore, binding of chromatin by cohesin and the establishment of sister chromatid occur separately and by distinct mechanisms.

In fission yeast the cohesin-associated protein, PDS5, has roles both in the establishment and maintenance of sister chromatid cohesion, as well as in chromosome condensation (Hartman et al., 2000, Panizza et al., 2000). PDS5 is related to the *Aspergillus nidulans* BimD protein which is implicated in chromosome cohesion in both mitosis and meiosis. PDS5 binds to chromatin in an RAD21 dependent manner, and hinders the establishment of cohesion until it is counteracted by ESO1 (*S. pombe* ECO1 orthologue) following which PDS5 is required for the maintenance of cohesion (Tanaka et al., 2001). PDS5 homologous have been identified and chracterised in both budding yeast and human (Panizza et al., 2000, Hartman et al., 2000, Sumara et al., 2000). Although not a member of the cohesin complex, PDS5 is essential for sister chromatid cohesion in budding yeast, and in fission yeast becomes essential for sister chromatid cohesion following prolonged time in G2 (Uhlmann, 2001). In vertebrates, PDS5 also appears to be involved in

both the stabilisation and destabilisation of cohesin mediated cohesion (Losada et al., 2005).

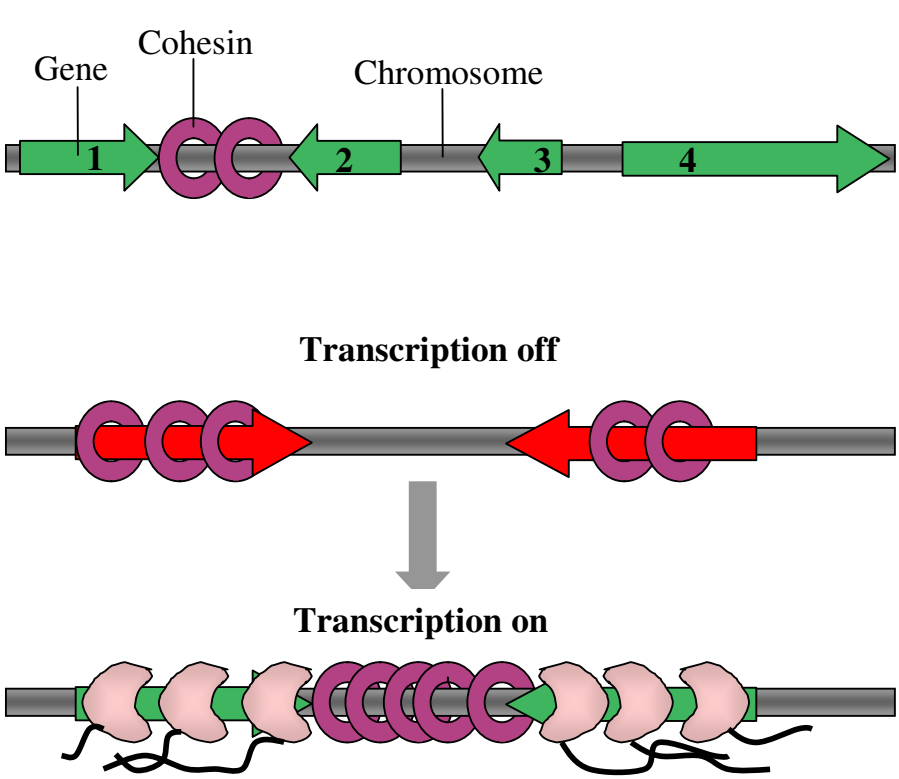

Figure 1. 8: *Cohesin is pushed to sites of convergent transcription by the transcription apparatus*

A: Hypothetical arrangement of genes organised in different orientations in the genome. Genes 1 and 2 are arranged in a tail to tail conformation, genes2 and 3 in a head to tail conformation and genes 3 and 4 in a head to head conformation. Green arrows indicate the direction of transcription. Analysis of cohesin location along chromosome arms shows that cohesin is most often found between genes that are convergently transcribed, i.e., arranged in a tail to tail conformation.
B: Cohesin is relocated following transcription. When transcription of a gene occurs, cohesin is relocated from the coding region to the intergenic region at the end of the gene. This relocation is thought to involve physical pushing of the cohesin complex by the transcription machinery, including RNA polymerase, shown in light pink. Newly synthesised RNAs are shown as black lines.
(Adapted from Ross and Cohen-Fix, 2004).

1.4.1.2 Dissolution of cohesion – The Metaphase to Anaphase transition

The cohesin complex is required to counteract the pulling forces of the mitotic spindle, preventing the separation of sister chromatids that are attached to the spindle via their kinetochores. Therefore, cohesion between sister chromatids must be dissolved at the time of chromosome segregation, to allow for the separation of sisters via the bipolar pulling forces of the spindle microtubules. Sister chromatid cohesion is maintained throughout mitosis until the onset of anaphase, when the simultaneous loss of cohesion from all chromosomes is necessary for the separation of sister chromatids. At the metaphase to anaphase transition at least two cohesin subunits, SCC3 and RAD21, dissociate from the chromosomes with the separation of the sister chromatids facilitated by the site-specific proteolysis of RAD21 by SEPARASE (ESP1).

SEPARASE is a site-specific protease of the caspase family and is kept inactive through physical interaction with PDS1 (SECURIN) (Hornig et al., 2002, Waizenegger et al., 2002, Herzig et al., 2002, Gorr et al., 2005, Nasmyth et al., 2000). SEPARASE activation at the metaphase to anaphase transition follows the anaphase promoting complex (APC) dependent degradation of SECURIN. SEPARASE is then able to cleave the RAD21 component of cohesin at either one of two cleavage sites, allowing the segregation of the sister chromatids at anaphase. Through tobacco etch virus (TEV) protease cleavage of recombinant RAD21 it was shown that cleavage of the RAD21 is necessary and sufficient for the segregation of sister chomatids (Uhlmann et al., 2000). Phosphorylation of RAD21 by the mitotic kinase, POLO/CDC5, at serine residues adjacent to the cleavage sites increases the efficiency of RAD21 cleavage by SEPARASE (Alexandru et al., 2001). The larger of the RAD21 cleavage products is subject to protein degradation via the N-end rule pathway, and RAD21 was the first physiological substrate of this pathway to be identified (Rao et al., 2001). This degradation is essential as failure to remove the RAD21 cleavage product could result in interference with the establishment and/or dissolution of cohesion in the following cell cycle, which could lead to aneuploidy and cell death (Rao et al., 2001).

In yeast, the total cellular pool of RAD21 is subject to proteolysis and protein levels decline rapidly in anaphase. By early G1 there is little to no detectable RAD21 in the cells (Michaelis et al., 1997, Guacci et al., 1997). This means that in yeast at least the RAD21 cohesin component must be resynthesised prior to S-phase when cohesin is leaded onto the chromosomes.

1.4.1.3 The meiotic cohesin complex

During meiosis, the RAD21 cohesin component is largely replaced by a related protein called REC8. Whilst *rec8* is non-essential for mitotic growth in yeast it is critical for the correct execution of meiotic specific events such as homologous recombination (Molnar et al., 1995). Analyses of the distribution of REC8-containing and RAD21-containing cohesin complexes during meiosis have revealed distinct roles for the two complexes (Klein et al., 1999, Watanabe and Nurse, 1999). RAD21-containing cohesin complexes are found to be removed from chromosome arms following SEPARASE cleavage of RAD21 at anaphase I, whilst REC8-containing cohesin maintains centromeric cohesion until the onset of anaphase II. Sister chromatid separation is triggered by the cleavage of REC8 by SEPARASE at anaphase II (Buonomo et al., 2000).

1.4.2 SISTER CHROMATID COHESION IN METAZOA

1.4.2.1 Cohesin complexes in metazoans

The cohesin complex is highly conserved and in higher eukaryotes homologues of the yeast cohesin proteins can be found. Cohesin complexes in higher eukaryotes are comprised of SMC1, SMC3 proteins, RAD21 and the SCC3 homologue which has at least two isoforms: SA1 and SA2. Overexpression of the human SMC3 cohesin subunit has been noted in a variety of transformed cells and primary tumours and alone is sufficient to transform NIH 3T3 cells (Ghiselli and Iozzo, 2000). In metazoan species, in addition to REC8, other meiosis specific isoforms of cohesin components exist. These include SA3 (orthologous to SCC3 (Prieto et al., 2001)) and SMC1β (Revenkova et al., 2001).

SA1 and SA2 belong to the stromalin antigen (SA) family of mammalian proteins and share limited homology with SCC3. SA proteins implicated in sister chromatid

cohesion have been identified in mouse and *Drosophila* in addition to those in human and *Xenopus* (Valdeolmillos et al., 1998, Valdeolmillos et al., 2004, Vass et al., 2003)Two different cohesin complexes have been identified in humans and *Xenopus,* those that contain SA1 (cohesin^{SA1}) and those that contain SA2 (cohesin^{SA2}) (Losada et al., 2000). Whilst cohesin^{SA1} and cohesin^{SA2} primarily function in mitosis, cohesin^{SA2} is also involved in meiosis in mammalian germinal cell maturation (Prieto et al., 2002). .

1.4.2.2 Regulation of cohesin in higher eukaryotes

1.4.2.2.1 Cohesin is removed from chromosomes in two distinct steps

In higher eukaryotes cohesin is present during all stages of the cell cycle. Unlike the yeast RAD21 proteins that oscillate in a cell-cycle dependent manner, the metazoan RAD21 homologues show few fluctuations. The cellular localisation of RAD21 homologues in higher eukaryotes varies in a cell cycle dependent manner, suggestive of post-translational regulation.

Although there are many similarities with yeast, the regulation of sister chromatid cohesion in eukaryotes also has many striking differences. Like yeast, cohesin is loaded onto chromosomes prior to S-phase and cohesion is established at the time of DNA replication with the aid of ECO1. However, at prophase/prometaphase, the majority of cohesin dissociates in a separase independent manner and is relocated to the cytoplasm, possibly to facilitate the condensation of chromosomes (Jager et al., 2001, Sumara et al., 2000, Losada et al., 1998) (Figure 1.9). In *Xenopus* the cleavage independent dissociation of cohesin from chromatids requires the Polo-like (Plk) and aurora B mitotic kinases (Sumara et al., 2002, Losada et al., 2002, Gimenez-Abian et al., 2004). In *Drosophila polo* mutants, the centromeres of sister chromatids are separated but cohesion along chromosome arms is maintained when cells are arrested in metaphase (Donaldson et al., 2001). Taken together these lines of evidence indicate that the prophase/prometaphase dissociation of cohesin is, at least in part, regulated by POLO in *Drosophila* and Plks in other metazoans.

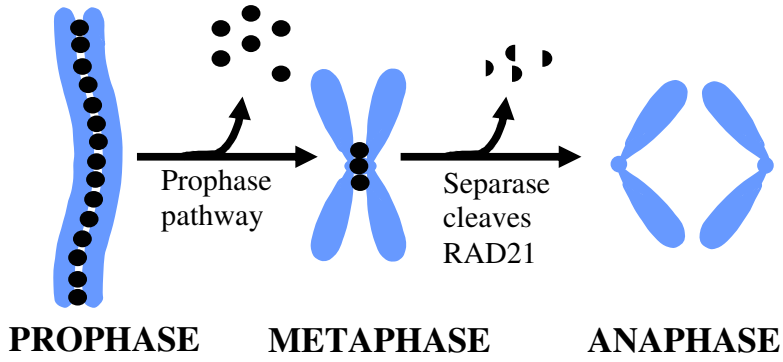

Figure 1. 9: *Cohesin is removed from metazoan chromosomes in two distinct steps*

Newly replicated chromosomes are held together by the cohesin complex (black dots) along their entire length at prophase. The majority of cohesin dissociates from the chromosome arms in a cleavage independent manner, and at metaphase sister chromatids are held together by cohesin in the vicinity of their centromere. Cleavage of the RAD21 cohesin component allows the sister chromatids to separate at anaphase and migrate to opposite spindle poles.

It has recently been shown that hyperphosphorylation of the human SCC3 cohesin component, SA2, is required for the prophase dissociation of cohesin, at least in HeLa cells (Hauf et al., 2005), however the function of this pathway remains unclear. Unphosphorylatable SA2 remained on chromosome arms until the metaphase-anaphase transition, whereby cohesin dissociation is presumably triggered by SEPARASE mediated proteolysis of RAD21. Intriguingly, the persistence of arm cohesion until the metaphase to anaphase transition did not interfere with the timely and efficient execution of mitosis. Therefore, while light is beginning to be shed on the mechanism of the prophase dissociation pathway, the reason for its existence remains unclear.

At metaphase sister chromatids are held together by centromeric cohesin and sister chromatid segregation results from the cleavage of the RAD21 component of this minor pool of centromeric cohesin (Figure 1.9). The cleavage sites of human RAD21 have been mapped, and overexpression of non-cleavable RAD21 in human cells results in the formation of anaphase bridges and a marked increase in

aneuploidy (Hauf et al., 2001). In this series of experiments Hauf et al (2001) observed that cells with sister chromatids still attached re-enter anaphase and re-replicate their DNA. This suggests that naturally occurring defects in SCC1 cleavage and/or separase activation would not result in cell cycle arrest but would be a possible cause of genomic instability through chromosomal non-disjunction events that persist in subsequent cell cycles. Such defects could also account for the abnormal karyotypes often associated with malignancy such as aneuploidy, chromosomal beaks and chromosomal fusions. Cleavage of the RAD21/SCC1 cohesin subunit has not been demonstrated in other metazoans, but is also likely to occur.

The differential regulation of cohesin at centromeres and along chromosome arms may not be restricted to metazoa. A SNF2 containing chromatin remodeling complex has been demonstrated to stably associate with the cohesin complex, in human cells, and to be required for the loading of cohesin onto chromatin (Hakimi et al., 2002). In *S. pombe* it has been shown that the heterochromatin associated protein SWI6, also involved in chromatin remodeling, is required for the establishment of centromere associated (but not chromosome arm associated) sister chromatid cohesion (Bernard et al., 2001a). This indicates that the establishment and possibly maintenance of cohesion along chromosome arms and at centromeres may be differentially regulated in unicellular eukaryotes also.

The means by which centromeric cohesin is protected from the prophase dissociation pathway has recently become somewhat clearer thanks to numerous studies of homologues of the *Drosophila* meiotic protein, MEI-S332. MEI-S332 has been studied extensively and was proposed to maintain sister chromatid cohesion until anaphase II of meiosis (Davis, 1971, Goldstein, 1980, Tang et al., 1998). Recent identification of homologous proteins in both yeast and human led to the designation of a new family of proteins called Shugoshin (SGO), conserved across all eukaryotes. The yeast SGO1 and SGO2 proteins appear to function solely in meiosis where they are required to maintain sister chromatid cohesion until anaphase II (Kitajima et al., 2005, Rabitsch et al., 2004, Katis et al., 2004, Indjeian et al., 2005, Marston et al., 2004, Kitajima et al., 2004). In vertebrates, this meiotic role appears to be mediated by SGO2, whilst SGO1 functions to protect the centromeric pool of

cohesin from premature chromosome dissociation (Salic et al., 2004, Tang et al., 2004, Kitajima et al., 2005).

Xenopus and human securins, like their yeast counterparts, are destroyed at the metaphase to anaphase transition in a APC dependent manner, and non-degradable forms of these proteins block the initiation of anaphase (Zou et al., 1999). The SECURIN destruction sequence is the same as that of the mitotic cyclins, and therefore APC mediated destruction of these molecules links mitotic exit with chromosome segregation. The human SECURIN is encoded by the pituitary-tumour transforming gene, *hPTTG*, which was independently isolated due to its overexpression in pituitary tumours (Pei and Melmed, 1997, Romero et al., 2001). hPTTG is overexpressed in a number of tumour types including those of the pituitary, breast and ovaries and over expression inhibits mitosis and causes p53 dependant and independent apoptosis (Yu et al., 2000, Heaney et al., 2000). In yeast, the loss of SECURIN results in the separation of sister chromatids with apparently normal kinetics (Alexandru et al., 1999). Additionally, in the absence of SECURIN, sister chromatids do not separate when cells are arrested in metaphase (Funabiki et al., 1996, Ciosk et al., 1998). This is opposite to what would intuitively be expected and suggests that SECURIN also plays a positive role in promoting sister chromatid separation. This has been shown to be the case in yeast where the nuclear localisation of SEPARASE is dependent on the presence of SECURIN. The molecular mechanism of this interaction remains to be elucidated, but recent evidence indicates that CDC28 may be involved. Pds1p is a substrate of CDC28 and phosphorylation of PDS1 by CDC28 increases the efficiency of binding to ESP1 and also the nuclear localisation of ESP1 (Agarwal and Cohen-Fix, 2002). The requirement for SECURIN in promoting the activity of SEPARASE was observed to be partially alleviated when SEPAEASE was fused to a strong nuclear localisation signal, supporting the contention that SECURIN also plays a positive role in SEPARASE activation (Jensen et al., 2001). Human cells lacking SECURIN, although viable grow at a slow rate and lose chromosomes at high frequency due to a defect in separating chromosomes at anaphase (Jallepalli et al., 2001). This suggests that SECURIN may not be essential for cellular viability in human cells. This contention is supported by the fact that SECURIN knockout mice appear to be completely normal, at least up to four weeks of age (Mei et al., 2001). A role for

SECURIN in the nuclear localisation of SEPARASE may not apply in the case of metazoans as progression into mitosis involves the breakdown of the nuclear envelope. However, SECURIN may play a role in stabilising or activating SEPARASE or targeting it to subnuclear structures (Jallepalli et al., 2001).

Until fairly recently it was thought that the inhibition of SEPARASE activity prior to the metaphase to anaphase transition was mediated solely by the binding of SECURIN. Given that the separation of sister chromatids and proteolysis of RAD21 are irreversible events this proposition did appear highly unlikely. Additional levels of regulation are likely to exist given the phenotypes observed in both yeast and human cells in the absence of SECURIN. Indeed, recent studies have revealed that SEPARASE is kept inactive during metaphase by two distinct and independent mechanisms. The first of these involves the inhibitory binding by SECURIN as already discussed above. The second of these mechanisms involves inhibitory phosphorylation of SEPARASE at one main serine residue. *In vitro* investigations implicate CDC2 and/or MAPK as the inhibitory kinase, although whether either of these kinases are required for the *in vivo* phosphorylation of SEAPARASE remains to be determined (Stemmann et al., 2001).

1.4.2.2.2 Studies of meiotic cohesion in mammalian systems

Studies of cohesin function in mammalian systems have indicated that descriptions of cohesin complexes as either meiotic or mitotic are not entirely accurate. Such studies have revealed roles for mitotic cohesin in meiosis and for meiotic cohesin in meiosis. This is exemplified in the phenotype of the *Rec8* mouse.

Similar to the meiotic dysfunction phenotypes of yeast cells lacking REC8, absence or mutation of REC8 in mice leads to complete meiotic failure (Bannister et al., 2004, Xu et al., 2005). Strikingly, in the absence of REC8, synapsis occurs between sister chromatids, not homologous chromosomes during prophase I of meiosis (Xu et al., 2005). In the wild-type situation, during synapsis of homologous chromosomes in meiosis I a protein complex binds homologous chromosomes and facilitates recombination between them. This complex, called the synaptonemal complex (SC),

dissociates or dissolves at the end of prophase I to facilitate the segregation of homologous chromosomes to opposite spindle poles, a process that also requires the resolution of sister chromatid cohesion along chromosome arms. In germ cells lacking REC8, SC formation was observed to occur between sister chromatids, not homologous chromosomes (Xu et al., 2005), indicating that meiotic cells require REC8 to differentiate between sister chromatids and homologous chromosomes. Whether sister chromatid cohesion is maintained in the meiotic cells of *Rec8* knockout mice was not examined, however RAD21 and SMC3 were found to be present along the entire length of the chromosomes, suggesting that RAD21-containing cohesin complexes may be mediating sister chromatid cohesion in the absence of REC8. Studies of RAD21 distribution in mammalian meiosis have indicated that RAD21-containing cohesin complexes co-exist with REC8 along meiotic chromosomes consistent with a role for the 'mitotic' cohesin complex in meiosis (Xu et al., 2004, Prieto et al., 2002, Parra et al., 2004). Although SMC3 and RAD21 are observed along chromosomes in the absence of REC8, it is unclear if they are functioning to mediate sister chromatid cohesion.

In addition to the meiotic phenotypes discussed, the absence of REC8 is reported to also cause somatic defects, indicating that REC8 may also function in mitosis. Specifically, pups lacking REC8 were born in sub-Mendelian ratios and exhibited in *utero* and post-natal growth retardation (Xu et al., 2005). These phenotypes suggest that in mice, REC8 is required for as yet unknown non-meiotic functions that are important for somatic growth and survival.

1.5 THIS STUDY

1.5.1 SISTER CHROMATID COHESION IN DROSOPHILA

Homologues of the mitotic cohesin proteins can be identified in *Drosophila*, and have been shown to form a complex in embryos (Vass et al., 2003). The *Drosophila* cohesin complex consists of SMC1, CAP/SMC3, DRAD21 and SA/SCC3. In addition, several other key components of cohesin regulation are conserved in *Drosophila*. These include the SCC2 cohesin loading factor, encoded by *nippedB,* the cohesion establishment factor ECO1/DECO (Williams et al., 2003) and the centromeric cohesion protector MEI-S332 (discussed in Section 1.4.2.2.1).

Dissociation of sister chromatid cohesion in *Drosophila* is largely controlled by three proteins, THREE-ROWS (THR), SEPARASE (SSE) and PIMPLES (PIM) (Leismann et al., 2000, Jager et al., 2001, Herzig et al., 2002). THR corresponds to the extensive N-terminal domain of non-dipteran SEPARASE proteins, and binds SSE to produce a functional protease (Jager et al., 2004, Herzig et al., 2002). PIM encodes the *Drosophila* SECURIN, and like securins of other species its degradation at anaphase onset is required for the separation of sister chromatids (Leismann and Lehner, 2003, Stratmann and Lehner, 1996).

1.5.2 THE ROLE OF *DRAD21*

Consistent with the RAD21 localisation data generated in *Xenopus* and human cell lines, *Drosophila* RAD21 (DRAD21) is observed to associate with chromosomes in interphase and is located between the sister chromatids following DNA replication (Vass et al., 2003, Warren et al., 2000b). As the chromosomes condense DRAD21 dissociates from chromosome arms and is relocated to the cytoplasm. A minor pool of DRAD21 is observed to remain attached to the condensed chromosomes in the region of the centromere and this cytoplasmic pool of DRAD21 is thought to facilitate cohesion until the metaphase to anaphase transition. At the metaphase to anaphase transition this minor centromeric pool of DRAD21 dissociates from the chromosomes and transiently associates with the centrosome (Warren et al., 2000b). In the absence of firm biochemical data it is tempting to speculate that the

centromere associated DRAD21 is cleaved by SSE at the metaphase to anaphase transition, and that this cleavage facilitates the separation of sister chromatids. Although the *Drosophila* separase homologue has been shown to be required for sister chromatid separation during mitosis (Jager et al., 2001, Herzig et al., 2002) at the commencement of this study it had not been shown to cleave DRAD21.

In the absence of DRAD21 mutants, insight into DRAD21 function had been gained through cell biological and biochemical analyses. DRAD21 forms a complex with the SMC1, SMC2 and SA (SCC3) cohesin molecules and depletion of DRAD21 in cultured cells destabilises the cohesin complex and causes mitotic defects such as failure of chromosomes to congress and premature sister chromatid separation (Vass et al., 2003). DRAD21 associates most strongly with the SA (SCC3) cohesin component, and these proteins are observed to co-localise throughout the cell cycle (Valdeolmillos et al., 2004). In cultured *Drosophila* cells, RNAi mediated DRAD21 depletion results in the destabilisation of the SA (SCC3) protein; however DRAD21 remains stable following SA depletion.

1.5.2.1 A role for DRAD21 in meiosis?

RAD21 and REC8 belong to a family of proteins with homologues identified in a number of eukaryotic species (Figure 1.10). Proteins in this family are characterised by blocks of evolutionary conservation within their N and C terminal regions, called the Rad21/Rec8 N and C terminal domains, and the RAD21 homologues of higher eukaryotes also have a conserved central region (Warren et al., 2000a). The conserved N and C terminal domains are necessary for the binding of the RAD21/REC8 proteins to the SMC proteins of the cohesin complex. The RAD21/REC8 family belongs to a protein super-family defined by their function as SMC protein partners, and thus their conserved N and C terminal domains. Proteins in this family are called kleisins, with those that form complexes with SMC1 and SMC3 (cohesins) and SMC2 and SMC4 (condensins) referred to as kleisin-α proteins. There are two identified kleisin-α proteins in *Drosophila*, DRAD21 and the distantly related synaptonemal component c(2)M (also known as mei-910)(Manheim and McKim, 2003).

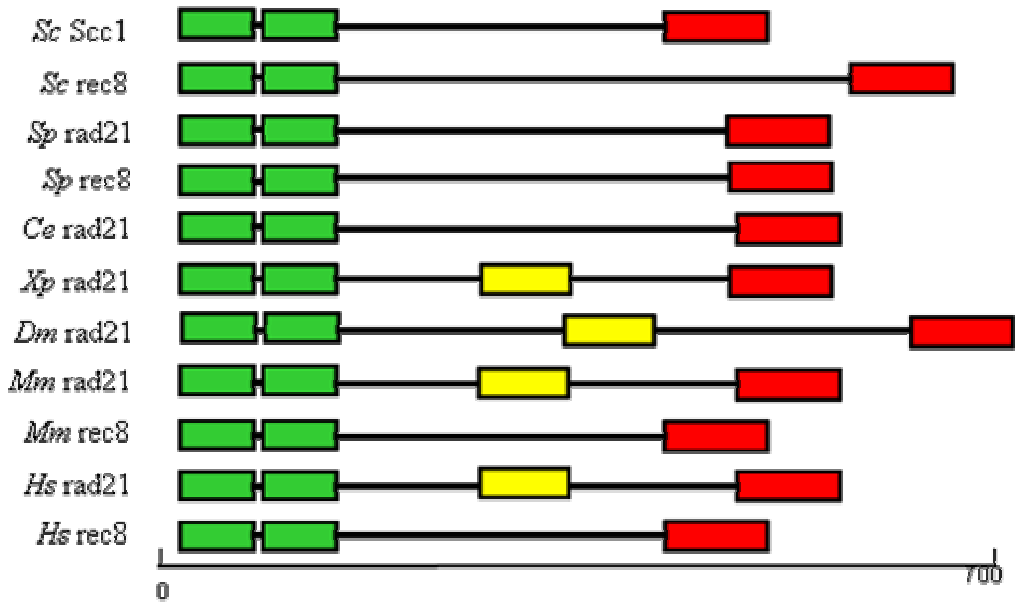

Figure 1. 10: *The RAD21/REC8 family of proteins*

Conserved protein regions at the N- (green) and C- (red) termini are represented, and are present in all eukaryotes. In yeast these regions have been shown to be required for Cohesin complex formation. The conserved region in the middle is present only in RAD21 orthologues of higher eukaryotes and is represented as the yellow box (Warren et al., 2000a).

c(2)M mutants have reduced meiotic recombination frequency and have been shown to have increased levels of chromosome non-disjunction in females at both meiosis I (homologous chromosomes) and meiosis II (sister chromatids) indicating a role in meiotic sister chromatid cohesion. c(2)M is capable of binding SMC3, however, it is unlikely to be performing as a member of the meiotic cohesin complex given that mutations appear to only affect female recombination and segregation, and the protein cannot be detected on chromosomes by meiosis I (Heidmann et al., 2004). If c(2)M was behaving as a Rec8-like cohesin we would predict that chromosomes would segregate prematurely and randomly in both male and female meiosis as is the case for *meiS332* mutants (Kerrebrock et al., 1992), and not remain together as observed. To date there is no evidence to suggest that c(2)M does function as a meiotic cohesin. This role could be assumed by *Drosophila* RAD21, as there are no other kleisin-α-like proteins encoded in the *Drosophila* genome.

1.5.3 *DROSOPHILA* AS A MODEL SYSTEM TO STUDY SISTER-CHROMATID COHESION

The mechanisms of sister chromatid cohesion are largely conserved from yeast to human, however there are striking differences in how this process is regulated. Higher eukaryotes appear to have evolved additional levels of regulation, presumably in order to deal with increases in genome size.

Defects in sister chromatid cohesion can lead to genetic instability and aneuploidy, which is a hallmark of many cancers and in meiotic cells can cause trisomies leading to birth defects. Whilst analyses in yeast led to the identification and characterisation of the cohesin complex, the differences in cohesin regulation between yeast and metazoan species suggests that the technical disadvantages of performing genetic analyses in *Drosophila* compared to yeast are offset by the multicellular nature of the organism and genome similarities to humans. This is exemplified by an analysis of known mutagen sensitive loci in *Drosophila* (discussed in Section 1.2.2.2) whereby greater 27% of loci that have been identified at the molecular level have orthologous proteins in mammals but not in yeast (Laurencon et al., 2004). Cohesin dynamics appear to be conserved among multicellular eukaryotes, making *Drosophila* the ideal model for genetic investigations of sister chromatid cohesion.

1.5.4 SCOPE OF THESIS

Traditional genetic approaches involve the analysis of mutant phenotypes to gain insight into gene function. At present there are no known *Drosophila* RAD21 mutants so alternative approaches have been used to elucidate the role(s) of this gene. In this study a reverse-genetic approach was employed to investigate the role of *Drad21* in chromosome segregation in *Drosophila*. Given the additional levels of cohesion regulation in metazoan species it was hypothesised that the generation of a metazoan model of chromosome missegregation would provide insight into how metazoans regulate the different pools of cohesin and would allow the identification of metazoan specific regulators of cohesion function. The following chapters examine the function of *Drosophila* RAD21 in cohesin regulation as well as describe a genome wide modifier screen for the identification of metazoan specific cohesin regulators and the identification of 13 interacting loci at the molecular level.

CHAPTER 2: MATERIALS AND METHODS

2.1 GENERATION OF PLASMIDS

Established molecular techniques not described here were performed as described in Sambrook and Russell (2001).

2.1.1 RESTRICTION ENDONUCLEASE DIGESTION OF DNA

All restriction digests were performed using manufacturer-recommended buffers at 1x concentration. 3-5 units of enzyme were added per microgram of DNA and incubated at 37°C for 1-2 hours.

2.1.2 AGAROSE GEL ELECTROPHORESIS

DNA fragments were separated by TAE (40mM Tris-acetate, 20mM sodium acetate, 1mM EDTA, pH 8.2) buffered agarose gel electrophoresis (0.8-1.5% agarose in TAE, supplemented with 50µg/ml ethidium bromide) at 90-120 volts. DNA samples were loaded with appropriate amounts of loading dye/buffer (Promega).

2.1.3 PHENOL/CHLOROFORM EXTRACTION OF DNA

Sterile TE (10mM Tris-Cl, pH 7.5, ImM EDTA) was added to the sample to give a volume of 100µl. 50 µl each of phenol and chloroform were added. The sample was then vortexed for approximately 1 minute and spun for 5 minutes at 13000 rpm in a microcentrifuge. The top phase was removed and added to a fresh microcentrifuge tube containing 100µl isoamyl-chloroform (25 parts phenol, 24 parts chloroform and 1 part isoamyl alcohol), vortexed for approx 1 minute and spun as previously. The top phase was removed and placed into a new sterile microcentrifuge tube and was DNA recovered by ethanol precipitation.

2.1.4 ETHANOL PRECIPITATION OF DNA

1/10th the volume of 3M NaOAC (pH 5.2) and 2x volumes of 100% ethanol were added to the sample and mixed. The tube was then incubated at –20°C for at least 20 minutes. The sample was then spun at 4°C for 20 minutes at 14000 rpm. The resultant pellet was then rinsed in 70% ethanol, air dried and resuspended in a suitable volume of TE.

2.1.5 DEPHOSPHORYLATION OF VECTOR DNA

The pUAST vector (Figure 2.1) used in this study is very large (>9kb) and throughout the course of this study it was consistently difficult to clone into. It was found that the efficiency of cloning increased when the linearised pUAST vector DNA was treated with shrimp alkaline phosphatase (SAP; Promega). This was observed to be the case in even in situations such as vector digestion with two enzymes that do not produce compatible ends and therefore where vector re-circularisation should not be possible. Therefore all vector preparations used in this study were treated with SAP prior to ligation. Linearised vector DNA was dephosphorylated by the addition of 1-2 units of SAP and incubating for at least 20 minutes at 37°C. SAP was then either heat-inactivated, or the DNA immediately purified by phenol/chloroform extraction and ethanol precipitation.

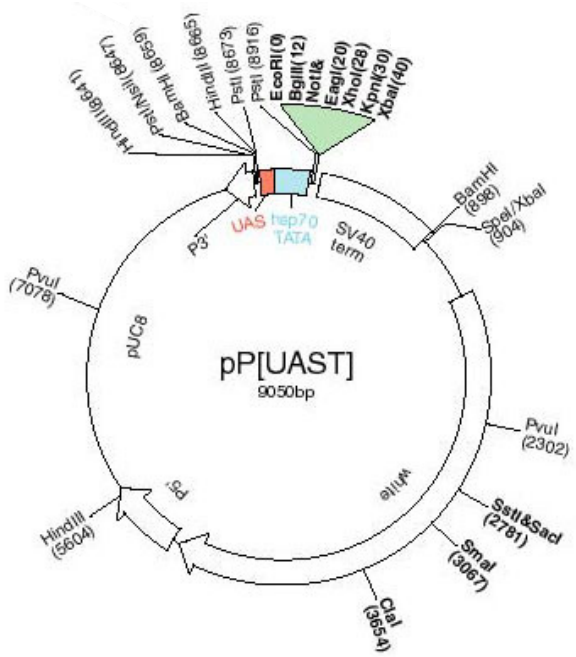

Figure 2. 1: *pUAST transformation vector*

pUAST is constructed from the pCaSpeR3 P-element vector and contains the P element ends (P3' and P5') and the white gene selectable marker. In addition, the pUAST vector contains five tandemly arrayed binding sites for Gal4 (orange), the *hsp70* TATA box and transcriptional start (blue) and the SV40 polyadenylation site. The polylinker (green) contains numerous unique restriction sites for cloning. For additional details see Brand and Perrimon (1993).

2.1.6 LIGATION

DNA fragments to be ligated were placed in a reaction mix with a total volume of 10-15 µl and incorporating 1-2 units of T4 DNA ligase (Promega) and 1x ligase buffer. Ligation mixes were incubated overnight at approximately 10°C.

2.1.7 TRANSFORMATION OF BACTERIA

100 µl aliquots of chemically competent *E. coli DH12S* or *DH5α* cells (Invitrogen; genotypes listed in Table 2.1) were thawed on ice. 5µl of the ligation mix to be transformed was added to the competent cells and incubated in ice for 20-30 minutes, heat shocked at 37°C for 2 minutes and returned to ice for a further 15 minutes. 800µl of LB (Luria-Bertani medium (Sambrook and Russell, 2001)) was added and the suspension incubated at 37°C with shaking for 40-60 minutes. The cells were pelleted for 1 minute at 5000 – 6000 rpm and the supernatant removed. Cells were resuspended in 100µl of LB and plated on LB-Agar plates supplemented with Ampicillin (75µg/ml). 20% IPTG (7µl) and 2% X-Gal (40µl) were spread on plates and allowed to dry before plating out the cell suspension when blue/white selection was possible. All plates were incubated at 37°C overnight.

Table 2. 1: *E.coli* strains and genotypes

***E. coli* strain**	**Genotype**	**Source**
DH5α	F^- φ80d*lac*ZΔM15 Δ(*lac*ZYA-*arg*F) U169 *rec*A1 *end*A1 *hsd*R17(r_k^-, m_k^+) *pho*A *sup*E44 λ^- *thi*-1 *gyr*A96 *rel*A1	Invitrogen
DH12S	80d*lac*ZΔM15 *mcr*A Δ(*mrr-hsd*RMS-*mcr*BC) *ara*D139 Δ(*ara*, *leu*)7697 Δ*lac*X74 *gal*U *gal*K *rps*L (Str^R) *nup*G *rec*A1/F' *pro*AB^+ *lac*I^qZΔM15	Invitrogen

2.1.8 PURIFICATION OF PLASMID DNA

2.1.8.1 Small scale preparation- Mini-preps

Individual 1.5 ml cultures of LB supplemented with Ampicillin (75µg/ml) were incubated overnight at 37°C with shaking. Cells were harvested by centrifugation at 5000-6000 rpm in a microcentrifuge for 2 min. The supernatant was aspirated off and cells were resuspended in 200 µl of Wizard solution I (cell resuspension solution: 50mM Tris-HCl, 10mM EDTA, 100 µg/ml RNaseA, pH 7.5) by vortexing. Cells were lysed by the addition of 200µl of Wizard solution II (Cell lysis solution: 1% SDS, 0.2M NaOH) and gentle mixing. Addition of 200µl of Wizard solution III (Netutralisation solution: 1.32M Potassium Acetate, pH 4.8) and centrifugation at 14000rpm for 5 minutes pelleted the cellular debris and chromosomal DNA. The supernatant, containing the plasmid DNA, was mixed with 1ml of Wizard solution IV (1.5g diatomaceous earth (Celite, Sigma) in 100ml 7M Guanidine HCL pH 5.5) by pippetting up and down and applied to a 3ml syringe barrel attached to a mini-column, and vacuum manifold (Promega). Application of the vacuum and rinsing with Wizard solution V (wash solution: 80mM Potassium Acetate, 8.3mM Tris-HCl (pH 7.5), 40µM EDTA, 50% ethanol) provided that the celite powder enter and remain in the mini-column. Minicolumns were removed from the manifold and spun for 1 minute at 14000 rpm in a microcentrifuge to remove excess Wizard solution V. Minicolumns were placed in fresh microcentrifuge tubes and 60 µl of TE applied to their centre. After 1-5 minutes DNA was eluted by centrifugation at 14000 rpm for 1 minute.

2.1.8.2 Large scale preparation- Midi and Maxi preps

Large scale preparation of high quality plasmid DNA was performed using QIAGEN Midi or Maxi kits according to manufacturer's specifications.

2.1.9 IN VITRO SITE DIRECTED MUTAGENESIS AND PLASMID GENERATION

In vitro site-directed mutagenesis was used to change the critical arginine residues of the putative separase cleavage sites in DRAD21 to alanines and to introduce diagnostic restriction sites using the *Drad21* cDNA clone pLD02527 (Genbank Accession number AA202271) as a template. Table 2.2 lists the oligonucleotide primers used in this study. Primers for site-directed mutagenesis were designed

according to the instruction manual of the Stratagene Quick-Change Site-Directed mutagenesis kit (Stratagene, La Jolla, CA), with the exception that the oligonucleotide primers were not HPLC purified. The reaction was carried out according the instructions in a 50µl reaction and cycled in an Eppendorf Mastercycler Personal or Bio-Rad iCycler using the following parameters: 95ºC 1 minute, pause (add 1 µl Pfu Turbo), 95ºC 30 seconds, followed by 16 cycles of 95ºC for 30 seconds, 60ºC for 1 minute and 68ºC for 11 minutes (2 minutes per kb). Following cycling, 1µl of DpnI (10U/µl) was added to the reaction mix and incubated at 37°C for 1 hour. Anywhere from 5-20µl of amplification product was used to transform *DH12S E. coli* cells. Plasmid DNA was isolated from the resultant colonies and tested for the presence of the introduced restriction site. Sequencing across the region of mutation confirmed the introduction of the desired sequence alterations (Table 2.2, primers DradN and DradP for R175A and RA474AG alterations respectively).

Table 2. 2: Oligonucleotides used in this study and their sequences

Number	Primer name	Sequence 5'-3'	Introduced restriction site	Introduced mutation
1	QC175R>A FOR	GCAGAAACGCCTGAAATTATAGCATGCTCTATACCTTCA	SphI	R175A
2	QC175R>A REV	TGAAGGTATAGAGCATGCTATAATTTCAGGCGTTTCTGC		
3	QC474RA>AGFOR	GGAAGCTCCGGAAGTCCTGGCCGGCAATCATAAATCTCTAG	NaeI	RA474AG
4	QC474RA>AGREV	CTAGAGATTTATGATTGCCGGCCAGGACTTCCGGAGCTTCC		
5	DradN	CCAAAAGAATCTCCAAACCCATC		
6	DradP	TACCAAAGAGAACGAGAACGCA		
7	M13_R	CAGGAAACAGCTATGACCAT		
8	DradA	CCTTGAAGCAGAAACGCCTGA		
9	DradK	GCCTGCAACCTCGCTCGTT		
10	DradL	GCTCTTTTGATACAATCTCCACAGA		
11	DradC	AAGTTTGGAAGCTCCGGAAGT		
12	DradI	CTGTACTAAGTGACAATGGCGTTTC		
13	DradE	CGCCAAGGACAGCTTGGAAC		
14	DradORF	GACTAGTTGAACATGTTCTATGAGCACA		
15	DradJ	TCGTCTTCAAAAAGGGCTGGT		
16	DradM	GCCTGGTTCTCGATTGGATG		

To create the double mutant plasmid (containing both arginine to alanine site-directed alterations), pLD02527*Drad21*^{RA474AG} was digested with both KpnI and BamHI and the pLD02527*Drad21*^{R175A} plasmid was digested with EcoRI and BamHI resultant DNA fragments separated by agarose gel electrophoresis. The 587bp BamHI-KpnI fragment from pLD02527*Drad21*^{RA474AG} and the 1613bp EcoRI-BamHI fragment from the pLD02527*Drad21*^{R175A} plasmid containing the site-directed changes were gel purified using the QIAquick purification kit (QIAGEN) to manufacturer's specifications. These fragments were subsequently ligated into EcoRI-KpnI linearised pBluescriptKS+ (Stratagene) that had been phenol/chloroform extracted and ethanol precipitated, in a three way ligation. Following complete sequencing of all of the mutagenised plasmid inserts using primers numbered 5-13 inclusive (Table 2.2), all three were subcloned into pUAST (Figure 2.1) using KpnI and EcoRI restriction endonucleases. Generation of the desired constructs was confirmed by restriction endonuclease digestion.

2.1.10 DNA SEQUENCING

Sequencing of *in vitro* mutagenised *Drad21* cDNAs was performed using the BigDye® Terminator cycle sequencing kit (Applied Biosystems) or DYEnamic™ ET terminator cycle sequencing kit (Amersham) as per manufacturers recommendations. Sequencing primers are listed in Table 2.2. Using BigDye Terminators each reaction contained 8.0µl or 4.0µl of 'Terminator ready mix', 200-500ng of plasmid template DNA, 3-5 ρmoles of sequencing primer and dH_2O to give a total reaction volume of 20µl. Cycling conditions were 96ºC for 30 seconds, followed by 25 cycles of 96ºC for 30 seconds, 55ºC for 15 seconds and 60ºC for four minutes. Using ET terminators each reaction contained 8.0µl of ET mix, 150-300ng of plasmid DNA, 5 ρmoles of sequencing primer and dH_2O to give a total reaction volume of 20µl. Cycling consisted of 35 cycles of 95ºC for 20 seconds, 50ºC for 15 seconds and 60ºC for 2 minutes. Reactions were analysed using an Amersham Megabse 1000 DNA analysis system.

2.2 SDS-PAGE AND WESTERN BLOTTING

2.2.1 PROTEIN EXTRACTION

Actively wondering third instar larvae were manually dissected in PBS (7.5 mM Na_2PO_4, 2.5 mM NaH_2PO_4, 145mM NaCl.) or EBR (129mM NaCl, 4.7 mM KCl, 1.9mM $CaCl_2$, 10mM HEPES pH 6.9). Thirty cleanly dissected eye-antennal imaginal discs were placed in 10µl of cold Lysis Buffer (10mM EDTA, 10mM DTT in 1 x PBS) supplemented with protease inhibitors (1 X PIC: 50µg/ml Phenylmethylsulphonylfluoride (PMSF), and 1µg/ml of antipain, leupeptin and pepstatin A) in the cap of a screw cap microcentrifuge tube. 10µl of 3xSample buffer (6% SDS, 150mM Tris pH 6.8, 30% Glycerol, 0.3% bromophenol blue, 6mM EDTA) was then added and the tube screwed into place followed by a quick spin to bring the contents to the bottom. Samples were boiled for 10 minutes, touch spun and then either loaded directly onto a polyacrylamide gel, or stored for up to one week at -20ºC for later electrophoresis.

2.2.2 PROTEIN SEPARATION BY ELECTROPHORESIS

Protein samples were boiled for 3-5 minutes before loading onto a 4-15% TrisHCl ready gel (BioRad) immersed in 1 x Running buffer (25mM Tris, 192mM Glycine, 0.1% SDS). Where possible a spare lane was kept between protein samples to limit potential overflow of proteins into adjacent samples. Samples and pre-stained size standards (SeeBlue Plus2, Invitrogen) were separated at 200V for 45-60 minutes at room temperature with an ice block in the apparatus using a MiniProtean3 electrophoresis cell (Bio-Rad). Separated proteins were transferred to Trans-Blot nitrocellulose membrane (BioRad) by wet electroblotting at 100V for 1 hour in Towbin buffer (25mM Tris, 192mM Glycine, 20% methanol, 0.5% SDS) using the mini TransBlot cell transfer tank system (BioRad).

2.2.3 Detection of proteins and Western Blotting

Nitrocellulose membranes were stained with 0.2% PonceauS in 3% TCA for 5-10 minutes and rinsed under running water to visualise transferred proteins. Following a 5-10 minute wash with gentle agitation in PBT (1 X PBS plus 0.1% Tween 20), membranes were blocked for at least 2 hours in PBT + 5% powdered skim milk. Blocked membranes were washed for at least three times in PBT at room temperature for a minimum of 10 minutes each; often washes were performed over several hours. Primary antibody, diluted in PBT, was incubated with the membranes for 1 hour at room temperature and the membranes were then washed again in PBT as described above. Primary antibodies used were rabbit anti-Drad21 (Warren et al., 2000b) (1:1000 dilution) and mouse anti-alpha tubulin (Sigma) (1:500 dilution). Horseradish-peroxidase conjugated secondary antibody diluted in PBT (1:10000) was added to the membrane and incubated for 1 hour at room temperature. Membranes were washed with PBT as described above. Antibody bound proteins were detected using enhanced chemiluminescence solutions (Amersham) and X-ray films (Kodak BioMax Light) were developed using a Kodak X-OMAT 1000 processor.

2.3 Staining of eye imaginal discs

2.3.1 Antibody staining of eye imaginal discs

Eye-antennal imaginal discs were roughly dissected from actively wondering third instar larvae in 1 x PBS or EBR, and fixed in 3.7% paraformaldehyde (in PBS) for at least 20 minutes. Fixed eye-antennal discs were dissected of extraneous material in 1 x PBS and then rinsed in 1 x PBT. Discs were then washed in antibody wash solution (1 X PBS, 0.2% BSA, 0.1% triton X-100) for 30 minutes and blocked in antibody block solution (1% BSA, 0.3% triton X-100, 10% donkey or goat serum, 1mg/ml RNase A, 1 X PBS) for at least 1 hour. Discs were incubated with primary antibody diluted in block solution overnight at 4ºC, then twice washed quickly in antibody wash solution, followed by four washes of at least 15 minutes each. Following incubation with secondary antibody diluted in block solution for 2 hours at room temperature, discs were washed twice quickly in wash solution followed by four washes of at least 15 minutes each. Discs were mounted directly onto glass microscope slides in Gel/Mount mounting medium (Biomedia) or in 80% Glycerol

0.5M EDTA (in PBS) and samples were sealed under glass coverslips using domestic nail varnish.

Primary antibodies used were rat anti-Elav (1:1000; Developmental Studies Hybridoma bank), or rabbit anti-phospho-histone3 (1:2500; Upstate Biotechnology, Lake Placid. NY). Secondary antibodies (Alexa Fluor 488 goat anti-rabbit and goat ant-rat: Molecular Probes) were used at 1:400 dilution.

2.3.2 ACRIDINE ORANGE STAINING OF EYE IMAGINAL DISCS

Eye antennal imaginal discs from actively wondering third instar larvae were initially roughly dissected in PBS. Eye discs with attached mouth-parts and other extraneous material were transferred to a drop of stain (Sigma; 1µg/ml) and eye-antennal imaginal discs were cleanly dissected in this drop of acridine orange. Dissections were performed in batches of 6-10 larvae and dissected tissues were soaked in acridine orange for a total of 5-10 minutes. Cleanly dissected eye-antennal imaginal discs were transferred to a drop of PBS on a clean microscope slide and de-stained in this drop for at least 5 minutes. Eye-antennal imaginal discs were carefully flattened on the microscope slide and mounted directly in this drop of PBS by slowly lowering a coverslip over them. Preparations were immediately viewed using the argon ion laser of the BIO-RAD Radiance 2000 laser scanning confocal microscope and images captured using BioRad LaserSharp2000 software.

2.4 SCANNING ELECTRON MICROSCOPY

2.4.1 PREPARATION OF SAMPLES

CO_2 anesthetised flies were placed in 25% acetone (in dH_2O) and incubated at room temperature for 1-2 hours. Dehydration of flies was achieved by incubation in an acetone series of 50% and then 75% acetone for 2 hours to overnight, and finally 100% acetone at least overnight. All incubations were performed with gentle agitation on a nutator platform. Dehydrated flies were stored in 100% acetone. Flies were removed from 100% acetone and placed on kim-wipe tissues to dry. Adhesive circles were placed on the sample stubs and the flies arranged on these with the aid of a stereo microscope (Lecia), taking care not to damage the eyes or head of the samples. Samples were then sputter-coated by in gold or platinum by Dr. Kevin

Blake using a JEOL sputter coating machine, with each sample being coated five or six times. Coated samples were viewed using a Jeol (JEOL JSM-5410LV) scanning electron microscope and images taken using Semaphore digital imaging system.

2.5 TRANSGENIC METHODS: GERM-LINE TRANSFORMATION OF *DROSOPHILA MELANOGASTER*

2.5.1 MICROINJECTION OF *DROSOPHILA* EMBRYOS

High quality DNA obtained from midi or maxi preparations (QIAGEN) was used in all injection mixes. Injection mixes were made by co-Ethanol precipitating (section 2.1.1.4) the transforming plasmid and pπ25.7wc (Δ2-3 transposase) and resuspending them in 1x injection buffer (5mM KCl, 0.1mM PO_4 pH 7.8) to give a final concentrations of 1µg/µl and 2µg/µl respectively. Injection mixes were centrifuged at 14000rpm for 5 minutes to remove any particulate matter immediately before use. *Drosophila* embryos were injected essentially as previously described (Spradling, 1986). Micro-injection needles were created by pulling 1mm thin walled borosilicate glass capillaries (Clark Capillaries) to a fine point using a Narishige PC-10 needle puller and were back-filled with several microlitres of injection mix. Capillaries were mounted on a micromanipulator and the volume of DNA injected per embryo controlled using an Eppendorf Femptojet microinjector.

w^{1118} embryos were collected from a small cage of 1-7 day old w^{1118} adults at 30 minute intervals on grape-juice agar plates supplemented with yeast paste. Embryos were manually dechorionated under an Olympus SZ60 dissecting microscope and aligned along a strip of non-toxic double-sided tape (3M) on a glass slide such that their posterior ends would face the microinjection needle. The embryos were air dehydrated for approximately 10 minutes and then covered liberally in Halocarbon oil (Sigma). The slide was placed on the Olympus BX51 light microscope stage, and the needle was positioned by micromanipulation. Embryos were injected by moving the stage of the microscope so that the needle pierced the embryo and a small amount of injection mix was deposited in the posterior cytoplasm.

Slides of injected embryos were placed in large Petri dishes with moist tissue paper and incubated for 24 hours at room temperature (approximately 25°C) in an oxygen

rich chamber. Surviving larvae were picked from the slides using small wedges of paper. Larvae were placed in a vial of standard cornmeal treacle medium supplemented with Instant *Drosophila* media (Sigma) to a density of 25-35 larvae per vial.

2.5.2 IDENTIFICATION OF TRANSGENIC FLIES

Surviving G_0 adults were crossed to w^{1118} flies and germline transformants identified in the G_1 progeny by virtue of their eye pigmentation. The constructs used to transform *Drosophila* embryos contain the mini *white* gene, which generates eye pigment when introduced into a w^- background, as a screenable marker. Independent G_1 transformants were then crossed to the double balancer stock *w, IF/CyO;MKRS/TM6B* and resultant doubly balanced flies were intercrossed to establish balanced stocks. Standard segregation analysis was performed by back crossing doubly balanced G_2 transgenics to w^{1118} flies to determine which chromosome the transgene inserted into in each independent line.

2.6 *DROSOPHILA MELANOGASTER* CULTURING

2.6.1 STOCKS

The w^{1118} white-eye mutant fly line was used as the wild-type strain in this study. The Deficiency Kit, comprising a set of overlapping deletions of the *Drosophila* genome, was obtained from the Bloomington Stock Centre.

Drosophila deficiency strains carry cytologically defined chromosomal deletions that each remove numerous genes at a time. The US *Drosophila* stock centre at Bloomington, Indiana houses a collection of overlapping deletion strains that are commonly referred to as the Deficiency Kit (DK). The Deficiency Kit release used in this study was that of February 6th 2004 (Appendix 1). This release was estimated to cover 90% of the *Drosophila* genome (Figure 2.2).

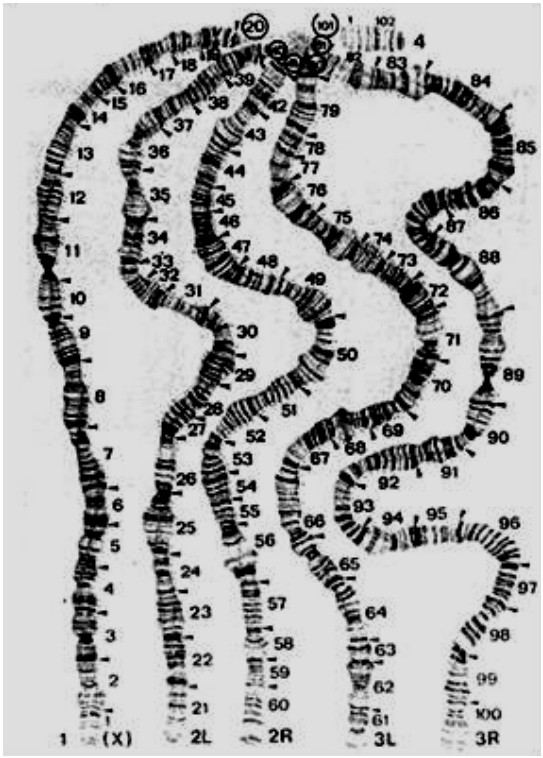

Figure 2. 2: *The* Drosophila *polytene chromosomes*

The four chromosomes of the *Drosophila* genome are divided into 102 sections called 'divisions'. The *Drosophila* salivary gland polytene chromosomes result from endoreplication, repeated rounds of DNA replication without subsequent cell division, and contain approximately 10 000 copies of the genome (10 doublings). The pattern of heterochromatin and euchromatin within these chromosomes can be visualised under the light microscope as a series of 5054 genetically stable light and dark bands (Drysdale et al., 2005), called polytene bands. The light and dark polytene bands are evident, chromosomal divisions are numbered and each of the chromosome arms is labeled at the base. Heterochromatic regions of polytene chromosomes remain grouped together in what is called the 'chromocentre'. In situ hybridisation on polytene chromosomes localises *Drad21* to the chromocentre (W. Warren, personal communication). Note the small size of chromosome 4.

Additional stocks used in this study, such as those used in the pilot screen (Section 4.2.1) and for identification of interacting loci (Chapter 5) are listed in Appendix 2.

2.6.2 MEDIUM AND MAINTENANCE

Drosophila melanogaster stocks were maintained on standard cornmeal treacle medium at 18ºC, 25ºC or 29ºC. Genetic crosses were performed at 18ºC, 25ºC or 29ºC as indicated in the text. All Deficiency Kit stocks were maintained solely at 25 º C and the genetic screen utilising these stocks were maintained at 25ºC.

2.6.3 *DROSOPHILA MELANOGASTER* SCORING/PHENOTYPIC ANALYSIS

Drosophila melanogaster crosses and stocks were analysed by anesthetising the flies with CO_2 and viewing with an Olympus SZ60 stereo microscope with an Olympus LG-PS2 fibre-optic light source. Low resolution images were captured using Olympus digital camera (CCD DP50) mounted on the microscope and ViewfinderLite and StudioLite image software (Olympus).

2.6.4 GENERATING RECOMBINANT STOCKS

Female meiotic recombination was used to generate recombinant stocks. P{UAS*Drad21*^{R175A}}16A and P{UAS*Drad21*^{DM}}24A transgenic lines bearing second-chromosome transgene insertions were separately recombined with the second-chromosome P{GAL4-ninaE.GMR}12. Flies bearing recombinant GMR,P{UAS*Drad21*^{DM}} second chromosomes were identified by their small and rough eyes and were balanced on CyO to produce the GMR,P{UAS*Drad21*^{DM}}/CyO line, hereafter referred to as GMR>DRAD21^{DM}. Flies bearing recombinant GMR,P{UAS*Drad21*^{R175A}}chromosomes were not able to be determined visually due to the absence of a discernable phenotype, and recombinant chromosomes were confirmed by diagnostic PCR amplifications using primers DradORF and DradJ (Table 2.2 and data not shown, PCR conditions described below in section 2.6.4.1). Confirmed recombinant chromosomes were balanced on CyO to produce the GMR,P{UAS*Drad21*^{R175A}}/CyO line, hereafter referred to as GMR>DRAD21^{R175A}. The P{UAS*Drad21*^{RA474AG}}P11a transgenic line on the X chromosome was used to create the P{UAS*Drad21*^{RA474AG}}; GMRGal4/CyO line (GMR>DRAD21^{RA474AG}) using standard genetic techniques.

2.6.4.1 PCR diagnostic test for confirmation of altered DRAD21cDNAs

Where required DNA from Individual flies was isolated (Gloor et al., 1993). In brief, flies were frozen for approximately 2 hours before being squashed on ice with a yellow pipette tip containing 50µl of freshly made SB (10mM Tris-HCl pH 8.2, 1mM EDTA, 25mM NaCl and 200µg/ml proteinase K) for 5-10 seconds. Remaining SB was then expelled into the microcentrifuge tube and the tube incubated at room temperature for 30 minutes, followed by incubation at 95°C for 1-2 minutes to inactivate the proteinase K. 1µl of this preparation was then used as the template in PCR reactions.

Individual flies of the genotype to be tested were prepared for PCR as described above. PCR reactions were performed using 1µl of single fly preparation as a template and primer pairs selected to span at least one intron and therefore only amplify *Drad21* cDNA and not endogenous *Drad21*. To identify *Drad21* cDNA spanning the regions of the R175A and RA474AG alterations respectively primer pairs DradORF and DradJ, and DradL and DradM (Table 2.2) were used at a concentration of 0.625µM in 20µl reactions containing 1mM $MgCl_2$ and 1U Taq polymerase (Fisher Biotech). Reactions were cycled for 2 minutes at 94ºC followed by 30 cycles of 94ºC for 20 seconds, 50ºfor 15 seconds and 72ºC for 1 minute, followed by a final extension of 10 minutes at 72ºC. The site-specific alteration introduces a diagnostic restriction site (Table 2.2) and the PCR products were digested with the appropriate restriction enzymes to diagnose the sequence alterations. Digested and undigested PCR products were resolved side-by-side on 1.5% agarose gels for direct comparison.

2.6.5 SCREENING FOR GENETIC INTERACTORS

Flies were raised on standard media at 25ºC unless indicated otherwise. GMR>DRAD21^{DM}/CyO virgin females were crossed to flies carrying a specific autosomal deletion or mutation. In the case of X-chromosome aberrations, GMR>DRAD21^{DM} males were crossed to virgin females carrying the mutated X chromosome. Adult flies were removed from the vial once the cross was established (usually 5-7 days). Flies carrying both the aberration being tested and GMR>DRAD21^{DM} (affected siblings) were compared to their siblings expressing

GMR>DRAD21^{DM} (control siblings) alone. An interaction was deemed significant if all or the majority of affected siblings exhibited a discernable eye specific phenotypic alteration. Stocks identified as interactors were crossed to the GMRhid-SM1/+ fly line (Kurada and White, 1998) to assess their ability to modify apoptosis. Any stocks capable of modulating the GMRhid phenotype and the GMR>DRAD21^{DM} in the same way (i.e. suppress both) were excluded from further analysis.

2.6.6 EMBRYO HATCHING ASSAY

Embryos of the desired genotype were collected from a small cage of 1-7 day old adults at 2 hour intervals on grape-juice agar plates supplemented with yeast paste. 100 embryos were aligned in a 10 x 10 grid formation on grape-juice agar plate supplemented with yeast paste. Hatching rate was assessed after 24 hours and 48 hours by individually assessing each embryo under an Olympus SZ60 stereo microscope. Embryos were scored as having hatched by virtue of empty chorion shell remaining on the grape-juice agar plate.

CHAPTER 3: GENERATION AND ANALYSIS OF A DOMINANT *DRAD21* ALLELE

3.1 INTRODUCTION

In the absence of a preexisting *Drad21* mutant, reverse genetic approaches such as RNA interference had been used to gain insight into *Drad21* function (Vass et al., 2003). However, as these prior studies were transient experiments performed in cultured *Drosophila* cells, or RNA microinjected embryos they had not taken full advantage of the wealth of genetic tools available to *Drosophila* geneticists. To perform a genetic analysis of DRAD21 function *in vivo* an alternative approach, creating a dominant *Drad21* allele, was pursued. As there are no known *Drad21* mutants any alleles generated would be expressed in the presence of endogenous, wild-type, DRAD21. Although expression of a recessive allele would be expected to be masked by endogenous DRAD21; the expression of a dominant allele should produce a demonstrable phenotype despite the presence of endogenous wild-type protein.

This chapter describes the rationale and approach used to generate and characterise a dominant *Drad21* allele. The separase cleavage sites of human and yeast RAD21 homologues have been previously identified (Tomonaga et al., 2000, Uhlmann et al., 1999, Hauf et al., 2001), and overexpression of non-cleavable human RAD21 results in the formation of anaphase bridges and a marked increase in aneuploidy. It was, therefore, predicted that a *Drad21* cDNA encoding a SEPARASE cleavage-resistant isoform of DRAD21 would act dominantly as cohesin complexes containing cleavage resistant DRAD21 isoforms would continue to hold the sister chromatids together in the vicinity of the centromere, despite the activation of SEPARASE. This chapter firstly describes the identification and targeting of the DRAD21 separase cleavage sites, and secondly, the characterisation of the dominant *Drad21*allele generated.

3.2 RESULTS

3.2.1 IDENTIFICATION OF PUTATIVE SEPARASE CLEAVAGE SITES IN DRAD21

In order for DRAD21 to be the functional equivalent of other previously studied RAD21 proteins it too must be cleaved by SEPARASE at the metaphase to anaphase transition. The identification of separase cleavage sites in human and yeast RAD21/REC8 proteins has lead to the identification of a minimal separase cleavage recognition sequence (Hauf et al., 2001) (Figure 3.1A and B). Careful examination of the DRAD21 amino acid sequence was undertaken to identify any amino acid sequence(s) that fit the consensus separase cleavage site (Figure 3.1C). There were four potential cleavage sequences in the DRAD21 protein identified in this way (Figure 3.2A).

Sequence alignment with RAD21orthologues from human and mouse (NCBI Homologene number 38161) indicates that SEPARASE cleavage of DRAD21 is most likely to occur following the arginine residue at amino acid position 175 (Figure 3.2 B). The more C-terminal separase cleavage site identified in Human RAD21 falls between two potential consensus sites in the *Drosophila* sequence (Figure 3.2 B, underlined); the failure of cleavage sites to align in this region is not surprising given that the C-terminal region of RAD21/REC8 family members is not as highly conserved as the N-terminal region (Warren et al., 2000a). To date, all but one confirmed α-kleisin separase cleavage sites have an glutamic acid (E) residue at amino acid position -3 in relation to the critical arginine residue (Figure 3.1A). SEPARASE cleavage of DRAD21 following the arginine at amino acid position 510 was deemed less likely, because the residue at amino acid position -3 is an aspartic acid (D), not an E. Supporting this contention, analysis of the surrounding residues indicate that this site is quite unlike any mapped separase cleavage sites, having large aromatic amino acid residues at positions -4 and -5 relative to the critical arginine (Figure 3.1C). The amino acid sequence surrounding the arginine at position 474 in the DRAD21 protein is more consistent with the separase consensus cleavage sequence (Figure 3.1B), and was therefore chosen for further analysis. The sites

surrounding DRAD21 amino acid residues 175 and 474 are hereafter referred to as the N-terminal and C-terminal putative cleavage sites, respectively.

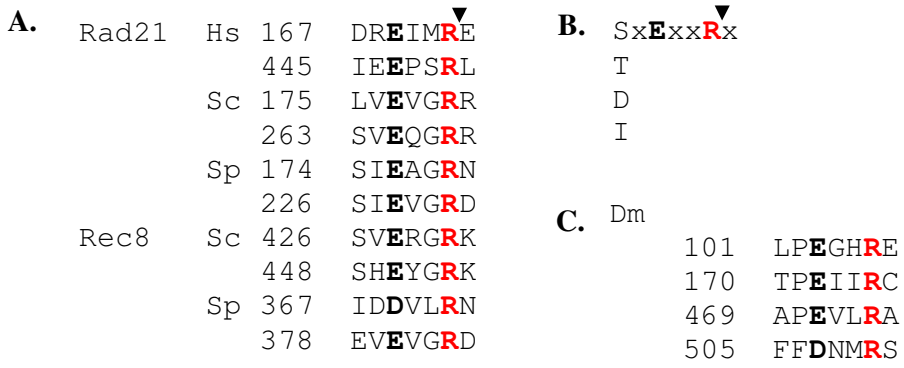

Figure 3. 1: *Separase cleavage sites*

A: Comparison of the two human Rad21 cleavage recognition sites with the published Rad21 and Rec8 cleavage site sequences of *S. cerevisiae* (Sc) and *S. pombe* (Sp).
B: The comparison in A has lead to the identification of a minimal separase cleavage recognition sequence (Hauf et al., 2001). The arrowheads indicate the peptide bond cleaved by SEPARASE following the invariant arginine residue (red).
C: Putative separase cleavage recognition sites identified in *Drosophila* RAD21 (Dm; this study). The numbers correspond to the position of the N-terminal most amino acid indicated in each instance.

A.

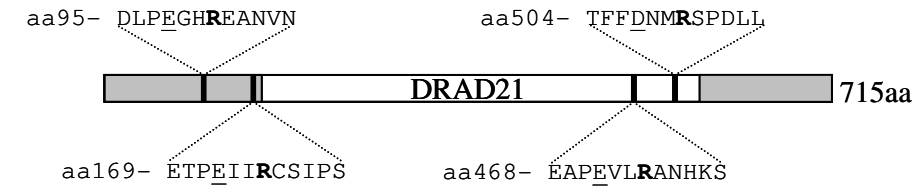
aa95- DLPEGHREANVN
aa504- TFFDNMRSPDLL
DRAD21
715aa
aa169- ETPEIIRCSIPS
aa468- EAPEVLRANHKS

B.

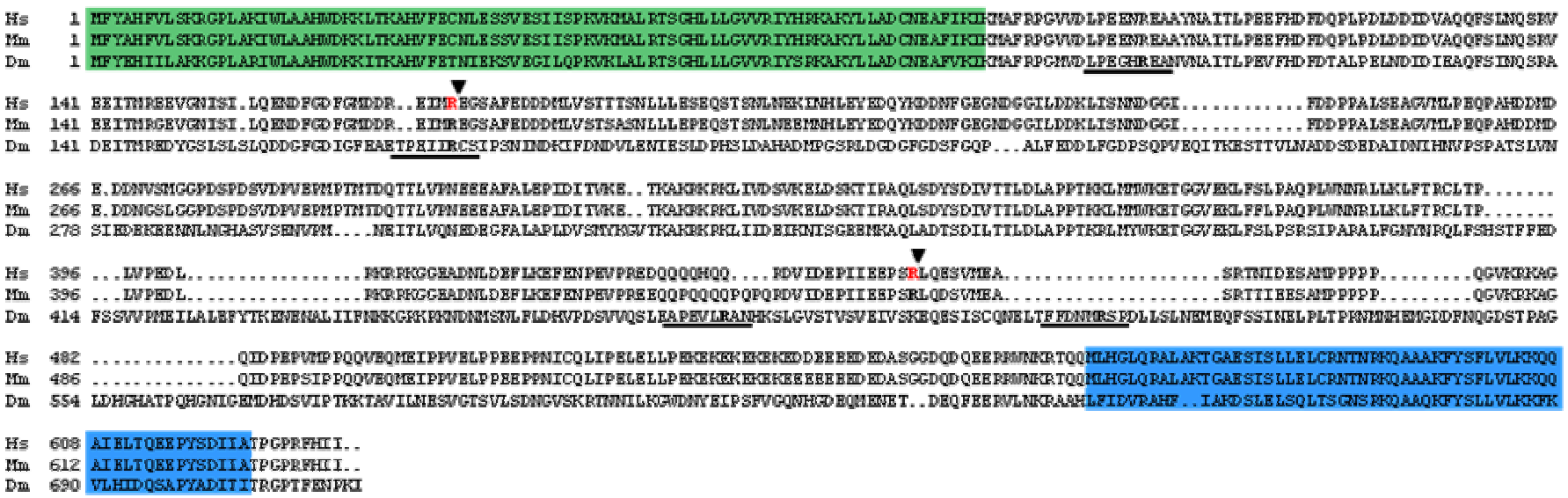
Hs 1 MFYAHFVLSKRGPLAKIWLAAHWDKKLTKAHVFECNLESSVESIISPKVKMALRTSGHLLGVVRIYHPKAKYLLADCNEAFIKHKMAFRPGVVDLPEENREAAYNAITLPEEFHDFDQPLPDLDDIDVAQQFSLNQSKV
Mm 1 MFYAHFVLSKRGPLAKIWLAAHWDKKLTKAHVFECNLESSVESIISPKVKMALRTSGHLLGVVRIYHPKAKYLLADCNEAFIKHKMAFRPGVVDLPEENREAAYNAITLPEEFHDFDQPLPDLDDIDVAQQFSLNQSKV
Dm 1 MFYEHIILAKKGPLARIWLAAHWDKKITKAHVFETNIEKSVEGILQPKVKLALRTSGHLLGVVRIYSPKAKYLLADCNEAFVKHKMAFRPGMVDLPEGHREANVNAITLPEVFHDFDTALPELNDIDIEAQFSINQSPA
Hs 141 EEITNREEVGNISI.LQEMDFGDFGMDDR..EIMREGSAFEDDDMLVSTTTSNLLLESEQSTSNLNEKINNHLEYEDQYKDDNFGEGNDGGILDDKLISNNDGGI.....FDDPPALSEAGVTLPEQPAHDDMD
Mm 141 EEITNRGEVGNISI.LQEMDFGDFGMDDR..EIMREGSAFEDDDMLVSTSASNLLLEPEQSTSNLNEEINNHLEYEDQYKDDNFGEGNDGGILDDKLISNNDGGI.....FDDPPALSEAGVTLPEQPAHDDMD
Dm 141 DEITNREDYGSLSLSLQDDGFGDIGFEAETPKIIRCSIPSNINDKIFDNDVLENIESLDPHSLDAHADMPGSRLDGDGFGDSFGQP...ALFEDDLFGDPSQPVEQITKESTTVLNADDSDEDAIDNIHNVPSPATSLVN
Hs 266 E.DDNVSMGGPDSPDSVDPVEPMPTNTDQTTLVPNEEEAFALEPIDITVKE..TKAKPKRKLIVDSVKELDSKTIRAQLSDYSDIVTILDLAPPTKKLMTMKETGGVEKLFSLPAQPLWNNRLLKLFTRCLTP.....
Mm 266 E.DDNGSLGGPDSPDSVDPVEPMPTNTDQTTLVPNEEEAFALEPIDITVKE..TKAKPKRKLIVDSVKELDSKTIRAQLSDYSDIVTILDLAPPTKKLMTMKETGGVEKLFFLPAQPLWNNRLLKLFTRCLTP.....
Dm 278 SIEDEKEENNLNGHASVSENVPM....NEITLVQNEDEGFALAPLDVSNYKGVTKAKPKRKLIIDEIKNISGEENKAQLADTSDILTILDLAPPTKRLMYMKETGGVEKLFSLPSRSIPARALFGNYNRQLFSHSTFFHD
Hs 396 ...LVPEDL.....PKRPKGGEADNLDEFLKEFENPEVPREDQQQQHQQ....RDVIDEPIIEEPSRLQESVMEA.....SRTNIDESAMPPPPP.....QGVKRKAG
Mm 396 ...LVPEDL.....PKRPKGGEADNLDEFLKEFENPEVPREEQQPQQQQPQPQRDVIDEPIIEEPSRLQDSVMEA.....SRTIIEESAMPPPPP.....QGVKRKAG
Dm 414 FSSVVPMEILALEFYTKENENALIIFNKKGKKPKNDNMSNLFLDHVPDSVVQSLEAPEVLRANHKSLGVSTVSVEIVSKEQESISCQNELTFFDNMRSPDLLSLNEMEQFSSINELPLTPRNTNHEMGIDFNQGDSTPAG
Hs 482 .....QIDPEPVMPPQQVEQMEIPPVELPPEEPPNICQLIPELELLPEKEKEKEKEKEDDEEEEDEDASGGDQDQEERRMNKRTQQMLHGLQRALAKTGAESISLLELCRNTNPKQAAAKFYSFLVLKKQQ
Mm 486 .....QIDPEPSIPPQQVEQMEIPPVELPPEEPPNICQLIPELELLPEKEKEKEKEKEEEEEEEDEDASGGDQDQEERRMNKRTQQMLHGLQRALAKTGAESISLLELCRNTNPKQAAAKFYSFLVLKKQQ
Dm 554 LDHGHATPQHGNIGEMDHDSVIPTKKTAVILNESVGTSVLSDNGVSKRTNNILKGWDNVEIPSFVGQNHGDEQMENET..DEQFEEEVLNKPAAHLFIDVRAHF..IAKDSLELSQLTSGNSPKQAAQKFYSLLVLKKFK
Hs 608 AIELTQEEPYSDIIATPGPRFHII..
Mm 612 AIELTQEEPYSDIIATPGPRFHII..
Dm 690 VLHIDQSAPYADITITRGPTFENPKI

Figure 3. 2: *Identification of putative DRAD21 separase cleavage sites*

A: Schematic of DRAD21 protein, predicted to consist of 715aa. Grey boxes indicate N and C terminal kleisin domains. The black bars indicate the relative positions of amino acid sequences that are similar to the published separase consensus cleavage sequence (Hauf et al., 2001), and the amino acid sequence at each of these sites is indicated. Cleavage by SEPARASE at such sites occurs following the invariant arginine residue, indicated in bold. The presence of a charged residue (Underlined, most commonly glutamic acid (E)) at position -3 in relation to the invariant arginine is a key feature of these sites.
B: T-Coffee sequence alignment of RAD21 homologues (Homologene number 38161) from *Homo sapiens* (Hs; accession number NP_0062561.1), *Mus musculus* (Mm; accession number NP_033035.2) and *Drosophila melanogaster* (Dm; accession number NP_001015132.1) (Notredame et al., 2000). N and C terminal kleisin domains are indicated by green and blue shading respectively. The four sites within DRAD21 that conform to the published SEPARASE consensus sequence are underlined and the critical arginine residues are indicated in bold. Arrow heads indicate the experimentally confirmed separase cleavage sites in *Homo sapiens* RAD21; the arginine following which cleavage occurs is represented in bold red font. The arginine at amino acid position 175 in the DRAD21 sequence clearly aligns with the identified N-terminal human cleavage site. The human C-terminal RAD21 cleavage site falls between the two more C-terminal consensus sites in the *Drosophila* (underlined) sequence.

3.2.2 GENERATION OF PUTATIVE CLEAVAGE-RESISTANT DRAD21 ISOFORMS

Amino acid substitution at the invariant arginine residues has previously been demonstrated to make separase cleavage sites refractory to SEAPARASE cleavage (Uhlmann et al., 1999, Tomonaga et al., 2000, Kitajima et al., 2003, Hauf et al., 2001, Buonomo et al., 2000). In order to determine which, if any, of the putative separase cleavage sites in DRAD21 are proteolytically cleaved during mitosis, *in vitro* site-directed mutagenesis was used to make specific changes in the hope of diminishing or abolishing cleavage. Previous studies had substituted the invariant arginine (R) residues for alanine (A) or glutamic acid (E) residues to make separase consensus sites refractory to SEPARASE cleavage (Uhlmann et al., 1999, Tomonaga et al., 2000, Kitajima et al., 2003, Hauf et al., 2001, Buonomo et al., 2000). Site-directed changes were made in the *Drad21*cDNA cloned in pBluescript so as to substitute the Arg residues at amino acid positions 175 and 474 for Ala residues, and to introduce a diagnostic restriction site (Figure 3.3). The resultant altered *Drad21* sequences are referred to as $Drad21^{R175A}$ and $Drad21^{R474A/A475G}$ (hereafter referred to as $Drad21^{RA474AG}$) for the N and C-terminal changes respectively.

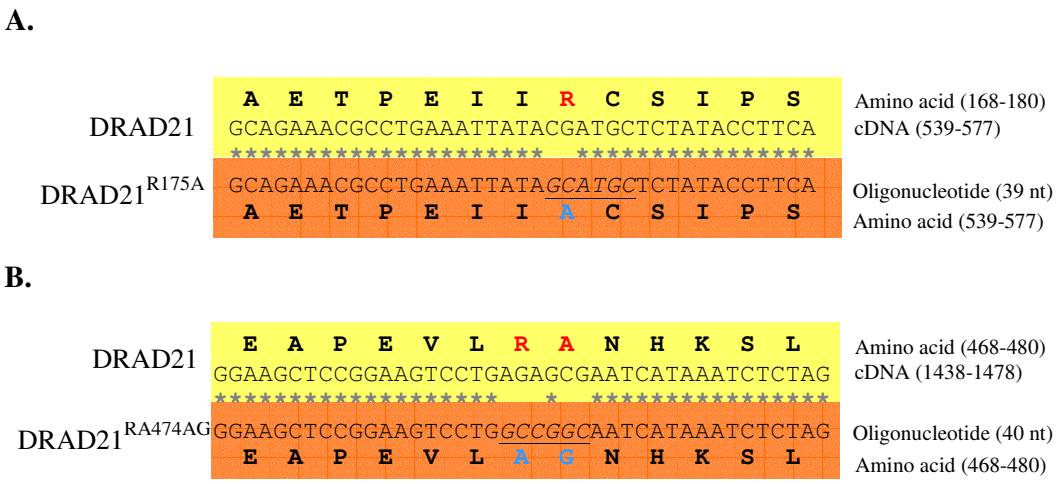

Figure 3. 3: *Site-directed mutagenesis to create cleavage-resistant DRAD21 isoforms*

Wild-type DRAD21 amino-acid and *Drad21* cDNA sequences are shown aligned with the sequence of oligonucleotides used to create the site-directed alterations. Mismatches between the cDNA and oligonucleotides are represented by the lack of asterisks and indicate the base changes used to engineer the desired protein sequences.
A: DRAD21^{R175A} was generated by site-directed mutagenesis using the 39nt oligonucleotide sequence indicated. This oligonucleotide introduced base changes to alter the wild-type arginine residue at position 175 (red) to alanine (blue) and to introduce the SphI diagnostic restriction endonuclease site (underlined, italics).
B: DRAD21^{RA474AG} was generated by site-directed mutagenesis using the 40nt oligonucleotide sequence indicated. This oligonucleotide introduced base changes to alter the arginine and alanine residues at amino acid positions 474 and 475 (red) to alanine and glycine residues (blue) and to introduce the NaeI diagnostic restriction endonuclease site (underlined, italics).

Diagnostic restriction sites were introduced into the *Drad21* cDNA to allow successfully mutagenised plasmids to be identified. Clones in which the *Drad21* cDNA contained the desired site-directed alterations were selected by restriction enzyme cleavage, and fully sequenced to ensure that no other nucleotide changes had been introduced. The altered cDNA was then sub-cloned into the *Drosophila* transformation vector, pUAST (Figure 3.4, see Figure 2.1 for full details of pUAST), and introduced into the *Drosophila* germline for the generation of transgenic insects.

Figure 3.4 shows a schematic of the three altered *Drad21* cDNA sequences used in this study. To create a mutant *Drad21* cDNA that would produce a DRAD21 protein with alterations in both putative separase cleavage sites recombinant DNA technology was used. The mutagenised sections of pBlueScript*Drad21*^{R175A} and pBlueScript*Drad21*^{R474A} were purified from agarose gels following EcoRI-BamHI and KpnI-BamHI digestion respectively. These fragments were then ligated into EcoRI-KpnI linearised pBlueScript and fully sequenced to ensure that no additional mutations had been introduced. The double mutant *Drad21*cDNA (*Drad21*^{DM}*)* was then sub-cloned into pUAST and introduced into the *Drosophila* germline for the generation of transgenic insects.

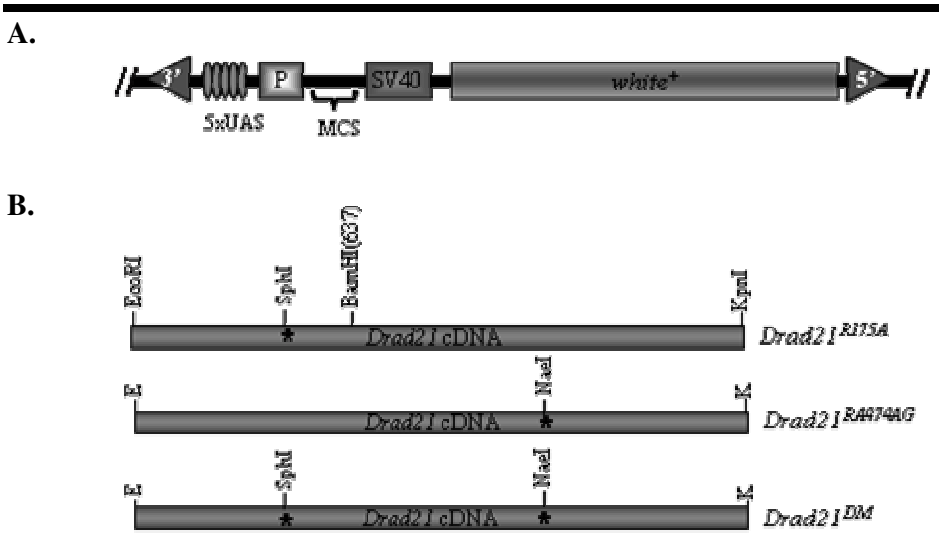

Figure 3. 4: *Transformation constructs*

A: Schematic of the pUAST transformation cassette. The double forward slashes indicate that the entire pUAST vector is not represented here. The P-element inverted repeats are shown as triangles. pUAST has five sequential Gal4 binding sites (ovals), HSP70 minimal promoter (P), a poly A signal from SV40 and the *white*$^{+}$ gene as a selectable marker for the generation of transgenic insects. For further detail see (Brand and Perrimon, 1993).
B: Schematic of the altered *Drad21* cDNAs used to transform embryos. The *Drad21* cDNA is approximately 2.2kb long, and encodes a polypeptide of 715 amino acids. The relative position of *in vitro* site-directed changes are indicated as asterisk. To create the double mutant cDNA (lower bar) a pLD02527*Drad21*^{RA474AG} BamHI-KpnI fragment and an EcoRI-BamHI fragment from pLD02527*Drad21*^{R175A} were ligated into EcoRI-KpnI linearised pBluescriptKS+ (Stratagene) in a three way ligation. Altered *Drad21* cDNAs were subcloned cloned into the EcoRI and KpnI sites of pUAST (within the MCS). Position of restriction enzyme cleavage sites are indicated.

3.2.2.1 Germline transformation of *Drosophila* embryos

P-element mediated transformation was used to introduce the altered *Drad21* sequences into the *Drosophila* genome in a quasi-random fashion. The level of transgene expression can vary considerably between independent transgenic lines carrying identical constructs in different genomic locations, such that integration events near a strong promoter or enhancer elements are likely to result in 'high expression' lines, whereas integration events in or near 'silent' genetic regions are likely to result in relatively 'low expression' lines (Weiler and Wakimoto, 1995). In addition, transgene integration into coding regions is likely to disrupt gene function and may influence viability or produce an insertion specific phenotype. Because of these reasons, several independent transgenic lines were generated and maintained as balanced stocks for each of the DNA constructs generated.

Single transgene insertions were mapped to the level of the whole chromosome by standard segregation analysis using dominantly marked balancer chromosomes. Table 3.1 lists the transgenic lines generated in this study and the chromosome to which each was mapped. None of the transgenic lines generated displayed a discernable phenotype when propagated in a w^{1118} background or when crossed to balancer chromosomes CyO, TM3 or TM6B.

Table 3. 1: Transgenic lines generated in this study

Transformation construct	Transgenic line	Chromosomal location of insert
P{UASTDrad21^{R175A}}	4B	2
	4A	2
	D1	3
	16A	3
	D2	3
P{UASTDrad21^{RA474AG}}	P11a	X
	20C	X
	20A	X
	53B	X
	3A	2
	53A	2
	15C	2
	53C	2
	15A	3
P{UASTDrad21^{DM}}	N1	X
	N5	X
	11B	X
	24A	2
	1B	2
	21	3
	38B	3
	21	3
	16A	3
	27B	3
	42A	3
	38B	3
	27C	3

3.2.3 ECTOPIC EXPRESSION OF PUTATIVE CLEAVAGE-RESISTANT DRAD21 ISOFORMS

3.2.3.1 Tissue specific expression of altered forms of DRAD21: The gal4 UAS system

One way to investigate the function of a gene is to express it in altered form(s) in defined tissues or developmental stages. This strategy is particularly useful when ubiquitous expression of such altered forms is predicted to be incompatible with cell viability, as is the case with *Drad21*. This study used the Gal4/UAS system to specifically induce transgene expression in tissues of interest using publicly available *Drosophila* stocks that express the Gal4 transcription factor a tissue specific pattern (Table 3.2). As *Drad21* isoforms had been cloned into a Gal4 responsive vector (pUAST), *Drad21* expression could be readily varied using different Gal4 "driver" lines. If the altered form of the DRAD21 protein adversely affected the tissue or developmental stage in which it is expressed, this could be readily identified.

3.2.3.2 Ectopic expression of putative cleavage-resistant DRAD21 isoforms

The effect overexpressing DRAD21^{R175A}, DRAD21^{RA474AG} and DRAD21^{DM} in different tissues and at different developmental times was assessed using a range of different Gal4 expression lines, called Gal4 drivers (Table 3.2). Balanced heterozygous transgenic flies bearing single P{UAST*Drad21*^{R175A}}, P{UAST*Drad21*^{RA474AG}} or P{UAST*Drad21*^{DM}} transgene insertions were crossed to a range of different Gal4 drivers and the effect of overexpression analysed in the F1 offspring. The presence of balancer chromosomes bearing dominant markers allowed individual F1 flies carrying a single *Drad21* transgene and a single Gal4-driver transgene to be compared to their siblings with the Gal4 driver alone. In this manner the effects of expression of the different *Drad21* transgenes was able to be directly assessed.

Table 3.2 summarises the results of overexpressing the three different DRAD21 forms in a number of different tissues and developmental stages. Overexpression of a single copy of DRAD21^{R175A} produced no discernable phenotype irrespective of the expression pattern or transgenic line used. Conversely, overexpression of single

copies of DRAD21^{RA474AG} and DRAD21^{DM} consistently produced dominant phenotypes in a range of tissue types that were overtly indistinguishable (Table 3.2). Given that the eye is a non-essential organ for laboratory cultured *Drosophila* and that the dominant eye phenotypes observed upon overexpression of DRAD21^{RA474AG} and DRAD21^{DM} were reproducible and relatively easy to score visually, the developing *Drosophila* eye was chosen as the experimental system for further analysis of DRAD21 cleavage.

Table 3. 2: Overexpression of altered DRAD21 forms

Gal4 Driver	*Expression Pattern*	*Temp (ºC)*	*Overexpression Phenotype*		
			DRAD21^{R175A}	*DRAD21^{RA474AG}**	*DRAD21^{DM}*
Nanos	*Embryo*	*25*	*None*	*Lethal*	*Lethal*
5818	*Embryonic PNS. Larval CNS*	*25*	*ND[1]*	*Lethal*	*Lethal*
Sev	*Eye imaginal disc*	*18*	*None*	*Lethal*	*Lethal*
		25	*None*	*Lethal*	*Lethal*
		29	*None*	*Semi-Lethal: slightly rough eyes*	*Semi-Lethal: Slightly rough eyes*
MS1096	*Wing imaginal disc*	*25*	*ND*	*Reduced wings*	*Reduced wings*
Ey	*Undifferentiated cells of eye imaginal disc*	*25*	*None*	*Small-no eyes*	*Small-no eyes*
		29	*WT*	*Small-no eyes*	*Small-no eyes*
GMR	*Differentiating cells of eye imaginal disc*	*18*	*WT*	*Disorganised eye*	*Disorganised eye*
		25	*WT*	*Reduced and disorganised eye*	*Reduced and disorganised eye*
		29	*None*	*Ablated eye*	*Ablated eye*
C689a	*CNS*	*25*	*None*	*None*	*None*
179	*Embryo*	*25*	*ND*	*Lethal*	*ND*

* 9 lines were tested using a range of Gal4 drivers. 4 of the lines consistently produced the results as tabulated. The remaining 5 lines (20A, 20C, 53C, 15A and 15C) did not produce any readily discernable phenotype and were tested further (see main text).
[1]ND, experiment not done.

3.2.3.3 Loss of *Drad21*cDNA sequences from some transgenic lines

To eliminate the possibility that the phenotypes observed were insertion specific, several different independent transgenic lines were tested for each construct. Each of the five DRAD21^{R175A} and seven DRAD21^{DM} lines tested produced consistent results (Table 3.2). The DRAD21^{RA474AG} transgenic lines tested produced variable results. Four of the nine DRAD21^{RA474AG} transgenic lines tested produced dominant phenotypes that appeared indistinguishable from those produced upon DRAD21^{DM} overexpression, whilst the remaining five lines did not produce a dominant phenotype when expressed in any of the examined patterns, including the developing eye. The failure to produce a dominant phenotype in these lines was not due to the insertion of the transgene into a region of silenced chromatin as each of the transgenic lines still had red eyes, indicating that the *white*$^{+}$ gene, present in the constructs as a screenable marker, was still being expressed. Before analysing the expression levels of the *Drad21*^{RA474AG} transgene expression in phenotype producing and non-phenotype producing transgenic lines, a PCR based assay was designed to confirm whether the correct *Drad21* isoform was present in all of the P{UAST*Drad21*^{RA474AG}} transgenic lines (Figure 3.5). This PCR assay determined that the lack of phenotype was due to the loss of *Drad21* cDNA sequences in the UAS construct (Figure 3.5). Consequently these transgenic lines were not characterised further.

A.

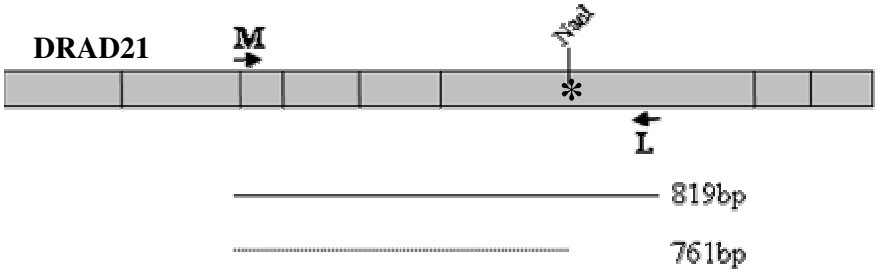

B.

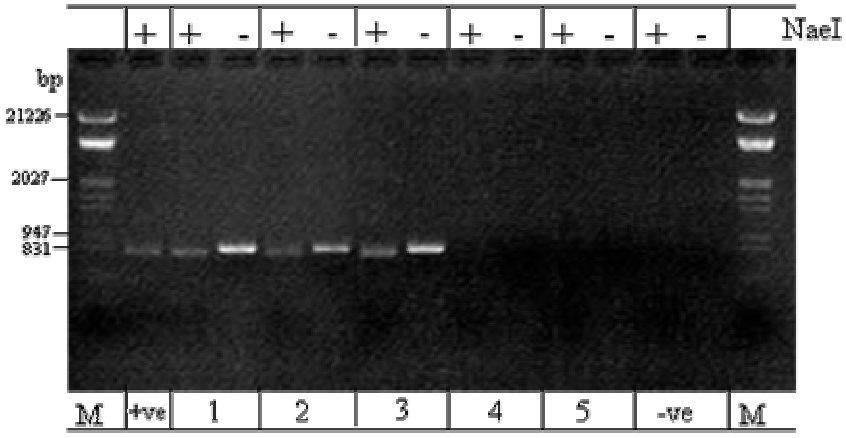

Figure 3. 5: *PCR diagnostic test for the presence of Drad21 transgenes*

A: Schematic of PCR design. *Drad21* cDNA (2.2kb) indicated as solid grey bar, with vertical lines indicating the position of intron-exon boundaries. Primers DradM (M) and DradL (L) were used to amplify a 819 bp fragment from the cDNA spanning the site of the introduced RA474AG alteration and associated diagnostic restriction site (NaeI). The PCR product is indicated before (solid line) and after treatment with NaeI (dotted line). *Drad21* genomic sequence was not amplified as the binding site of primer DradM spans an intron-exon boundary and amplification conditions favour the production of smaller products.
B: Results of PCR diagnostic test. PCR products were left untreated, or incubated with NaeI before electrophoresis as indicated. **M**, EcoRI/HindIII lambda DNA marker; size of selected fragments indicated in base pairs (bp). **+ve**, positive control PCR from P{UASDrad21^{DM}}42A transgenic fly. **–ve**, negative control PCR from w^{1118} fly. Individual P{UASDrad21^{RA474AG}} transgenic flies were tested for the presence of cDNA and the introduced mutation. **1**, transgenic line 53A. **2**, transgenic line PIIa. **3**, transgenic line 3A. **4**, transgenic line 20C. **5**, transgenic line 15A. Lines 20C and 15A, as well as lines 20A, 53C and 15C consistently failed to generate a PCR product.

3.2.3.4 Ectopic expression of putative cleavage-resistant DRAD21 isoforms in the differentiating cells of the eye imaginal disc

Balanced heterozygous virgin females of each of P{UAST*Drad21*^{R175A}}, P{UAST*Drad21*^{RA474AG}} or P{UAST*Drad21*^{DM}} were crossed to males of the P{GAL4-ninaE.GMR}12 transgenic line (hereafter referred to as GMR-Gal4) to assess the effect of overexpression in the developing eye. GMR-Gal4 induces transgene expression in all cells of the eye-antennal imaginal disc posterior to the morphogenetic furrow (MF) (Wolff and Ready, 1993). Overexpression of one copy of DRAD21^{R175A} in this pattern at 25ºC produced no discernable perturbation of eye development, with the resultant eyes indistinguishable from wild-type (Figure 3.6 B). Overexpression of DRAD21^{RA474AG} or DRAD21^{DM} in the GMR-GAL4 defined pattern, however, produced uniformly roughened and reduced eye phenotypes indistinguishable from one another (Figure 3.6 D). If DRAD21 was cleaved at either separase cleavage site with equal efficiency it would be expected that expression of DRAD21 isoforms with only one mutant cleavage site would not produce a dominant phenotype, or would produce a phenotype more mild than that of the double mutant. These suggest that DRAD21, unlike RAD21 proteins of other species, is cleaved by SEPARASE at only one cleavage site, or at one preferred cleavage site.

To further investigate the effect of overexpression of these DRAD21 isoforms in the developing *Drosophila* eye, transgene expression levels were increased by increasing transgene copy number, and by increasing the level of transgene expression through increasing Gal4 activity by elevating the temperature at which the flies were raised. In all cases the severity of the phenotype increased with copy number and expression level, consistent with the phenotypes observed being a direct result of overexpression of the DRAD21 isoforms. Increasing the expression levels of DRAD21^{RA474AG} and DRAD21^{DM} by increasing the rearing temperature to 29ºC or increasing transgene copy number produced an even further reduced eye phenotype with no discernable individual ommatidial structures evident, resulting in a smooth and shiny eye surface with black necrotic spots (Figure 3.6 E, F, H and I).

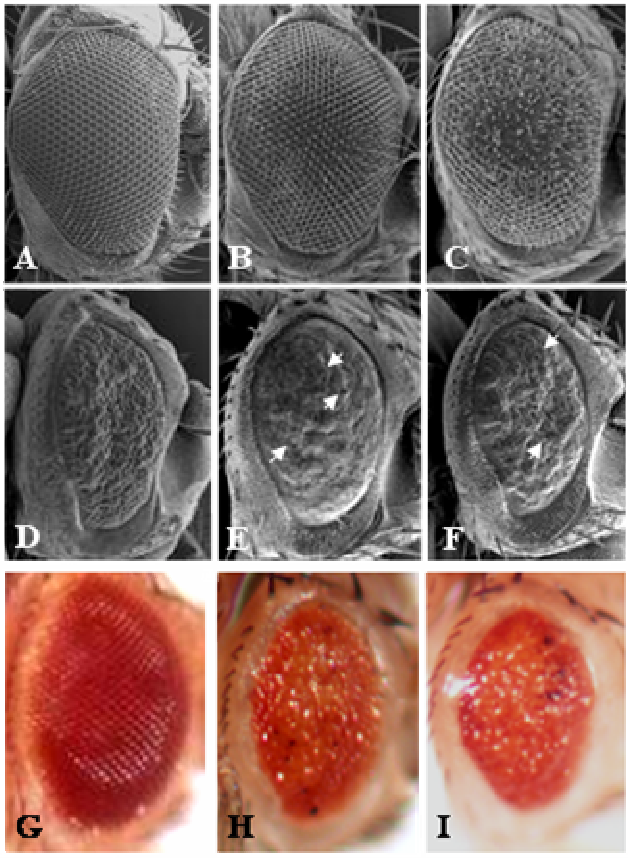

Figure 3. 6: *GMR-Gal4 overexpression of putative cleavage-resistant DRAD21 isoforms*

A-F: Scanning electron micrographs of adult *Drosophila* eyes. **A:**Wild-type eye (w^{1118}). **B:** Overexpression of one copy of $Drad21^{R175A}$ (GMR>DRAD21^{R175A}) does not significantly alter the appearance of the eye. **C:** Overexpression of two copies of $Drad21^{R175A}$ (GMR>DRAD21^{R175A}/ GMR>DRAD21^{R175A}) results in a moderately rough eye phenotype. **D:** Overexpression of $Drad21^{DM}$ (GMR>DRAD21^{DM}) results in a uniformly reduced and roughened eye. **E** and **F:** Increasing transgene copy number (GMR>DRAD21^{DM}/ GMR>DRAD21^{DM}) or raising GMR, $Drad21^{DM}$/CyO animals at elevated temperatures (29ºC) increases the severity of the small and rough eye phenotype (E and F respectively). Overexpression of elevated levels of $Drad21^{DM}$ in the developing eye imaginal disc produces an adult eye with almost no ommatidial structure and with evident necrotic spots (arrows). **G-I:** Low resolution images of adult *Drosophila* eyes. **G:** Wild-type eye (w^{1118}). **H** and **I:** GMR>DRAD21^{DM} animals raised at 29ºC, necrotic spots are clearly evident as black dots.

Interestingly, a weak 'rough eye' phenotype was observed in flies carrying two copies of both DRAD21^{R175A} and GMR-Gal4 transgenes (Figure 3.6 C). Although GMR-GAL4 homozygosity has been noted to produce a slightly disordered eye phenotype in flies cultured at 25ºC this phenotype is only ever observed in females. Homozygosity of GMR-GAL4 was ruled out as the cause of the weak 'rough eye' phenotype observed when DRAD21^{R175A} overexpression was increased as this phenotype was not sex limited and occurred in both males and females to equivalent degrees. These data are consistent with a small proportion of DRAD21 being cleaved by SEPARASE at position 175 during mitosis and inhibition of SEPARASE activity at this site can potentially inhibit correct chromosome segregation by strengthening centromeric cohesion.

Overexpression of the C-terminal cleavage mutation in the developing *Drosophila* eye, however, produces a dominant rough-eye phenotype when transgenic flies are heterozygous for both the *Drad21^{RA474AG}* transgene and the Gal4 driver. This rough eye phenotype can be modified in a dose and temperature dependent fashion. Interestingly, over-expression of the C-terminal mutation alone and the N-and C-terminal mutations in combination (*Drad21^{DM})* produce indistinguishable phenotypes, consistent with DRAD21 being preferentially cleaved by SEPARASE at or adjacent to position 474.

3.2.3.5 Generation of stable lines expressing the putative cleavage-resistant DRAD21 isoforms

Expression of DRAD21^{RA474AG} or DRAD21^{DM} in the eye imaginal disc cells posterior to the MF (using GMR-Gal4) consistently produced a reduced and roughened eye phenotype. This expression pattern was therefore chosen for further analysis of the effects of overexpression of DRAD21 cleavage mutants. A combination of traditional genetic approaches and female meiotic recombination was used to generate transgenic stocks that consistently inherited the altered DRAD21 forms expressed in the GMR-Gal4 defined pattern.

P{UASTD*rad21*^{R175A}} and P{UAST*Drad21*^{DM}} transgenic lines bearing second-chromosome transgene insertions were meiotically recombined with the second-chromosome GMR-Gal4 line. Flies bearing recombinant GMR-Gal4, P{UAST*Drad21*^{DM}} second chromosomes were identified by their small and rough eyes and were balanced on CyO to produce the GMR-Gal4,P{UAST*Drad21*^{DM}}/CyO line, hereafter referred to as GMR>DRAD21^{DM}. Flies bearing recombinant GMR-Gal4, P{UAST*Drad21*^{R175A}} were not able to be determined visually due to the absence of a discernable phenotype, and recombinant chromosomes were confirmed by diagnostic PCR amplifications (Section 2.6.4.1). Confirmed recombinant chromosomes were balanced on CyO to produce the GMR-Gal4, P{UAST*Drad21*^{R175A}}/CyO line, hereafter referred to as GMR>DRAD21^{R175A}. In addition a P{UAST*Drad21*^{RA474AG}}transgenic line on the X chromosome was used to create the P{UAST*Drad21*^{RA474AG}}; GMR-Gal4/CyO line (GMR>DRAD21^{RA474AG}) using traditional genetic crossing techniques.

3.2.4 Analysis of the dominant reduced and roughened eye phenotype

3.2.4.1 Preferential cleavage of DRAD21 following arginine 474

Genetic evidence presented in section 3.2.3.4 is consistent with DRAD21 being preferentially cleaved by SEPARASE after the arginine residue at position 474, and that only a minor pool of DRAD21 is cleaved after arginine 175. This hypothesis was tested directly by examination of the DRAD21 proteins of eye imaginal discs from transgenic flies expressing the three altered DRAD21 isoforms. In flies expressing DRAD21^{R175A}, cleavage by separase would be expected to occur at the favoured R474 cleavage site, and therefore the cleavage product would not be able to be distinguished from wild-type DRAD21 cleavage products. The only DRAD21 cleavage products that would be evident in flies expressing DRAD21^{DM} would be those of wild-type DRAD21, as DRAD21^{DM} would remain as a full length protein. In flies expressing DRAD21^{RA474AG} separase cleavage cannot occur at the preferred cleavage site, however, the small amount of cleavage at the R175 site would be expected to result in the production of a unique DRAD21 cleavage fragment. This cleavage product would be expected to be only observed in the eye imaginal discs of GMR>DRAD21^{RA474AG} animals, despite the presence of wild-type protein (Figure

3.7). This hypothesis was tested by examining the proteins produced in the eye imaginal discs of w^{1118} (wild-type), GMR>DRAD21^{R175A}, GMR>DRAD21^{RA474AG} and GMR>DRAD21^{DM} third instar larvae by western blotting.

An additional protein band, not present in the protein extracts of any other genotype, was observed in protein extracts from imaginal discs expressing DRAD21^{RA474AG} (Figure 3.8). The presence of this band can only be explained if DRAD21 is indeed cleaved by SEPARASE at the R175 and R474 sites as hypothesised (Figure 3.7). Taken together, the biochemical and genetic evidence indicate that DRAD21 has two separase cleavage sites and that the C-terminal cleavage site is preferred.

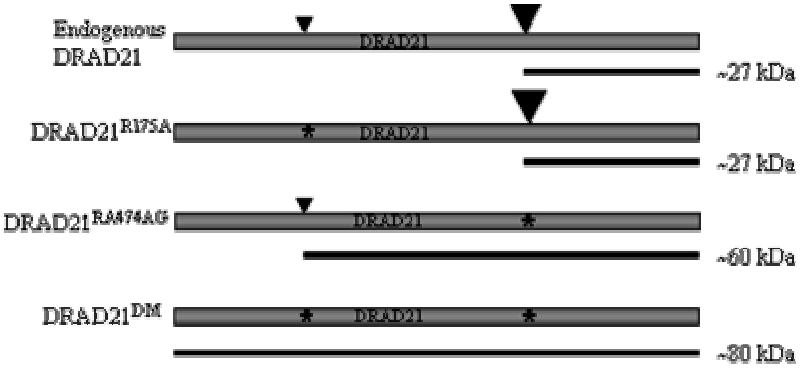

Figure 3. 7: *Biochemical analysis of DRAD21cleavage*

Schematic of DRAD21 proteins analysed in this study. Arrow-heads indicate the putative sites of SEPARASE cleavage, and their size indicates the hypothesised preferential cleavage at the more C-terminal site. Asterisks designate putative SEPARASE cleavage-resistant sites engineered in this study. The predicted cleavage products are shown under each schematic and the predicted size of cleavage products detectable by an antibody raised to a C-terminal DRAD21 epitope (Warren et al., 2000b) are indicated. Because all experiments are performed in the presence of endogenous DRAD21, protein extracts from transgenic flies overexpressing engineered DRAD21 proteins would be expected to contain both endogenous protein and endogenous cleavage products.

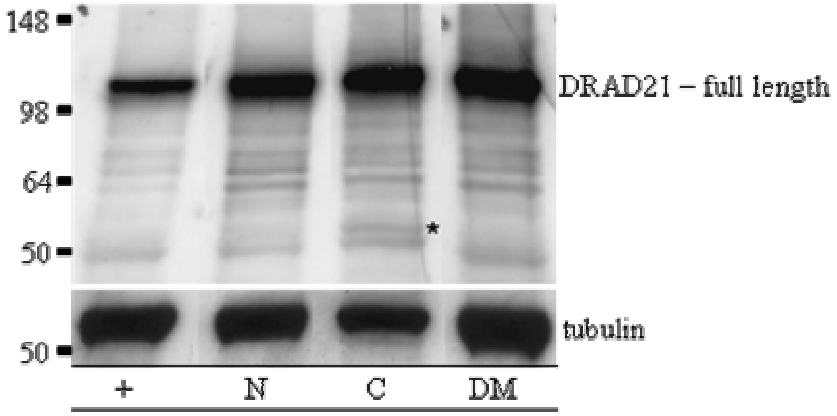

Figure 3. 8: *Western blot of eye imaginal disc extracts*

Proteins were extracted from eye-antennal imaginal discs of third instar larvae. Proteins from 30 discs were loaded per lane. DRAD21 proteins were identified using an antibody raised to an epitope towards the C-terminus of the protein (Warren et al., 2000b). **+,** w^{1118}; **N**, GMR>DRAD21^{R175A}; **C**, GMR>DRAD21^{RA474AG}; **DM**, GMR>DRAD21^{DM}. Asterisk marks the band unique to lane C that confirms that DRAD21^{RA474AG} is not cleaved near position 474 and is cleaved near position 175. Note that full length DRAD21, predicted to be 80 kDa, migrates abnormally slowly in standard Laemmli SDS-PAGE buffered gels (Warren et al., 2000b). α-tubulin is shown as a loading control.

3.2.4.2 GMR>DRAD21^{DM} eye disc cells are disorganised

Development of the eye imaginal disc during late larval and early pupal life is marked by the progression of the morphogenetic furrow (MF) (Wolff and Ready, 1993). Cells anterior to the MF are undifferentiated and progressing through the cell cycle asynchronously in what is referred to as the first mitotic wave. Cells posterior to the MF undergo a synchronous S-phase and mitosis (the second mitotic wave) following which cells are recruited into their specific terminal fates. As GMR>DRAD21^{DM} is expressed in imaginal disc cells posterior to the MF the rough eye phenotype may be due to either disruption of cell fate adoption or insufficient cell numbers to allow correct eye development. To assess whether cells expressing GMR>DRAD21^{DM} were undergoing normal differentiation, third instar eye discs from WT and GMR>DRAD21^{DM} animals were stained with an antibody to Elav to mark cells that have adopted a neuronal fate (Figure 3.9). This analysis showed that whilst neuronal cells of GMR>DRAD21^{DM} were still adopting their fates, the eye discs were generally smaller than their WT counterparts and had more disorganised Elav-positive clusters, which is consistent with the rough and disorganised adult eye phenotype (Figure 3.9).

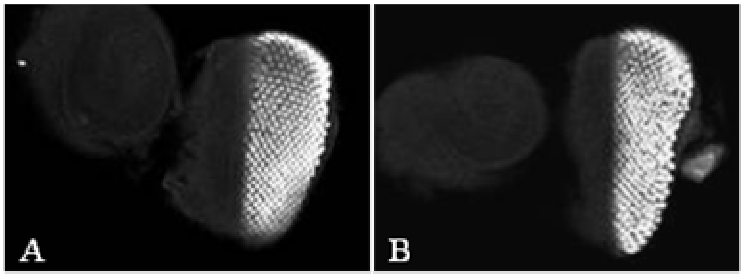

Figure 3. 9: *Neuronal cells in the imaginal disc are disorganised*
Elav staining of eye imaginal discs of w^{1118} wild-type (**A**) and GMR>DRAD21^{DM} (**B**) third instar larvae. Elav marks cells that have adopted a neuronal cell fate.

3.2.4.3 Overexpression of cleavage-resistant DRAD21 leads to increased levels of apoptosis

Overexpression of *Drad21*^{DM} causes a reduction in the size of eye imaginal discs and adult tissue in the *Drosophila* eye (Figures 3.6). These data may be explained by an increase in the level of cell death, or alternatively, failure of the cells to proliferate. To examine whether the reduced size of the adult eye was due to increased levels of apoptosis, the baculovirus apoptosis inhibitor was simultaneously overexpressed in GMR>DRAD21^{DM} eye imaginal discs. Overexpression of the baculovirus apoptosis inhibitor p35 in cells expressing DRAD21^{DM} suppressed the small and rough eye phenotype when analysed in the adult eye (Figure 3.10 compare B and C). This result indicates that the dominant small and roughened eye phenotype is in part due to increased levels of programmed cell death.

To further substantiate the involvement of apoptosis in the generation of the reduced and roughened eye phenotype, eye imaginal discs of both wild-type and GMR>DRAD21 ^{DM} third instar larvae were stained with acridine orange to identify apoptotic cells. A massive increase in acridine orange positive cells was observed posterior to the morphogenetic furrow coincident with DRAD21 ^{DM} expression, as compared to the same set of cells in wild-type (compare Figures 3.10 D and E). Consistent with this result, ubiquitous expression of either *Drad21*^{DM} or *Drad21*^{RA474AG} during embryogenesis causes dominant lethality (Table 3.2), with 98% of embryos failing to hatch into first-instar larvae after 24 hours. These results confirm that over-expression of cleavage resistant DRAD21 isoforms results in significantly increased levels of apoptosis.

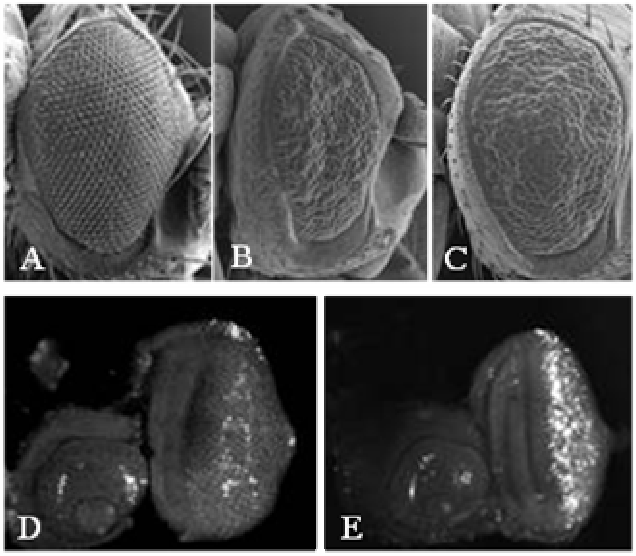

Figure 3. 10: *Over-expression of Drad21 cleavage mutants causes increased apoptosis*

A-C: Scanning electron micrographs of *D. melanogaster* eyes.
A: wild-type (w^{1118}) and **B:** GMR>DRAD21^{DM} are reproduced from Figure 3.6.
C: Co-expression of the apoptosis inhibitor, p35, with DRAD21^{DM} partially suppresses the small and rough eye phenotype.
D: Acridine orange staining of wild-type (w^{1118}) eye imaginal discs reveals a limited amount of apoptosis occurring as part of normal development.
E: GMR>DRAD21^{DM} eye imaginal discs have many more acridine orange staining cells, indicative of increased levels of apoptosis.

3.2.4.4 Mitotic progression is disrupted in GMR>DRAD21^{DM} eye discs

Overexpression of non-cleavable forms of DRAD21 would be predicted to perturb mitosis by stabilising the cohesin complex at the metaphase to anaphase transition. To investigate mitosis in the eye imaginal discs, eye imaginal discs from WT and GMR>DRAD21^{DM} animals were stained with an antibody to the phosphorylated form of Histone 3 (PH3) to identify mitotic cells. The second mitotic wave in eye imaginal discs of GMR>DRAD21^{DM} animals is evident as a much broader band than in wild-type, indicating that the cells are either arresting or delaying in mitosis (Figure 3.11, particularly evident in panels C and D). Also consistent with a mitotic defect, increasing the number of mitoses occurring in cells expressing GMR>DRAD21^{DM} by simultaneously overexpressing CYCLIN E caused a dramatic enhancement of the eye phenotype (compare Figures 3.11 E and F).

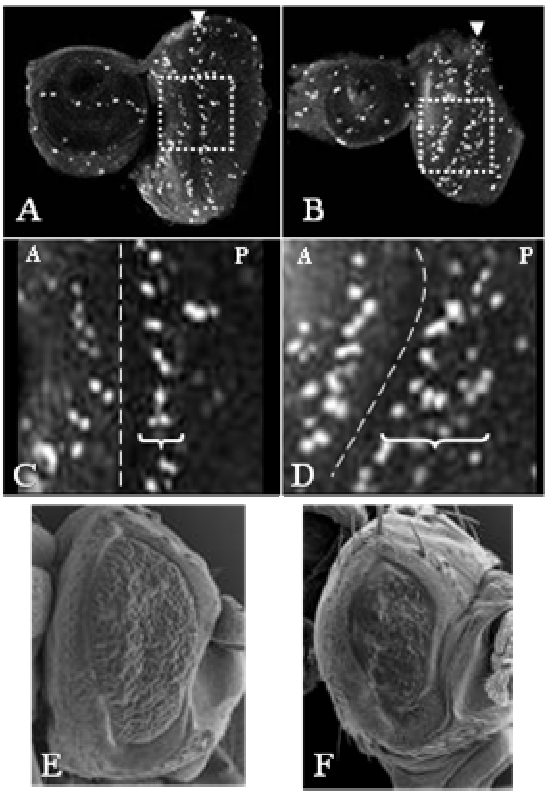

Figure 3. 11: *Progression through mitosis is perturbed in eye discs expressing GMR>DRAD21^{DM}*

Eye imaginal discs were stained with anti-bodies raised against the phosphorylated form of histone 3 (PH3).
A: Wild-type (w^{1118}) eye imaginal disc. **B:** GMR>DRAD21^{DM} eye imaginal disc.
The second mitotic wave is evident in A and B in the posterior region of the disc (arrow heads), however it is wider in the GMR>DRAD21^{DM} disc. Dotted boxes indicate region enlarged in **C** and **D**. **C** and **D**: dashed line indicates the position of the morphogenetic furrow, A=anterior and P=posterior, the widening of the second mitotic wave in GMR>DRAD21^{DM} is clearly evident. **E** and **F**: Scanning electron micrographs of GMR>DRAD21^{DM} (reproduced from Figure 3.6) and GMR>DRAD21^{DM}, UAS Cyclin E animals respectively. Overexpression of Cyclin E in the GMR>DRAD21^{DM} background (F) enhances the eye phenotype to an extent that distinct ommatidial structures can no longer be seen.

3.2.5 ECTOPIC EXPRESSION OF CLEAVAGE-RESISTANT DRAD21 ISOFORMS IN THE DEVELOPING EYE AND WING

3.2.5.1 Ectopic expression of cleavage-resistant DRAD21 isoforms in the asynchronously cycling cells of the eye imaginal disc

To demonstrate that the reduction in the size of the adult eye observed with overexpression of cleavage-resistant DRAD21 isoforms was not a GMR-Gal4 specific phenomenon ectopic expression of DRAD21 transgenes in a different subset of cells in the developing eye imaginal disc was examined.

Balanced heterozygous virgin females of each of DRAD21^{R175A}, DRAD21^{RA474AG} and DRAD21^{DM} were crossed to males of the P{GAL4-ey.H}4-8 transgenic line (hereafter referred to as *ey*-Gal4) to assess the effect of overexpression in the undifferentiated cells of the developing eye. *ey*-Gal4 induces transgene expression throughout the anterior asynchronously dividing cells of the eye imaginal disc extending posteriorly to the MF and a few cells beyond the MF. Overexpression of DRAD21^{R175A} in this pattern at both 25ºC and 29ºC (where Gal4 induced gene expression is increased at higher temperatures) had no effect on eye development, with the eyes of non-balanced progeny (containing both UAS-*Drad21*^{R175A} and *ey*-Gal4) appearing covertly wild-type. In contrast, overexpression of one copy of the *Drad21*^{RA474AG} or of *Drad21*^{DM} transgenes in this pattern resulted in a reduction in the amount of adult eye tissue but did not appear to affect the organisation of the ommatidia. Phenotypes produced from these crosses varied from a slight reduction in the size of the eye to some flies having almost no eye tissue evident at all (Figure 3.12).

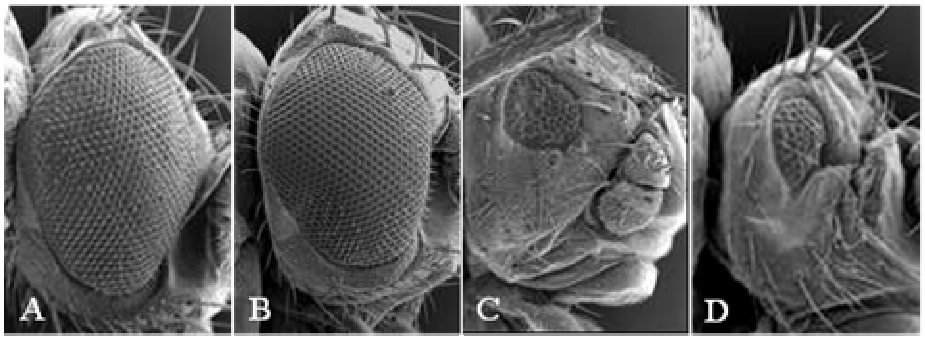

Figure 3. 12: ey-*Gal4 overexpression of cleavage-resistant DRAD21 isoforms*

Scanning electron micrographs of *Drosophila* eyes.
A: wild-type (w^{1118}), reproduced from Figure 3.6.
B: *ey*-Gal4 heterozygote raised at 29ºC
C: w^{1118}, P{UAS*Drad21*^{RA474AG}}/*ey*-Gal4 heterozygote raised at 25ºC
D: w^{1118}; P{UAS*Drad21*^{DM}}/*ey*-Gal4 heterozygote raised at 29ºC
All images are shown at the same magnification.

3.2.5.2 Ectopic expression of cleavage-resistant DRAD21 isoforms in the wing imaginal disc

To demonstrate that the reduction in the size of the adult tissue was not an eye-specific phenomenon, these transgenic lines were used to produce DRAD21 isoform expression in the developing *Drosophila* wing imaginal disc using the MS1096Gal4 driver line. Flies expressing DRAD21^{RA474AG} or DRAD21^{DM} in this pattern had a massive reduction in the amount of adult wing tissue, with their wings appearing as rudimentary wing stubs, similar in phenotype to the *Drosophila* vestigial wing mutant (Figure 3.13). In addition, the third pair of legs of these flies had a twisted appearance and most flies were observed to drag them as they walked around. These results confirm that overexpression of cleavage-resistant forms of DRAD21 are detrimental to cell viability and lead to an increase in the level of cell death, ultimately resulting in the reduction in the size of adult tissues. These results demonstrate that the increased levels of apoptosis observed are specifically due to overexpression of the cleavage-resistant DRAD21 isoforms and are not an artifact of the particular GMR-Gal4 induced expression pattern chosen for analysis in the developing eye, nor are they eye-specific.

Figure 3. 13: *Overexpression of cleavage-resistant DRAD21 isoforms in the developing wing*

Scanning electron micrographs of adult *Drosophila*
A: wild-type (w^{1118}) adult female *Drosophila*
B: MS1096 Gal4/P{UAS*Drad21*^{RA474AG}} heterozygote, expression of cleavage-resistant forms of DRAD21 in this pattern resulted in a dramatic reduction in the amount of wing tissue in the adult fly.

3.3 DISCUSSION

3.3.1 METAZOAN MODEL OF ANEUPLOIDY

Careful sequence analysis allowed the identification of separase cleavage sites in the *Drosophila* cohesin subunit, DRAD21. *In vitro* mutagenesis and subsequent overexpression of cleavage-resistant DRAD21 isoforms in the presence of wild-type DRAD21 showed that, consistent with orthologues in other species, DRAD21 is cleaved by SEPARASE at two sites. This is the first study to demonstrate *Drosophila* RAD21 cleavage.

In yeasts and human cells, expression of RAD21 isoforms with both separase cleavage sites mutated is required to generate any observable phenotype. RAD21 cleavage studies in *S. cerevisiae* indicate that all molecules are cleaved at the C-terminal cleavage site, and that not all are cleaved at the N-terminal cleavage site (Uhlmann et al., 1999). Irrespective of predominant cleavage of *S. cerevisiae* RAD21 at the C-terminal cleavage site, mutation of this cleavage site alone does not perturb chromosome segregation or mitotic progression (Uhlmann et al., 1999). In contrast, overexpression of altered DRAD21 proteins mutated at either the C-terminal cleavage site alone, or at both cleavage sites in combination, produce indistinguishable dominant phenotypes indicating that unlike other species examined to date, DRAD21 is predominantly cleaved at the C-terminal cleavage site. Preferential cleavage of DRAD21 at the C-terminal R474 was confirmed by western-blot analysis (Figure 3.8). It remains to be seen whether this aspect of RAD21 biology is conserved in other Diptera.

In the absence of a *Drad21* mutant all overexpression studies were performed in the presence of endogenous, wild-type DRAD21 protein. Overexpression of either $DRAD21^{DM}$ or $DRAD21^{RA474AG}$ in this context caused mitotic delay or arrest, consistent with a decrease in the efficiency of chromosome segregation. Overexpression of these altered forms of DRAD21 during a single round of mitosis was sufficient to produce a striking phenotype as is evidenced when using GMR-Gal4 to define the expression pattern (Figure 3.6). Indeed, the eyes of GMR>$DRAD21^{DM}$ are significantly smaller and less organised than that of wild-type

animals. These results suggest that the presence of even a small amount of 'non-cleavable' DRAD21 is inconsistent with correct execution of mitosis. Supporting this contention, increasing the number of mitoses occurring in GMR>DRAD21^{DM} eye discs by overexpressing CYCLIN E dramatically enhanced the eye phenotype (Figure 3.11). In addition, mitosis in GMR>DRAD21^{DM} eye discs was observed to be delayed (Figure 3.11). These results indicate that the presence of DRAD21^{DM} makes it difficult for cells to correctly segregate their chromosomes and exit mitosis in a timely manner. Some of these cells undergo apoptosis (Figure 3.10, and further discussion below), however, in the cells that do not undergo apoptosis, reducing the ability of sister chromatids to disjoin in anaphase is likely to produce a proportion of cells with an aneuploid chromosome complement, as is observed upon overexpression of non-cleavable human RAD21 in cell culture (Hauf et al., 2001).

3.3.2 A ROLE FOR DRAD21 IN APOPTOSIS?

The overexpression phenotypes described in this chapter are at least in part due to increased levels of cell death (section 3.2.4.3). Acridine orange staining of GMR>DRAD21^{DM} eye imaginal discs showed that the increase in apoptosis is restricted to cells expressing the transgene, and therefore is cell-autonomous. Cleavage of human RAD21 by caspases 3 and 7 has been shown to occur before the condensation of apoptotic chromatin and the resultant ~65kDa protein is required to amplify the cell death signal (Chen et al., 2002, Pati et al., 2002). A link between RAD21 and apoptosis has not been explored in other species, however, the results presented in this chapter indicate that amplification of the cell death signal is not occurring in the *Drosophila* eye imaginal disc, since acridine orange staining is limited specifically to the region of the eye disc in which GMR>DRAD21^{DM} is expressed. Further analysis such as double-labeling of eye imaginal discs with UAS-GFP, to identify cells expressing cleavage-resistant DRAD21 isoforms, in combination with an apoptosis marker such as TUNEL or acridine orange would be necessary to definitively rule out the occurrence of non cell-autonomous apoptosis. Such analyses will be informative in determining if the cohesin and apoptotic functions of human RAD21 co-evolved, or if these functions have evolved independently of one another.

3.3.3 GMR>DRAD21^{DM} AND GENETIC MODIFIERS

This chapter describes the generation and characterisation of the first known *Drad21* mutants. The dominantly acting 'cleavage-resistant' *Drad21* alleles generated in this study have provided the first genetic tools with which the function and regulation of DRAD21 and the *Drosophila* cohesin complex can be investigated. Importantly, the nature of these alleles, predicted to strengthen centromeric cohesion and perturb the correct execution of mitosis, makes them ideal tools for investigating the role of cohesin regulators in chromosome segregation.

CHAPTER 4: A GENOME-WIDE MODIFIER SCREEN TO IDENTIFY NOVEL REGULATORS OF METAZOAN CHROMOSOME SEGREGATION

4.1 INTRODUCTION

4.1.1 COHESIN AND GENETIC SCREENS

Most of what is understood about the function of the cohesin complex has come from genetic and biochemical studies in yeast and biochemical studies in vertebrate cell culture and *Xenopus* cell free extracts. As outlined in Chapter 1, genetic screens in yeast have greatly added to our understanding of the complex nature of sister chromatid cohesion and have identified many of the highly conserved players in the process. Indeed, *Rad21* was initially identified in a genetic screen for Radiation sensitive mutants in *S. pombe* and its homologue in *S.cerevisiae* is called *Scc1* from its isolation in a screen for sister chromatid cohesion mutants. In metazoan species, including *Drosophila,* it is quite evident that cohesin is subject to additional levels of regulation that are not present in yeast. At the commencement of this study it was clear that genetic studies in a metazoan species, such as *Drosophila*, could offer unique insights into how metazoan species regulate the structure and stability of their chromosomes.

4.1.4 STRATEGIES FOR GENETIC SCREENS IN *DROSOPHILA*

External organs such as the eye or wing have been used extensively for genetic screens in *Drosophila*. In both cases phenotypic alterations are relatively easy to score and interpretation of the results is aided by the fact that the development of these tissues is very well understood. Most genetic screens in *Drosophila* are used to identify genes that enhance the effects of a null or weak mutation, or enhance or suppress the effects of a dominant allele expressed in a tissue restricted pattern. Following the development of the DRAD21^{DM} allele (Chapter 3), a sensitised genetic screen to identify second site modifiers of chromosome segregation was undertaken. By expressing the DRAD21^{DM} in a subset of cells in the eye using GMRGal4, centromeric cohesion is artificially strengthened and the correct execution of mitosis prevented (section 3.2.4.4). This eye specific GMR>DRAD21^{DM} provides the appropriately sensitised genetic background in which to perform a screen for second site modifiers of cohesin function and chromosome segregation (this chapter). By introducing second site modifications into this sensitised background loci that enhance (increase) or suppress (decrease) the severity of the small and rough eye

phenotype that would not be penetrant in an otherwise wild-type background can be identified. Indeed, the specificity of such genetic interactions can be ensured by confirming that the phenotypic modulation is specific to the sensitised tissues alone, in this case in the eye.

The deficiency kit release used in this study was that of March 2004, which consists of 232 individual deletion strains estimated to cover 90% of the genome (Appendix 1). The stocks that make up this DK delete a minimum of 4569 out of 5054 polytene bands across the *Drosophila melanogaster* genome with the exception of the Y chromosome (Figure 2.2). Chromosomes X, 2, 3 and 4 are represented by deletion strains in the DK. As each of these deletions strains is the equivalent of a null mutation for all of the genes that are removed in the deleted region, screening this collection of deficiencies allows us to rapidly scan the genome a few hundred genes at a time.

It was previously shown that the severity of the dominant GMR>DRAD21^{DM} phenotype can be modulated in a dose dependent manner (Section 3.2.3.4); with increasing severity correlating with increases in transgene copy number and expression levels (Figure 3.6). This study uses the eye phenotype resulting from GMR>DRAD21^{DM} expression in the posterior differentiating cells of the eye imaginal disc to identify novel regulators of chromosome segregation.

4.2 RESULTS

4.2.1 THE GMR>DRAD21^{DM} PHENOTYPE CAN BE MODIFIED BY BOTH KNOWN AND PREDICTED COHESIN REGULATORS

To determine whether the DRAD21^{DM} eye phenotype was sufficiently sensitive to identify second-site modifiers likely to encode novel regulators of chromosome segregation, flies expressing DRAD21^{DM} in the posterior differentiating cells of the eye imaginal disc were crossed to a collection of *Drosophila* strains heterozygous for recessive mutations in known cohesin regulators (Table 4.1). When GMR>DRAD21^{DM} was expressed in animals heterozygous for a null mutation in *sse*, the gene encoding SEPARASE, a significant, eye specific, enhancement of the DRAD21^{DM} phenotype was observed (Figure 4. 1). Halving the dose of *see* significantly enhanced both the size and organisation defects of the GMR>DRAD21^{DM} eye phenotype, to the extent that obvious ommatidial structures were no longer evident. Conversely, in individuals with a constitutional genotype heterozygous for a null-mutation in the cohesin loading factor Scc2 (NIPPED B) a significant suppression of the eye specific phenotype is observed (Figure 4.1). Halving the dose of *nippedB* significantly suppressed the GMR>DRAD21^{DM} size and organisation defects to a marked extent. Clear ommatidial structures are evident, particularly in the anterior-ventral region of the compound eye. These results indicate that the GMR>DRAD21^{DM} phenotype is suitably sensitive to identify second site modifiers of chromosome segregation.

To assess whether the phenotypic modification observed with *sse* and *nippedB* was broadly applicable to other genes involved in chromosome regulation, a range of known and predicted cohesin interactors were analysed (Table 4.1). The listed stocks (Table 4. 1) were crossed to the GMR>DRAD21^{DM} line and the eye phenotype in the affected progeny was scored. A number of different genetic alterations were tested and it was shown that modulation of the eye phenotype was not specific to the type of genetic lesion, with suppression and enhancement noted for a variety of aberrations. Interactions were classified as either enhancers or suppressors and also by strength of the interaction, in ascending order, with 1 indicating a relatively weak interaction and 4 a strong interaction. Importantly, some

of the tested alleles failed to modulate the GMR>DRAD21^{DM} phenotype, indicating that the genetic interactions observed are specific and consistent with previous studies where not all components of a given process are dose-sensitive.

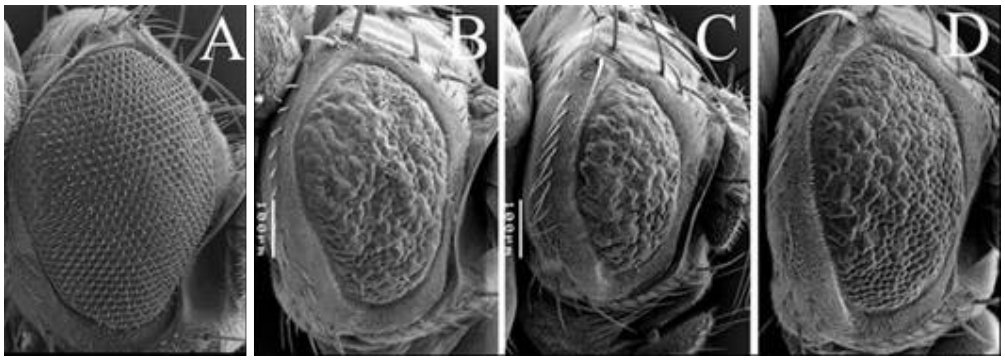

Figure 4. 1: *The GMR>DRAD21^{DM} eye phenotype can be modified by known cohesin regulators*

Scanning electron micrographs of adult *Drosophila* eyes. **A:** Wild-type eye (*w^{1118}*). **B:** Moderately disorganised eye resulting from expression of DRAD21^{DM} in the eye imaginal disc using the eye-specific GMR-Gal4 transgene. **C:** Enhancement of the phenotype shown in B caused by heterozygosity for a loss of function mutation in the *separase* gene. (D) Suppression of the GMR>DRAD21^{DM} phenotype shown in B caused by heterozygosity for a null mutation in the cohesin loading factor encoded by *nipped B*. Eyes are oriented with anterior to the right and dorsal side up. All are shown at the same magnification. Scale bar= 100µm.

Table 4. 1: Modulation of the GMR>DRAD21^{DM} eye phenotype by known and predicted cohesin interactors

Gene Name	Allele Tested	CG number	Mutation Type	Interaction	Strength	BL stock #
Scc3	*Dp(2;2)C619*	CG3423	Duplication	Enhancer	4	1065
mus209	*mus209^{k00704}*	CG9193	Insertion	Enhancer	3	10361
sumo2	*Df(3L)XDI98*	CG10107	Deficiency	Enhancer	2	4393
top2	*Df(2L)TW158*	CG10223	Deficiency	Enhancer	2	3784
separase	*Df(3L)CH18*	CG10583	Deficiency	Enhancer	1	6463
auroraB	*Df(2L)J39*	CG6620	Deficiency	Enhancer	1	1469
Grapes	*grp^{06034}*	CG17161	insertion	None	0	12219
sumo2	*CG10107^{KG05095}*	CG10107	insertion	None	0	13870
aurora	*aur^{87Ac-3}*	CG3068	amorphic	None	0	6188
thr	*thr^{3}*	CG5785	EMS generated	None	0	6275
Top1	*Df(3L)ri-XT1*	CG6146	deletion	None	0	5878
sZW10	*mit(1)15^{5}*	CG6600	amorphic	None	0	4282
mei-41	*mei-41^{2}*	CG4252	strong	None	0	4183
DTS3	*l(3)DTS3^{1}*	l(3)DTS3	EMS generated	None	0	3014
sumo2	*Dp(1;1)B^{S}TAG*	CG10107	duplication	None	0	4484
sumo	*CG10107^{KG05095}*	CG1010	Insertion	Suppressor	1	13870
fzy	*fzy^{1}*	CG4274	Point	Suppressor	1	2492
prod	*prod^{k08810}*	CG18608	Insertion	Suppressor	1	10814
lin 19	*lin19^{BG02329}*	CG1877	Insertion	Suppressor	1	12764
pasc	*wapl^{EY03441}*	CG3707	Insertion	Suppressor	2	15438
polo	*polo^{1}*	CG12306	Null	Suppressor	2	546
polo	*polo^{01673}*	CG12306	Insertion	Suppressor	2	11543
Pros26	*Pros26^{1}*	CG4097	Point	Suppressor	2	6182
pim	*pim^{IL}*	CG5052	Point	Suppressor	2	3117
cyclin B	*CycB^{2}*	CG3510	Deletion	Suppressor	3	6630
timeout	*Df(3R)ry619*	CG8148	Deficiency	Suppressor	3	6171
nipped B	*Nipped-B^{02047}*	CG17704	Insertion	Suppressor	4	11143
Scc3	*Df(2L)spd^{j2}*	CG3423	Deficiency	Suppressor	4	2414
mei-S332	*mei-S332^{1}*	CG5303	Truncation	Suppressor	4	671

4.2.2 GENOME-WIDE SCREEN FOR SECOND SITE MODIFIERS OF GMR>DRAD21^{DM} REDUCED AND DISORGANISED EYE PHENOTYPE

4.2.2.1 Overview

The 232 individual *Drosophila* deficiency strains that comprise the March 2004 deficiency kit were individually crossed to the GMR>DRAD21^{DM} recombinant stock in an effort to rapidly screen the *Drosophila* genome to determine genomic regions capable of modifying the GMR>DRAD21^{DM} phenotype. Due to the large number of crosses involved, the deficiency kit was screened in sections corresponding to the major linkage groups: the X chromosome, second chromosome, third chromosome and fourth chromosome. GMR>DRAD21^{DM} virgins were crossed to deficiency kit males bearing second, third and fourth chromosome deletions. In the case of X chromosome deletions, GMR>DRAD21^{DM} males were crossed to deficiency kit virgin females. All crosses to deficiency kit stocks were maintained at 25ºC due to the temperature sensitivity of the GMR>DRAD21^{DM} phenotype, and also due to the reduced fitness of many deficiency kit stocks at temperatures that deviate from 25ºC. The use of balancer chromosomes bearing dominant marker genes in both the test and deficiency kit stocks allowed the genotypes of each cross to be determined visually and a direct comparison of the effects of GMR>DRAD21^{DM} expression in the presence or absence of each chromosomal deficiency to be made. An alteration in the GMR>DRAD21^{DM} phenotype was deemed significant if all or the majority of affected siblings (those expressing GMR>DRAD21^{DM} in the presence of the deficiency) exhibited an eye specific phenotypic alteration that was not present in siblings carrying GMR>DRAD21^{DM} alone.

4.2.2.2 X-chromosome Deficiency Kit stocks that modify the GMR>DRAD21^{DM} phenotype

The X chromosome section of the Deficiency Kit used in this study deletes approximately 924 out of the total 1011 X chromosome polytene bands, thus providing approximately 91% coverage of the entire chromosome. The 44 stocks that were used to screen the X chromosome for modifiers of the GMR>DRAD21^{DM} phenotype are listed in Appendix 1. Figure 4. 2 shows an example of the crossing scheme employed for the identification of X chromosome GMR>DRAD21^{DM}

modifiers as well as a specific example of an interaction deemed significant based on the criterion given above (section 4.2.2.1).

Of the 44 deficiency kit deletions tested for the X chromosome, 12 deletion strains were observed to significantly modify the GMR>DRAD21^{DM} phenotype. Five deletions were found to enhance the eye specific phenotype, whilst the remaining seven deletions suppressed the phenotype (Table 4. 2). The deletions of two of the suppressor deletions, S158 (stock 940) and S82 (stock 944; see Table 4. 2), overlap significantly and suppress the GMR>DRAD21^{DM} phenotype to a similar extents (Figure 4. 3). Therefore the locus causing the suppression is likely to be common to in both deficiencies, reducing the total number of X chromosome suppressor regions to six.

Table 4. 2: X Chromosome modifiers of GMR>DRAD21^{DM} eye phenotype

BL Stock #	Chr	Deficiency	Break Points[±]	Unique Identifier[※]
939	1	Df(1)dm75e19	3C11;3E4	S72
940	1	Df(1)A113	3D6-E1;4F5	S158
944	1	Df(1)JC70	4C15-16;5A1-2	S82
945	1	Df(1)C149	5A8-9;5C5-6	S169
959	1	Df(1)HA85	10C1-2;11A1-2	S256
966	1	Df(1)N12	11D1-2;11F1-2	S79
971	1	Df(1)JA27	18A5;18D	S63
935	1	Df(1)JC19	2F6;3C5	E73
952	1	Df(1)C52	8E;9C-D	E185
957	1	Df(1)KA7	10A9;10F6-7	E277
964	1	Df(1)JA26	11A1;11D-E	E126
6217	1	Df(1)RR79	16C;16F	E157

[±] Break points are mapped cytologically, and the locations refer to polytene bands.

[※] Identifier used consistently throughout this study.

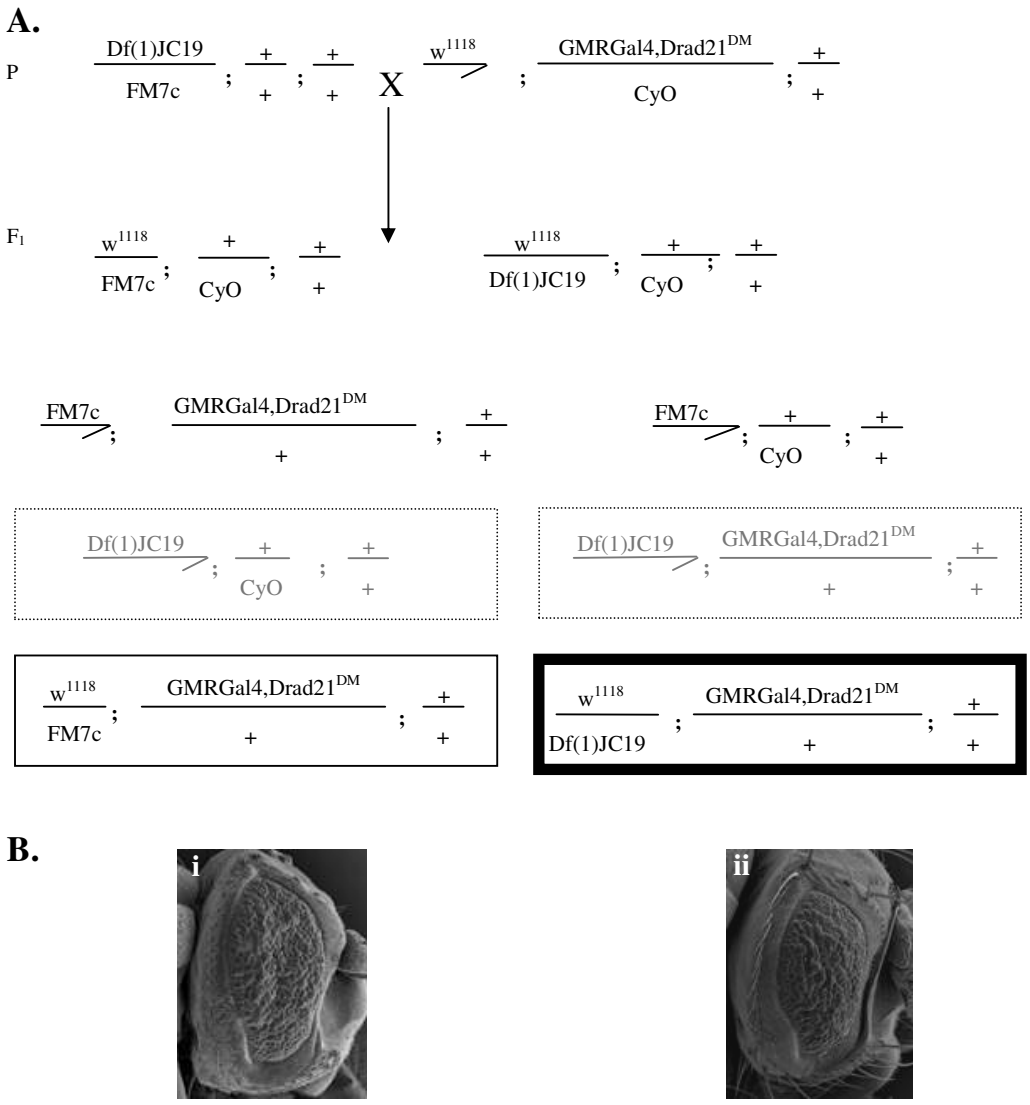

Figure 4. 2: *Identification of X chromosome modifiers of GMR>DRAD21^{DM}*

A: Females carrying X chromosome deletions (Df(1)JC19 in this example) were crossed to males carrying the GMR>DRAD21^{DM} recombinant chromosome. The F1 progeny, of which there are eight distinct classes, were examined visually. Comparison of individuals carrying both the deficiency and GMR>DRAD21^{DM} ("test class"; bold black box) with those carrying an X chromosome balancer and the GMR>DRAD21^{DM} chromosome ("control class"; black box) revealed whether the deficiency was capable of modifying the GMR>DRAD21^{DM} phenotype. F1 progeny classes that did not survive to adulthood due to the presence of the X chromosome deficiency are indicated in grey dotted boxes.
B: Example of GMR>DRAD21^{DM} phenotype (i) and 'test' progeny (ii). In this example the deficiency Df(1)JC19 enhances the small and rough eye phenotype shown in (i). This interaction was assigned the identifier E73.

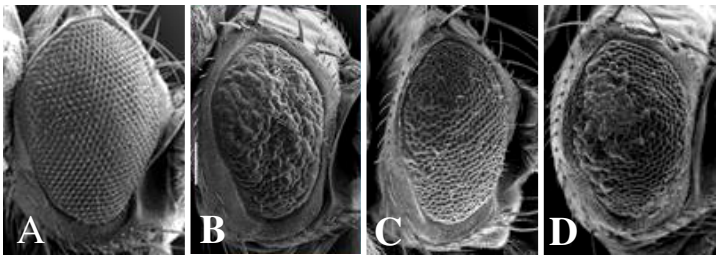

Figure 4. 3: *S82 and S158 suppress the GMR>DRAD21^{DM} eye phenotype to similar extents*

Scanning electron micrographs of adult *Drosophila* eyes, dorsal side is up and anterior to the right. **A:** The reduced and roughened eye phenotype of GMR>DRAD21^{DM}. **B** and **C:** The size and organisation defects of GMR>DRAD21^{DM} are strongly suppressed to similar extents by the introduction of Df(1)JC70 (S82) and Df(1)A113 (S158) respectively.

4.2.2.3 Second chromosome deficiency kit stocks that modify the GMR>DRAD21^{DM} phenotype

The second chromosome Deficiency Kit used in this study covered a minimum of 1788 out of 1936 polytene bands, thus providing approximately 92% coverage of the entire second chromosome. The 93 stocks that were used to screen the second chromosome for modifiers of the GMR>DRAD21^{DM} phenotype are listed in Appendix 1. Figure 4. 4 shows an example of the crossing scheme used for the identification of modifiers as well as a specific example of an interaction deemed significant based on the criteria listed in Section 4.2.2.1.

Of the 93 individual stocks carrying deletions tested for the second chromosome, 29 significantly modified the GMR>DRAD21^{DM} eye phenotype. 14 deficiencies were found to enhance the eye specific phenotype, whilst 15 deletions suppressed the phenotype (Table 4. 3).

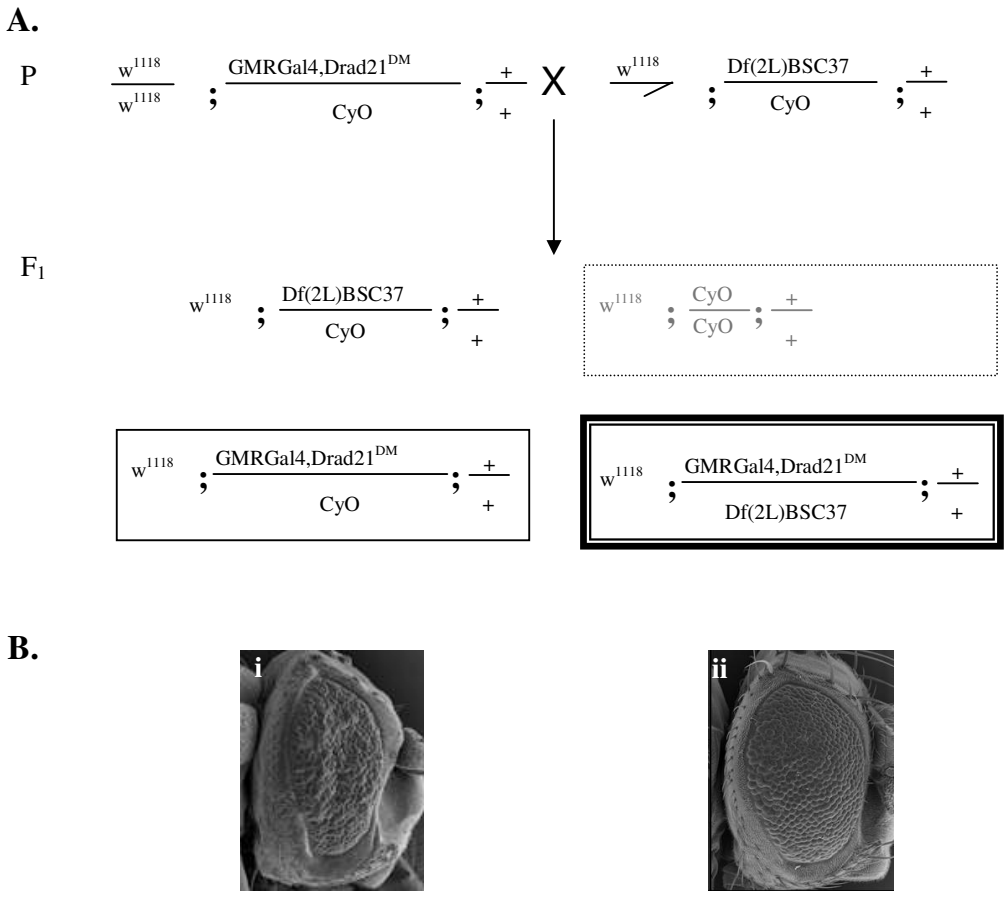

Figure 4. 4: Identification of second chromosome modifiers of GMR>DRAD21^{DM}

A: Males carrying second chromosome deletions (Df(2L)C144 in this example) were crossed to males carrying the GMR>DRAD21^{DM} recombinant chromosome. The F1 progeny, of which there are four distinct classes, were examined visually. Comparison of individuals carrying both the deficiency and GMR>DRAD21^{DM} ("test class"; bold black box) with those carrying a second chromosome balancer and the GMR>DRAD21^{DM} chromosome ("control class"; black box) revealed whether the deficiency was capable of modifying the GMR>DRAD21^{DM} phenotype. F1 progeny classes that did not survive to adulthood due to homozygosity for recessive lethal marker(s) on the CyO chromosome are indicated in grey dotted boxes. Individuals carrying the deficiency over a balancer chromosome were identified by their wild-type eyes and were not analysed further (unboxed).
B: Example of GMR>DRAD21^{DM} eye phenotype (i) and 'test' progeny (ii). In this example the deficiency is Df(2L)C144, and is clearly suppressing the small and rough eye phenotype evident in (i). This interactor was assigned the identifier S81.

Table 4. 3: Second chromosome modifiers of the GMR>DRAD21^{DM} phenotype

BL Stock #	Chr	Deficiency	Break Points[±]	Unique Identifier[*]
7144	2	Df(2L)BSC37	22D2-3;22F1-2	S101
90	2	Df(2L)C144	22F3-4;23C3-5	S81
693	2	Df(2L)sc19-8	24C2-8;25C8-9	S279
6299	2	Df(2L)BSC5	26B1-2;26D1-2	S107
2414	2	Df(2L)spd[j2]	27C1-2;28A	S103
5420	2	Df(2L)Dwee1-W05	27C2-3;27C4-5	S48
2583	2	Df(2L)cact-255rv64	35F-36A;36D	S168
420	2	Df(2L)TW137	36C2-4;37B9-C1	S78
198	2	Df(2R)H3C1	43F;44D3-8	S150
201	2	Df(2R)H3E1	44D1-4;44F12	S127
4966	2	Df(2R)w45-30n	45A6-7;45E2-3	S61
1743	2	Df(2R)B5	46A;46C	S239
3518	2	Df(2R)Jp1	51D3-8;52F5-9	S67
757	2	Df(2R)P34	55E2-4;56C1-11	S164
6866	2	Df(2R)BSC26	56C4;56D6-10	S91
6608	2	Df(2L)BSC16	21C3-4;21C6-8	E276
1567	2	Df(2L)JS17	23C1-2;23E1-2	E240
5330	2	Df(2L)ed1	24A2;24D4	E92
6374	2	Df(2L)BSC7	26D10-E1;27C1	E94
4956	2	Df(2L)XE-3801	27E2;28D1	E151
7147	2	Df(2L)BSC41	28A4-B1;28D3-9	E100
3366	2	Df(2L)J2	31B;32A	E281
3079	2	Df(2L)Prl	32F1-3;33F1-2	E159
739	2	Df(2R)M41Aa4	41A;41A	E134
1007	2	Df(2R)nap9	42A1-2;42E6-F1	E60
1702	2	Df(2R)X1	46C;47A1	E64
190	2	Df(2R)en-A	47D3;48B2	E274
442	2	Df(2R)CX1	49C1-4;50C23-D2	E68
3520	2	Df(2R)Jp8	53F5-9;52F10-53A1	E71

[±] Break points are mapped cytologically, and the locations refer to polytene bands.

[*] Identifier used consistently throughout this study.

4.2.2.3.1 Redundancy in the number of interacting regions on the second chromosome

Screening the second chromosome using the deficiency kit identified 29 deficiency kit stocks capable of significantly modifying the GMR>DRAD21^{DM} phenotype. Although the stocks of the deficiency kit are chosen to have minimal overlap, it remains possible that some of the identified interacting deletions may be removing the same locus as another deletion and, therefore, that the number of interacting deficiency kit stocks is not an accurate reflection of the total number of interacting loci. In order to address this possible over-estimation of GMR>DRAD21^{DM} interactors, the breakpoints of the interacting deficiencies were analysed, and the strength of interaction compared for overlapping deficiencies that both modify the GMR>DRAD21^{DM} phenotype. Below are the results of such analysis for six individual interacting deficiencies, which are likely to represent three interacting genomic regions.

Df(2L)cact-255rv64 and Df(2L)TW137 (interactions S168 and S78, see Table 4. 3) have the breakpoints 35F-36A;36D and 36C2-4;37B9-C1 respectively. These breakpoints significantly overlap and both S168 and S78 moderately suppress the GMR>DRAD21^{DM} size defect whilst only weakly suppressing the organisation defect (Figure 4.6). It is likely, therefore, that the primary interacting locus falls within the region of the genome that is common to both deletions. In addition, the deletion Df(2L)spd^{j2} completely spans that of Df(2L)Dwee1-W05 (S103 and S48 respectively). The suppression phenotypes of S103 and S48 strongly suppress both the size and organisation defects of GMR>DRAD21^{DM} (Figure 4. 5), suggesting that the suppression observed in these two cases are predominantly due to the one locus. The S48 interaction is not quite as strong as that of S103 and it remains possible that there are additional loci influencing the interaction that are unique to the S103 deletion Df(2L)spd^{j2}. Finally enhancer regions E151 and E100 significantly overlap, with breakpoints of 27E2;28D1 and 28A4-B1;28D3-9 respectively. Both of these deletions significantly enhance both the size and organisation defects of the GMR>DRAD21^{DM} phenotype (Figure 4. 5), and it is likely that the primary interacting locus falls within a region of the genome common to both deletions.

Taken together these data reduce the number of likely GMR>DRAD21^{DM} interacting regions on the second chromosome from an initial estimate of 29 to 26.

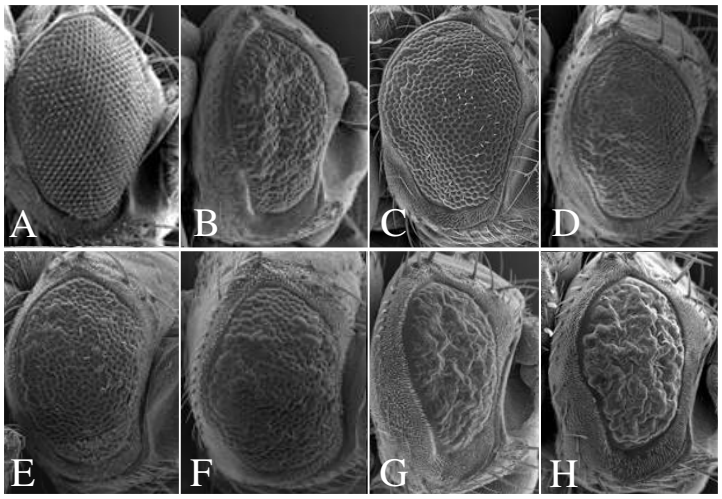

Figure 4. 5: Overlapping deficiencies modify GMR>DRAD21^{DM} to similar extents

A: wild-type (w^{1118}) eye. **B:** The GMR>DRAD21 small and rough eye. **C-H:** Modification of the GMR>DRAD21^{DM} small and rough eye by chromosome 2 deficiencies. **C** and **D:** Strong suppression mediated by regions S103 and S48 respectively. These deficiencies suppress the eye phenotype dramatically. **E** and **F:** Moderate-strong suppression phenotypes of S168 and S78 respectively, note that in both cases the eye appears round and organised. **G** and **H:** Moderate to strong enhancement of both the GMR>DRAD21^{DM} size and organisation defects mediated by both E100 and E151 (G and H respectively).

4.2.2.4 Third chromosome deletions that modify the GMR>DRAD21^{DM} phenotype

The third chromosome Deficiency Kit used in this study deletes a minimum of 1834 out of 2062 polytene bands, thus providing approximately 89% coverage of the entire third chromosome. The 93 stocks that were used to screen the third chromosome for modifiers of the GMR>DRAD21^{DM} eye phenotype are listed in Appendix 1. Figure 4. 6 shows an example crossing scheme employed for the identification of modifiers as well as a specific example of an interaction deemed significant based on the criteria listed in Section 4.2.2.1.

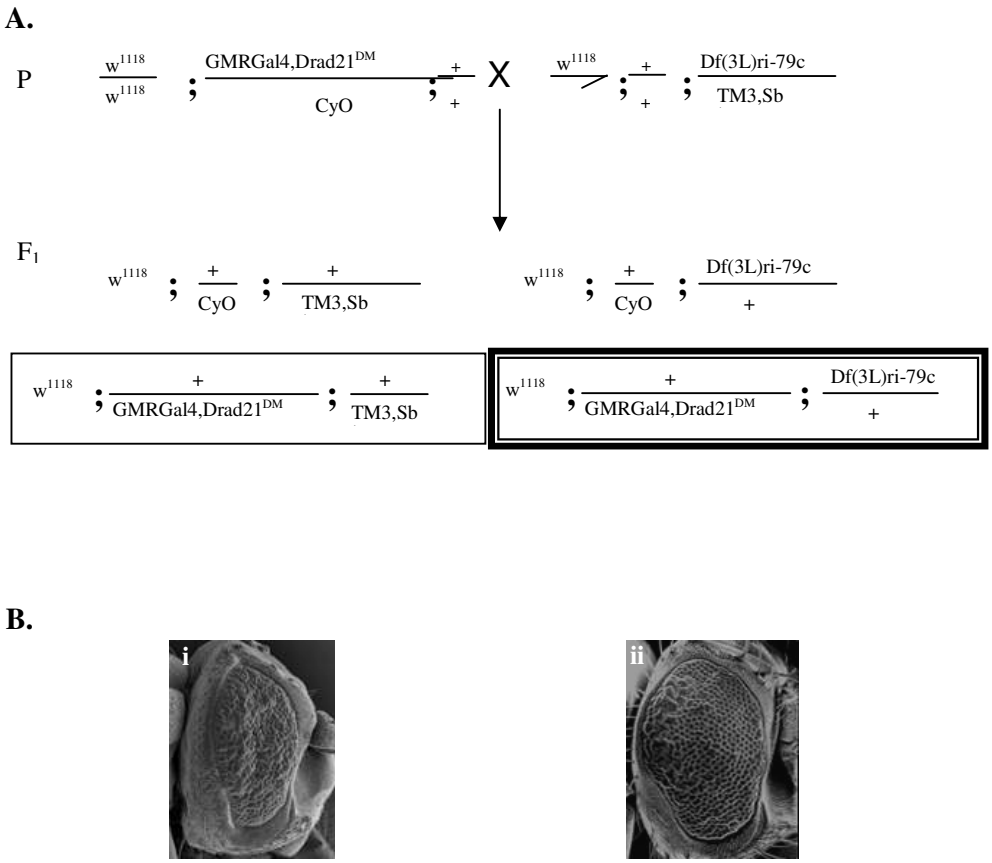

Figure 4. 6: *Identification of third chromosome modifiers of GMR>DRAD21^{DM}*

A: Males carrying third chromosome deletions (Df(3L)ri-79c in this example) were crossed to males carrying the GMR>DRAD21^{DM} recombinant chromosome. The F1 progeny, of which there are four distinct classes, were examined visually. Comparison of individuals carrying both the deficiency and GMR>DRAD21^{DM} ("test class"; bold black box) with those carrying a third chromosome balancer and the GMR>DRAD21^{DM} chromosome ("control class"; black box) revealed whether the deficiency was capable of modifying the GMR>DRAD21^{DM} phenotype. Individuals carrying the deficiency over a balancer chromosome or two balancer chromosomes were identified visually and were not analysed further (unboxed).
B: Example of GMR>DRAD21^{DM} phenotype (i) and 'test' progeny (ii), in this case the deficiency is Df(3L)ZP1, and is clearly suppressing the small and rough eye phenotype evident in (i). This interaction was assigned the identifier S93.

Of the 91 individual deletions tested for the third chromosome, 21 were found to significantly modify the GMR>DRAD21^{DM} phenotype. Nine of these deletions enhanced the eye specific phenotype, whilst the remaining 12 deletions suppressed the phenotype (Table 4. 4).

Table 4. 4: Third Chromosome modifiers of the GMR>DRAD21^{DM} eye phenotype

BL Stock #	Chr	Deficiency Name	Break Points[±]	Unique Identifier[※]
5877	3	Df(3L)ZP1	66A17-20;66C1-5	S93
6471	3	Df(3L)BSC14	67E3-7;68A2-6	S84
2612	3	Df(3L)vin7	68C8-11;69B4-5	S122
6457	3	Df(3L)BSC12	69F670A1;70A1-2	S98
6551	3	Df(3L)XG5	71C2-3;72B1-C1	S86
3128	3	Df(3R)M-Kx1	86C1;87B1-5	S120
3007	3	Df(3R)ry615	87B11-13;87E8-11	S128
3011	3	Df(3R)Cha7	90F1-F4;91F5	S123
4962	3	Df(3R)H-B79	92B3;92F13	S132
4940	3	Df(3R)mbc-30	95A5-7;95C10-11	S119
2585	3	Df(3R)mbc-R1	95A5-7;95D6-11	S124
823	3	Df(3R)D605	97E3;98A5	S105
5492	3	Df(3L)eyg[C1]	69A4-5;69D4-6	E95
3640	3	Df(3L)brm11	71F1-4;72D1-10	E161
5126	3	Df(3L)XS533	76B4;77B	ES129
3127	3	Df(3L)ri-79c	77B-C;77F-78A	E170
5878	3	Df(3L)ri-XT1	77E2-4;78A2-4	E97
4506	3	Df(3L)Ten-m-AL29	79C1-3;79E3-8	E155
1968	3	Df(3R)p712	84D4-6;85B6	E133
1962	3	Df(3R)p-XT103	85A2;85C1-2	E104
2425	3	Df(3R)e-N19	93B;94	E125

[±] Break points are mapped cytologically, and the locations refer to polytene bands.

[※] Identifier used consistently throughout this study.

4.2.2.4.1 Redundancy in the number of interacting regions on the third chromosome

Screening the third chromosome using the deficiency kit identified 21 separate deletions capable of significantly modifying the GMR>DRAD21^{DM} phenotype. In order to address possible redundancy of GMR>DRAD21^{DM} interactors (as discussed above in section 4.2.2.3.1), the breakpoints of the interacting deficiencies were analysed, and the strength of GMR>DRAD21^{DM} interaction was compared for any overlapping deficiencies. Of the third chromosome interactors, only two individual interacting deficiencies, are likely to represent a single interacting genomic locus. Df(3R)p712 and Df(3R)p-XT103 (stocks E133 and E104, see Table 4. 4) have the breakpoints 84D4-6;85B6 and 85A2;85C1-2 respectively. These breakpoints significantly overlap and both E133 and E104 moderately enhance the GMR>DRAD21^{DM} size defect whilst having little if any effect on the organisation defect (Figure 4. 7). It is likely, therefore, that the primary interacting locus falls within the region of the genome that is common to both deletions. This reduced the number of interacting regions on the third chromosome to 20.

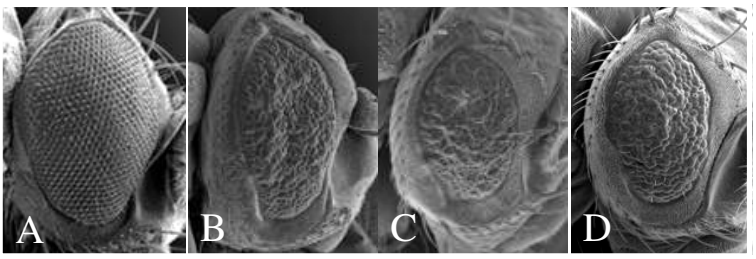

Figure 4. 7: *Overlapping deficiencies modify GMR>DRAD21^{DM} to similar extents*

A: wild-type (*w^{1118}*) eye. **B:** The GMR>DRAD21 small and rough eye. **C** and **D:** moderate-strong enhancement mediated by regions S103 and S48 respectively. These deficiencies enhance the size defect of the GMR>DRAD21^{DM} eye phenotype, but have little to no effect on the organisation defect.

4.2.2.5 Fourth chromosome deletions that modify the GMR>DRAD21^{DM} phenotype

The fourth chromosome of *Drosophila melanogaster* is approximately 1.2 Mb in size and roughly accounts for 1% of the entire genome (the euchromatic portion of the genome is ~120 Mb (Adams et al., 2000)). Given its small size and the lack of markers the fourth chromosome is often ignored or excluded from genetic studies. The fourth chromosome Deficiency Kit used in this study deletes a minimum of 16 out of 45 polytene bands, thus providing approximately 36% coverage of the entire chromosome. None of the four deletions tested for chromosome four were observed to modify the GMR>DRAD21^{DM} eye phenotype.

4.2.3 PHENOTYPIC SUB-CATEGORIES OF GMR>DRAD21^{DM} MODULATION

4.2.3.1 Overview

Consistent with the results obtained with the pilot screen (Table 4. 1), the degree of interaction observed within each of the general categories of enhancer and suppressor varied quite significantly. Although assigning individual modifiers to either enhancer or suppressor categories was mostly straightforward, occasionally difficulties were encountered. Although assignment of modifiers to categories is highly subjective, classification served the purpose of ordering, or structuring, the genome-wide screen data and to provide a foundation for further analysis.

4.2.3.2 Suppressors clearly fall into six phenotypic classes

Detailed examination of the Scanning Electron Micrographs generated for each of the suppression interactions allowed each of them to be assigned to one of six different phenotypic classes: strong suppression, moderate-strong suppression, mixed, and three classes of weak suppression (numbered 1-3). Table 4.5 presents an example and description of each phenotypic class. Strong, moderate-strong and mixed suppressors are shown in Figure 4.8, and the three classes of weak suppressors are shown in Figure 4.9.

Table 4. 5: Suppressor interactions fall into six phenotypic classes

Suppressor Class	Example	Description
Strong	S103	Increased both the size and organisation Resultant eye phenotype almost wild-type in appearance
Moderate-strong	S81	Increased both size and organisation but not to the same extent as interactors in the strong suppressor category
Mixed	S93	Moderately increased the size and organisation of the eye. Had an additional distinct overgrowth phenotype
Weak 1	S120	Weakly suppressed both the size and organisation of the eye
Weak 2	S127	Weakly suppressed only the size defect
Weak 3	S128	Very weakly suppressed both the size and organisation. Had an additional increase in the number of bristles in the adult eye

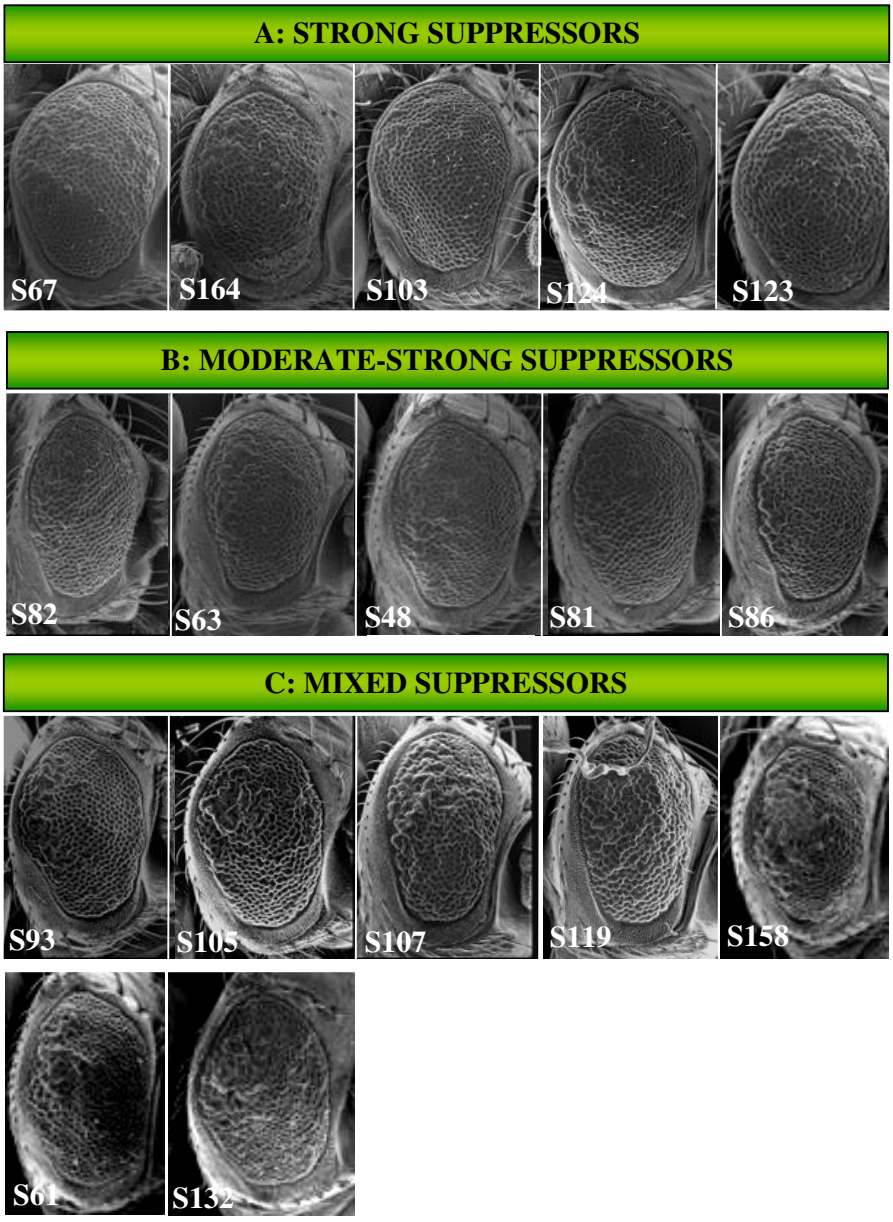

Figure 4. 8: *Strong, Moderate-Strong and Mixed suppressor classes*

A: Strong suppressors dramatically increased the size and organisation of the GMR>DRAD21^{DM} eye phenotype. Five suppressor interactions, S67, S164, S103, S124 and S123 were placed in this category. **B:** Moderate-strong suppressors also significantly increased both the size and organisation of the eye, however not to the same extent as strong suppressors. Five suppressor interactions, S82, S63, S48, S81 and S86 were placed in this category. **C:** Mixed suppressors increased the size and organisation of the eye and also exhibited a distinct overgrowth phenotype in the posterior region of the eye, usually occurring more dorsally. The seven suppressors that belong to this category were S93, S105, S107, S119, S158, S61 and S132.

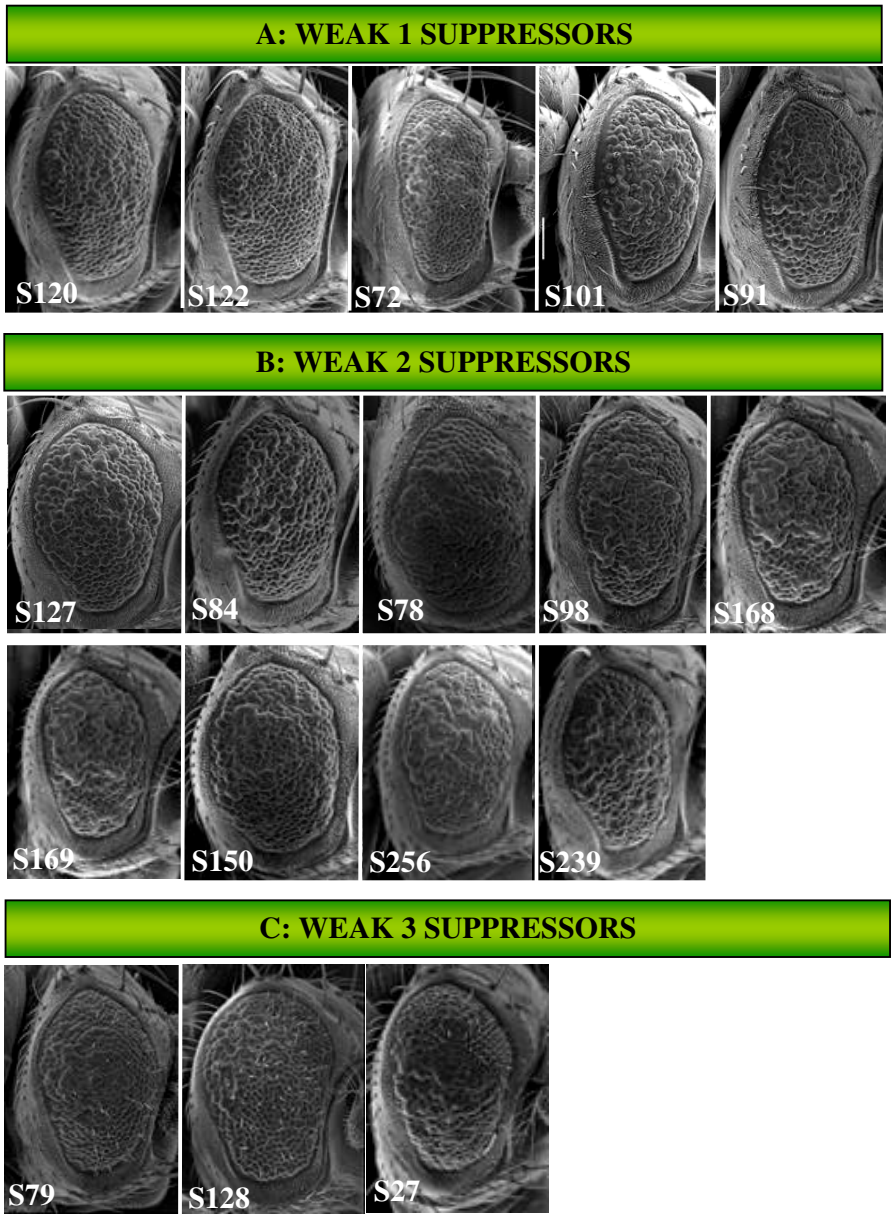

Figure 4. 9: *Weak1, Weak 2 and Weak 3 suppressor classes*

A: Weak 1 suppressors moderately increased both the size and organisation of the GMR>DRAD21^{DM} eye phenotype. Five suppressor interactions, S120, S122, S72, S101 and S91 were placed in this category. **B:** Weak 2 suppressors also moderately increased the size of the eye, however they had little to no effect on the organisation of the ommatidial array. Nine suppressor interactions, S127, S84, S78, S98, S168, S169, S150, S256 and S239 were placed in this category. **C:** Weak 3 suppressors moderately increased the size and organisation of the eye and also weakly suppressed the GMR>DRAD21^{DM} bristle defect. The three suppressors belonging to this category were S79, S128 and S27.

4.2.3.3 Enhancers fall into three phenotypic classes

Detailed examination of the Scanning Electron Micrographs generated for each of the enhancer interactions allowed each of them to be broadly assigned to one of three different phenotypic classes: strong enhancement, moderate enhancement and weak enhancement. Table 4. 6 presents an example of each phenotypic class and a description of each category. Strong and moderate enhancers are shown in Figure 4. 10, and weak enhancers are shown in Figure 4. 11.

Table 4. 6: Enhancer interactions fall within three broad categories

Enhancer Class	Example	Description
Strong	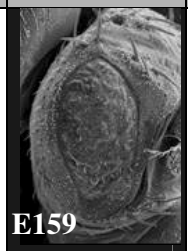	Strongly decreased both the size and organisation
Moderate		Decreased the size and organisation of the eye resulting in a slight protrusion of eye material
Weak	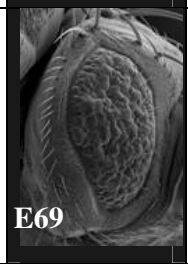	Slightly decreased the size and/or organisation of the eye neither to any great extent

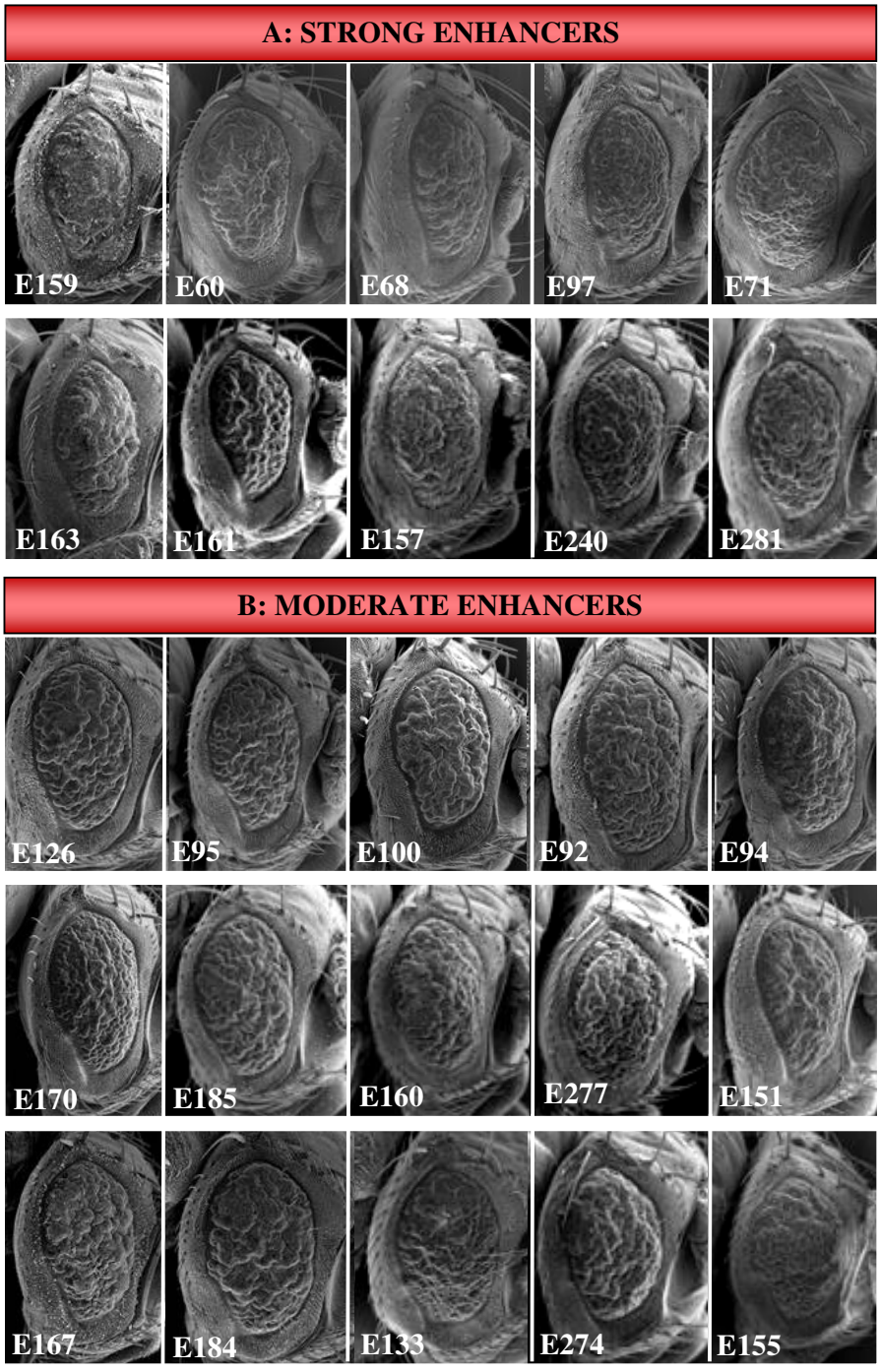

Figure 4. 10: Strong and moderate enhancer classes

A: Strong enhancers decrease both the organisation and size of the GMR>DRAD21^{DM} eye phenotype quite dramatically. The ten enhancers that fall into this category are E159, E60, E68, E97, E71, E163, E161, E157, E240 and E281. **B:** Moderate enhancers also decrease the size and organisation of the eye and have a distinct 'globby' appearance. The fifteen enhancers that fall into this category are E126, E95, E100, E92, E94, E170, E185, E160, E277, E151, E167, E184, E133, E274 and E155.

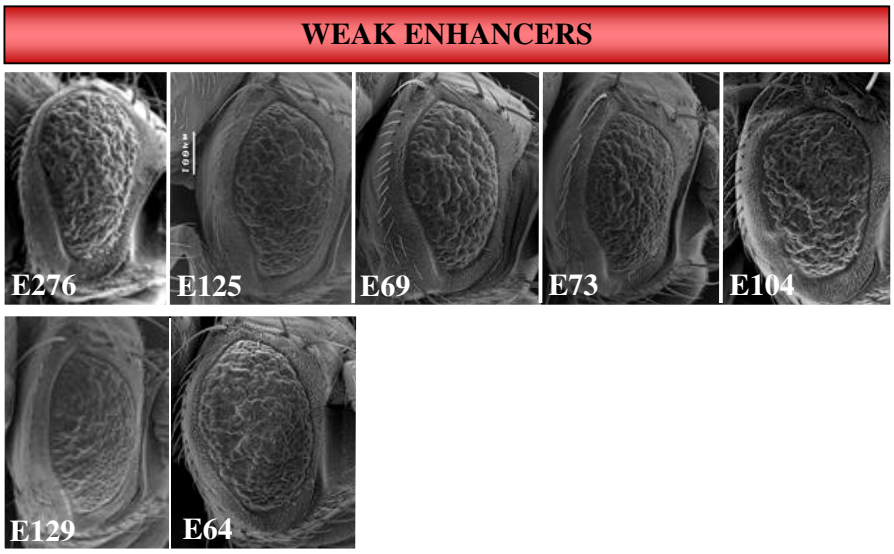

Figure 4. 11: *Weak enhancer class*

Interactors were classed as weak enhancers if they slightly enhanced the size and/or organisation defects of the GMR>DRAD21^{DM} phenotype, but neither to any great extent. The seven enhancer interactions that fall into this category were E276, E125, E69, E73, E104, E129 and E64.

4.2.4 SECOND-PASS SCREENING TO ELIMINATE MODIFIERS OF APOPTOSIS

As it had been demonstrated that the reduced and roughened GMR>DRAD21^{DM} was at least in part caused by increased levels of apoptosis (Section 3.2.4.3) a second-pass screening strategy was employed to identify modifiers that were acting via modulation of apoptotic pathways. Interacting deficiencies were crossed to a P{GMRhid}-SM1 (Kurada and White, 1998) fly line, which has a small eye phenotype caused by increased apoptosis in the developing eye (Figure 4. 12C). Expression of GMR>DRAD21^{DM} in the GMRhid background strongly enhanced the GMRhid eye phenotype (Figure 4. 12D), indicating that this screen would be successful at identifying modifiers of apoptosis.

Deficiency Kit stocks found to be capable of modifying the GMRhid phenotype in a similar way in which they modulated the GMR>DRAD21 ^{DM} phenotype (for example, suppressing both eye phenotypes) were assumed to be altering the GMR>DRAD21^{DM} phenotype by modulating apoptosis and were excluded from further analysis. Using these criteria modifier stocks, representing 9 interacting regions, were eliminated from further analysis (Table 4. 7). These included seven enhancer regions and two suppressor regions (see Figure 4. 12 for examples). Interestingly stocks that were grouped together as deleting the same interacting locus behaved consistently in the second-pass screen, supporting the initial assumption (E100 and E151 for example).

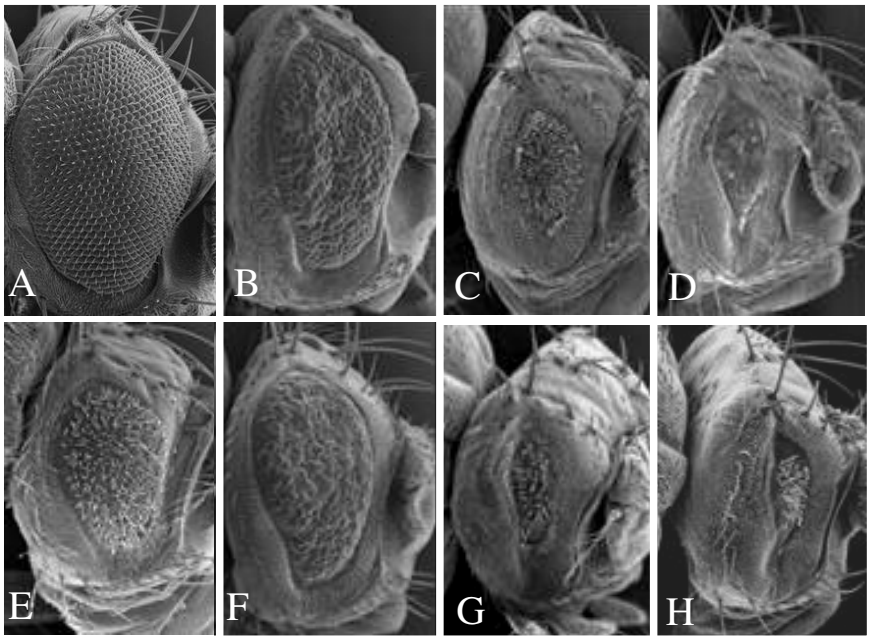

Figure 4. 12: *Second-pass screening to identify modifiers of apoptosis*

Scanning electron micrographs of adult *D. melanogaster* eyes. Dorsal is to the top, posterior to the left. **A:** w^{1118} used as the wild-type control in this study. **B:** The GMR>DRAD21^{DM} small and roughened eye used to screen the deficiency kit for modifiers. **C:** The GMRhid eye phenotype was used to determine which of the interactors identified in the genome-wide screen modulate apoptosis. **D:** Increasing apoptosis in this genetic background by expressing GMR>DRAD21^{DM} enhances the size defect and results in no obvious ommatidial structures are evident. **E** and **F:** Two regions of the genome that suppress the GMR>DRAD21^{DM} eye phenotype also suppress the GMRhid eye phenotype (S123 and S127 respectively). **G** and **H:** Seven genomic regions capable of enhancing the GMR>DRAD21^{DM} eye phenotype when present in only one copy also significantly enhance the GMRhid eye phenotype, examples of E94 and E126 (Df(1)JA26) are shown in **E** and **F** respectively. All images are shown at the same magnification.

Table 4. 7: Modifiers eliminated from further analysis due to alteration of the GMRhid phenotype

BL stock#	Df name	Chr	Interaction Name	GMRhid Interaction
952	Df(1)C52	1	E185	lethal
964	Df(1)JA26	1	E126	enhanced
5330	Df(2L)ed1	2	E92	enhanced
6374	Df(2L)BSC7	2	E94	enhanced
4956	Df(2L)XE-3801	2	E151	enhanced
7147	Df(2L)BSC41	2	E100	enhanced
442	Df(2R)CX1	2	E68	enhanced
1968	Df(3R)p712	3	E133	enhanced
1962	Df(3R)p-XT103	3	E104	enhanced
201	Df(2R)H3E1	2	S127	suppressed
3011	Df(3R)Cha7	3	S123	suppressed

4.3 DISCUSSION

4.3.1 SUITABILITY OF THE GMR> DRAD21^{DM} EYE PHENOTYPE FOR USE IN A GENETIC SCREEN

The reduced and roughened eye phenotype produced upon GMR>DRAD21^{DM} overexpression was found to be dose sensitive, and capable of being modified by a number of known cohesin regulators. A global reduction in the loading of the cohesin complex onto chromatin caused by halving the dose of the NIPPED B cohesin loading factor was found to suppress the reduced and rough eye phenotype, whilst decreasing the genetic dose of *separase* enhanced the phenotype (Figure 4.1). A molecular model for the enhancing and suppressing effects of halving the dose of *Sse (separase)* and *NippedB* is presented in Figure 4.13. These results demonstrated the suitability of this phenotype for use in a genetic screen for regulators of chromosome segregation in *Drosophila*.

In metazoan species the majority of cohesin dissociates from chromosome arms in a separase independent manner before metaphase (Waizenegger et al., 2000). The presence of non-cleavable DRAD21 is therefore expected to only affect the minor centromeric pool of cohesin that is thought to maintain centromeric cohesion from prophase until the metaphase to anaphase transition. DRAD21^{DM} containing cohesin complexes would be expected to strengthen centromeric cohesion between sister-chromatids yet have little or no effect on the regulation of cohesin loaded onto chromosome arms. It is reasonable to assume therefore, that loci capable of suppressing the GMR>DRAD21^{DM} phenotype are likely to act by reducing the strength of cohesion, either globally (as is the case of Scc2 (NIPPED B)) or in the vicinity of the centromere. An example of the latter is the *MeiS332* mediated suppression observed (Table 4.1). MEI-S332 is the founding member of a family of proteins with roles in protecting centromeric cohesin in both mitosis and meiosis (for recent review see Lee et al., 2005). Reducing the amount of functional MEI-S332 through *mei-S332^{1}* heterozygosity was observed to weaken centromeric cohesion (LeBlanc et al., 1999, Lee et al., 2004), presumably by failing to protect this pool from the separase-independent prophase dissociation pathway. In the context of GMR>DRAD21^{DM} expression, reduction of MEI-S332 activity and therefore

reduction in the strength of centromeric cohesion acted to suppress the small and roughened eye phenotype of GMR>DRAD21^{DM}.

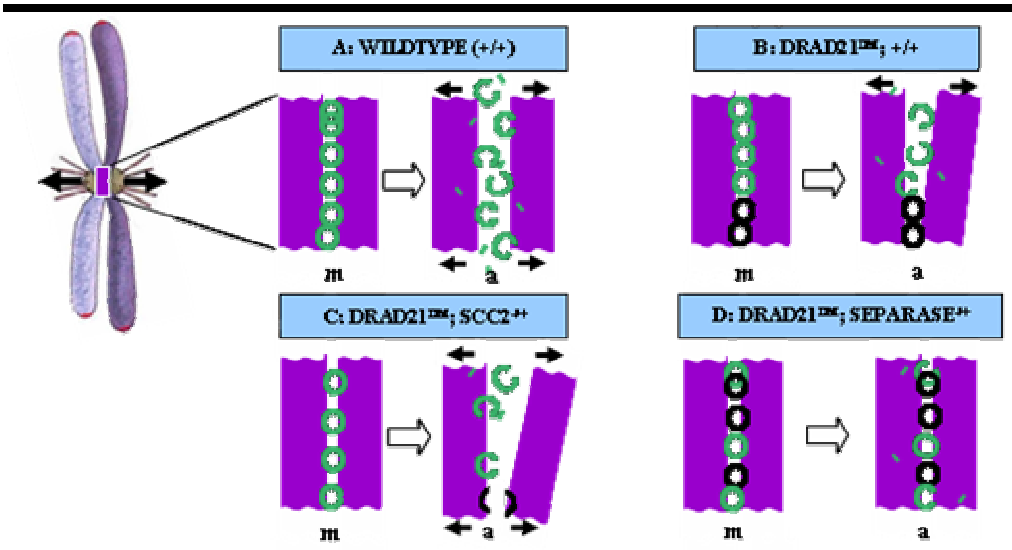

Figure 4. 13: *Model for enhancement/suppression by separase and scc2*

A: In a wild-type background, wild-type cohesin (green circles) maintains sister chromatid cohesion at metaphase in the vicinity of the centromere, with cleavage of the DRAD21 component of cohesin in anaphase (a). **B:** Expression of DRAD21^{DM} causes a proportion of cohesin to be cleavage-resistant (black circles) leading to a failure of chromatid separation at anaphase. **C:** Heterozygosity for the cohesin loading factor SCC2 causes a global reduction in both wild-type and DRAD21^{DM} -containing cohesin, allowing more cells to correctly separate their sister-chromatids in anaphase. The cohesion mediated by DRAD21^{DM}-containing cohesin may be able to be overcome by the pulling forces of the spindle to allow fir chromosome segregation in some cells. **D:** Heterozygosity for separase, the enzyme that cleaves DRAD21, causes a global reduction in DRAD21 cleavage, increasing the number of cells that fail to accurately segregate their genome, leading to and increased level of cell death.

In contrast to suppressor loci, enhancer loci may be acting in a number of ways, these could include decreasing the amount of cleavage of the wild-type DRAD21 containing complexes, as was observed for Separase, or by further increasing the strength of cohesin. Indeed any loci that have the result of preventing or decreasing the prophase dissociation of the cohesin complex should behave as an enhancer. Using the GMR>DRAD21^{DM} phenotype in a genetic screen is, therefore, likely to provide insight into the differential regulation of both arm and centromeric cohesin.

Interestingly, whilst a deficiency that removes *Sumo2* dominantly enhances the GMR>DRAD21^{DM} eye phenotype, duplication of the same region, and heterozygosity for an insertion allele do not modify the phenotype (Table 4.1). These results indicate that it is the deletion of another locus, and not the deletion of *sumo2* that is interacting with the non-cleavable form of DRAD21 in these flies. Alternatively, the interaction may indeed be due to the deletion of *sumo2*, but the insertion allele of *sumo2* that was tested failed to modify the GMR>DRAD21^{DM} phenotype as it is not functioning as a null allele. As P-element insertions have a general tendency to only partially inhibit gene function (Spradling et al., 1995), it is likely that the *CG10107*^{KG05095} insertion allele tested in this case is behaving as a hypomorphic allele and not a complete null. These results highlight the difficulties faced when using deficiencies to identify interacting genomic regions, and identifying the causative loci.

4.3.2 SUMMARY OF GENOME WIDE SCREEN USING THE DEFICIENCY KIT

As previously described in Section 4.2.2.1, an interaction was deemed significant if all or the majority of the affected siblings exhibited the eye-specific phenotypic alteration. Using these criteria 62 genomic regions, spanning chromosomes X, 2 and 3, were identified as containing loci capable of modifying the GMR>DRAD21^{DM} eye phenotype. Analysis of the breakpoints of the associated deletions and comparison of the strength of the interactions observed (in the case of overlapping deletions) allowed the number of interacting regions to be refined to 57. 31 of these regions contain suppressor loci, whilst the remaining 26 harbour enhancer loci. Whilst no interacting regions were identified on chromosome 4, this is likely a reflection of the poor representation of this chromosome in the current Deficiency Kit. Figure 4.14 shows that aside from chromosome four, interacting loci were observed to be distributed across the remainder of the genome, and that the screen did not detect any major clustering of loci.

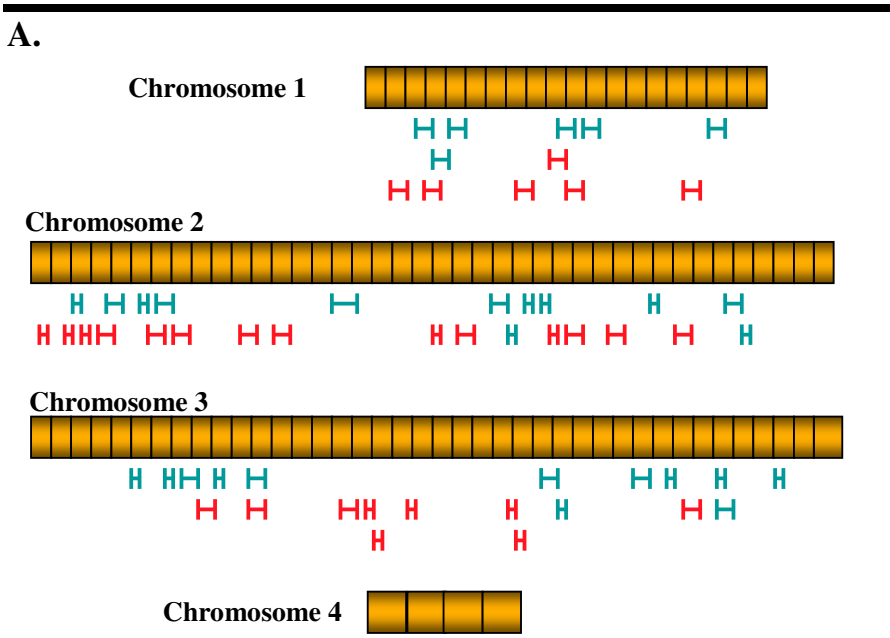

Figure 4. 14: *Suppressor and enhancer regions occur throughout the genome*

A: The divisions of each chromosome are indicated and approximate positions of interacting deficiencies are shown as green (suppressors) and red (enhancers) brackets.
B: The total minimum number of polytene bands represented by each of the interacting regions was determined for both suppressors and enhancers. These are presented as a percentage of the total number of polytene bands per chromosome, and shows that each of the three major linkage groups were sampled evenly in the genome-wide screen.

Each of the interacting regions identified are likely to contain at least one locus that is acting to modify the reduced and roughened eye phenotype and thus likely to be involved in the regulation of sister-chromatid cohesion and chromosome segregation. If we assume that each interaction is due to a single locus, which given the density of interactors will be true for the majority of the interacting regions, then we can state that approximately 57 interacting loci were identified by screening ~90% of the genome. As the *Drosophila* genome has been estimated to contain 14 000 genes (Adams et al., 2000), screening 90% of the genome means that approximately 12 600 genes for were tested for their ability to dominantly modify the GMR>DRAD21^{DM} phenotype. Consequently only 57/12600 (0.45%) of the genome was observed to interact with GMR>DRAD21^{DM}. Based on this calculation it is estimated that were it possible to screen the remaining 10% of the genome an additional 6 interacting regions/loci would be expected to be found.

4.3.3 POTENTIAL IDENTIFICATION OF NOVEL PRO AND ANTI-APOPTOTIC GENES

The focus of this study was to identify novel regulators of chromosome segregation. The GMRhid second-pass screen was utilised to eliminate genetic modifiers that also significantly modified the levels of apoptosis in the GMRhid background as assessed by eye phenotype. Interacting regions eliminated from further analysis in this study based on the results of the second-pass screen may be useful in the identification of novel regulators of apoptosis. Two examples in which this may be the case are discussed below.

The enhancer region on the X chromosome responsible for the E185 interaction (Table 4.7) was lethal in combination with the GMRhid chromosome. This could possibly be due to the presence of an anti-apoptotic gene within this region, the removal of which results in levels of cell death incompatible with viability. The deficiency responsible for the E185 deletion (Df(1)C52) has the breakpoints 8E;9C-D, deleting a minimum of 106 genes. Analysis of the annotations of the genes in this region does not reveal any obvious anti-apoptosis candidates, indicating that it is possible that there is a novel anti-apoptotic gene in this region.

Suppressor region S127 strongly suppressed the GMRhid eye phenotype (Figure 4.12). This level of suppression could be attributed to the presence of a pro-

apoptotic gene within this region, the deletion of which decreases the levels of cell death occurring in the cells expressing GMRhid. The deficiency responsible for the S127 interaction (Df(2R)H3E1) has the breakpoints 44D1-4;44F12, deleting a minimum of 84 genes. Analysis of the annotations of the genes in this region does not reveal any obvious pro-apoptotic candidate genes, indicating there may be a previously undescribed pro-apoptotic gene in this region. Identification and analysis of the genomic regions eliminated from further analysis in this study may identify the postulated novel regulators of apoptosis. In addition, such analysis could potentially provide a substantive link between cohesin, in particular the DRAD21 component, and apoptosis in *Drosophila*.

More exciting prospects arising from the genome-wide screen presented in this chapter are identifying the genes responsible for modifying GMR>DRAD21^{DM} at the molecular level. Such genes are likely to have important roles in the regulation of metazoan chromosome dynamics, and chromosome segregation. It is likely that along with known regulators of the cell cycle and of mitosis, such as those presented in the pilot screen (Table 4.1), this screen will allow the identification of novel regulators of chromosome segregation.